RRCAT Newsletter

Vol. 36 Issue 2, 2023

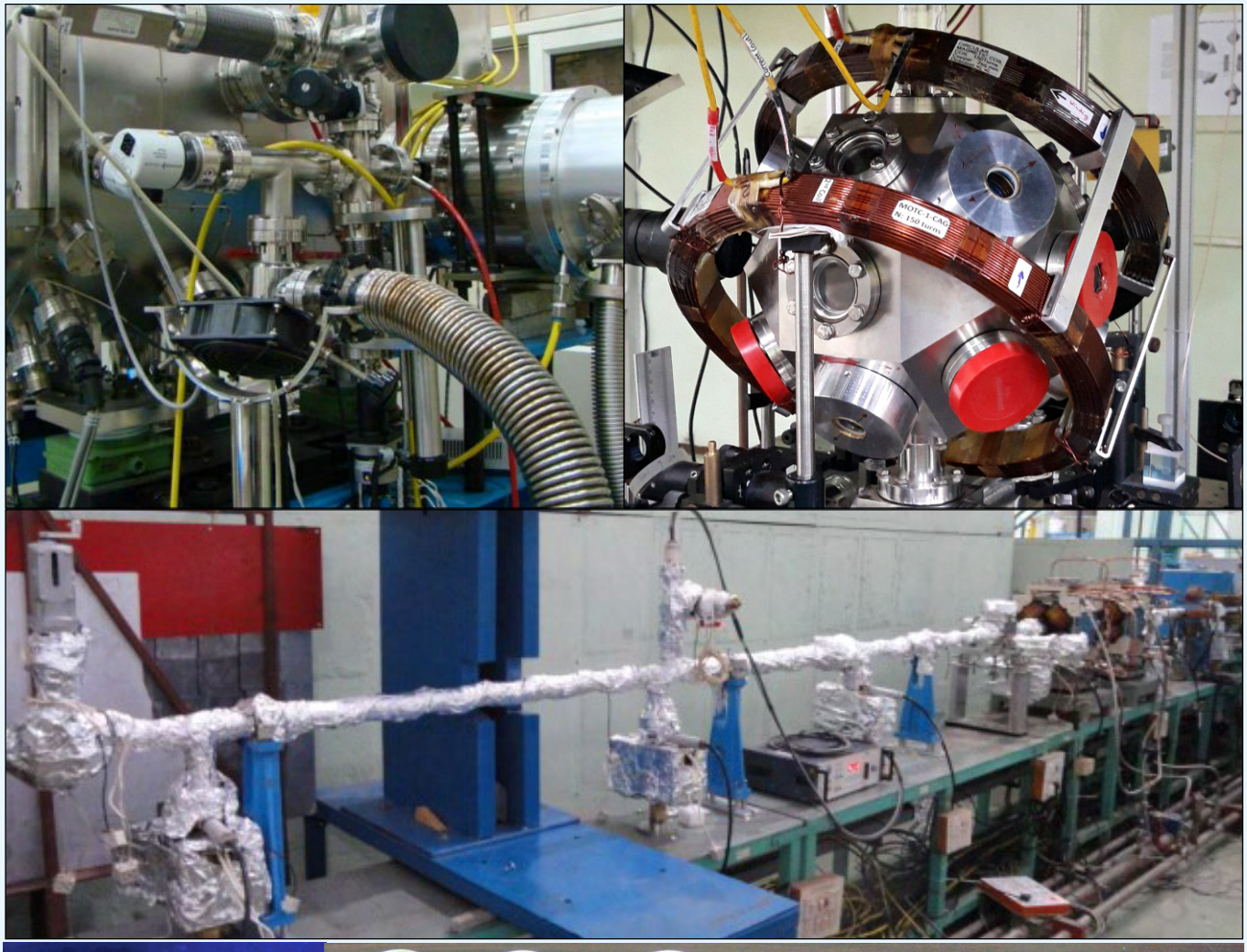

Raja Ramanna Centre for Advanced Technology, Indore
Website : https://www.rrcat.gov.in/

In this issue...

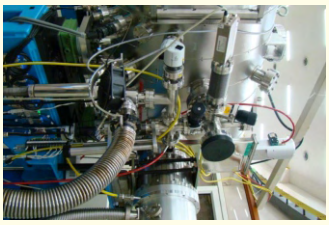

Soft x-ray fluorescence based absorption measurement setup installed in the downstream of the reflectometer station of Indus-2 soft x-ray reflectivity beamline BL-3.

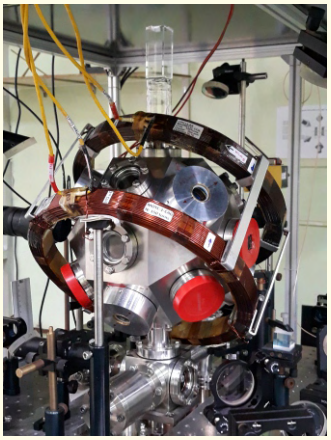

Cold atom gravimeter at RRCAT.

Photograph of newly installed vacuum system of TL-2 (Indus-1 hall).

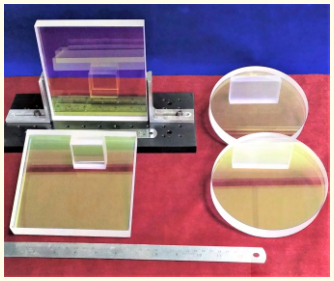

AR coated, 150 mm dia. & 150 x 150 mm optics at RRCAT.

Diffusion bonded titanium-SS tubular joints.

From the Director's Desk...

I am delighted to see the publication of the second issue of RRCAT Newsletter for the year 2023 highlighting various R&D and infrastructural accomplishments of the Centre from January - June 2023.

In this period, the two synchrotron radiation facilities Indus-1 and Indus-2 were operated smoothly in round-the-clock mode for 165 days excluding the two planned shutdown sessions for performing various experiments and undertaking preventive maintenance jobs. A total of 524 user experiments have been carried out at Indus beamlines during the period of January - June 2023. During this period more than 90 papers based on the experiments carried at Indus beamlines have been published in international peer-reviewed journals covering a wide range of topics in physics, chemistry, and materials science.

The electron beam radiation processing facility of RRCAT is used for sterilization of several batches of intravenous cannula, and other medical devices have been irradiated as per the guidelines. These products otherwise would have been sent outside India for e- beam processing. The work associated with Indus facilities highlights development of power converter for combined function corrector magnet to carry out closed orbit distortion corrections, upgradation of the vacuum system of Transport Line-2 connecting Booster to Indus-1 storage ring and low-conductivity water cooling system for Indus-2 with $\pm 0.5\ ^{0}C$ temperature stability. Other activities related to the development of accelerator technology includes the processing of high-β nitrogen-doped single-cell superconducting RF cavity at 650 MHz with extremely low field emission, setting up of a soft x-ray fluorescence-based x-ray spectrometer at the x-ray reflectivity beamline, BL-03 of Indus-2, design and development of a four-layer VME delay generator based on field programmable gate array board producing multiple delayed trigger outputs with low timing jitter, which will be beneficial for future accelerators, and UHV compatible electrical feedthroughs.

The achievements in the areas of laser technology, laser based spectroscopy, and allied fields of laser science are highlighted in the second section. Towards development of various lasers, an AO Q-switched Yb-doped fiber laser producing 3.3 mJ pulse energy and 100 W average power for potential cleaning and decontamination application and a fiber based ultrafast Mamyshev oscillator, which can circumvent the limitations of pulse energy of conventional all normal dispersion configuration oscillators have been developed. Development of laser based cold atom gravimeter providing an accuracy in the measurement of *g* up to fifth digit has also been done. Gallium nitride and its alloys with Aluminium and Indium are important due to their numerous applications in light emitters and detectors. A Nitride MBE facility has been set up at RRCAT, which can be used to grow high crystalline quality layers of nitride materials e.g., GaN, AlGaN, InGaN, InAlN. Realizing the importance of two-dimensional materials in optoelectronics and quantum technology, a microscopic mechanical exfoliation setup has been built at RRCAT to prepare two-dimensional semiconductors. Besides, the developmental works, laser application in basic science involving measurement of charge density wave in quasi-two-dimensional metallic samples of $EuTe_4$ using time-resolved x-ray diffraction technique has also been performed.

The section on *Theme Articles* constitutes an important part of the RRCAT newsletter. In this edition, we have presented three *Theme Articles* providing detailed reviews of some of the selected R&D activities carried out at the Centre over a long period of time. First theme article reviews the progress made in the material joining technologies and the second one is devoted to the development of optical thin-film coating and characterization facilities at RRCAT. The third *Theme Article* is based on a Ph. D. thesis devoted to the study of acceleration and transport of energetic electrons generated by high-power, ultra-short, intense laser pulses in dense plasma.

During this period several events and functions have been organized at RRCAT, which has been presented in the section on *Events and Happenings*. 40th Foundation Day function of RRCAT was celebrated on 20th February 2023 with Shri K. N. Vyas, Chairman, Atomic Energy Commission and Secretary, Department of Atomic Energy as the Chief Guest. On this occasion, RRCAT also signed four incubation and one technology transfer agreements with industries and startups. To commemorate, the discovery of Raman Effect, National Science Day was celebrated at RRCAT on 25th and 26th February 2023 with a theme on "Global Science for Global Wellbeing". On this occasion, visits were organized for the school and college students, teachers, family members and guests of RRCAT staff and invitees from public. This section also contains other reports on organization of workshop, theme meeting, activities devoted to the radiation and fire safety, clean and green campus, RRCAT Staff Club, accomplishments of AECS, Indore and Women's Welfare Committee.

I congratulate all the scholars, who have been awarded Ph. D. degrees by HBNI and all the staff members who have won accolades for their contributions in R&D work. We have also included a list of new members who have joined RRCAT and welcome them to the RRCAT family and we remember all those colleagues, who have superannuated from their services during this period and we wish them a happy and healthy post retirement life.

I earnestly appreciate the efforts put in by the Editorial Board to bring out this issue of the Newsletter, showcasing the wide spectrum of accomplishments of the Centre.

With best wishes,
May 3, 2024

S. V. Nakhe
Director, RRCAT

From the Editor's Desk...

The RRCAT Newsletter Editorial Board is happy to bring out second issue of the RRCAT Newsletter for year 2023 showcasing the various achievements of the Centre during the period **January - June 2023**.

The first section contains nine reports on various R&D activities associated with the Accelerator programme, which includes regular reports on the operation and usage of the two synchrotron facilities, expansion of the electron beam radiation processing facility for sterilization of various medical equipment, and development of components and utilities for the present and future accelerators. The reports devoted to the R&D activities of Laser programme are presented in the second section, which contains a total of seven reports covering various achievements in the areas of laser technology and application of lasers and to address the problems of materials science. The third section contains two reports highlighting the achievements of the Centre towards infrastructure.

Like previous issues, this edition of Newsletter also contains three *Theme Articles* appraising three chosen long term R&D activities carried at the Centre. One of them originated from the Ph. D. thesis of an HBNI scholar devoted to the study of laser-based electron acceleration. The other two articles review the development that took place at RRCAT in the areas of metal joining technology and optical thin film coating technology.

The last section on *Events and Happenings* comprises reports on the various events and functions organized at RRCAT. This section includes reports on two important functions, namely, the celebration of RRCAT's 40th Foundation Day on 20th February 2023 and National Science Day celebration at RRCAT on 25th and 26th February 2024.

The Editorial Board thanks all the contributors for their cooperation and support in bringing out this issue. We take this opportunity to express our sincere gratitude to Director, RRCAT, for his keen interest, guidance, and active support in publication of RRCAT Newsletter. We look forward to receiving constructive comments and suggestions from readers for improving the content of RRCAT Newsletter.

Arup Banerjee
Chairman, Editorial Board
(on behalf of RRCAT Newsletter Editorial Board)

May 3, 2024

A.1: Status report on operation of Indus accelerators

The Indus synchrotron radiation (SR) sources, constituting a national facility, provided SR beam to the users on round-the-clock (RTC) basis. Both Indus-1 and Indus-2 maintained excellent operational performance during the first half of year 2023 (January - June).

In the said period, both the machines were operated smoothly following the prescribed safety procedures. One planned shutdown of four days was taken in the month of May for preventive maintenance. A relatively longer shutdown of 11 days was taken in February for upgradation of vacuum system of Transport Line-2 (TL-2) and other major activities possible in parallel. Taking this into account, the machine was operated in round-the-clock mode for 165 days during these six months. The beam availability in Indus-1 was 3442 hours (~20.8 hours/day) whereas in Indus-2 it was 2711 hours (~16.4 hours/day). This performance is largely in line with performance in recent years. Indus-2 clocked its best yearly performance ever in terms of beam availability of 5601 hours in the calendar year 2022. Figures A.1.1 and A.1.2 show the typical user mode operation of Indus-1 and Indus-2, respectively.

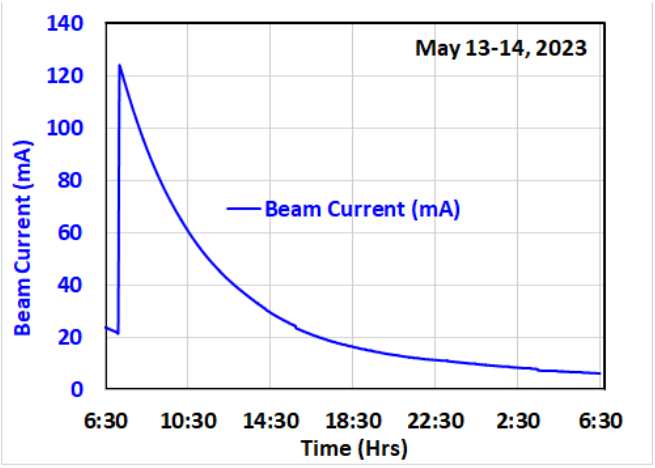

Fig. A.1.1: Typical user mode operation of Indus-1.

Utilization: A total of seven beamlines in Indus-1 and eighteen beamlines in Indus-2 are operational. Users from large number of universities and research institutes carried out experiments at these beamlines. The number of users from pharmaceutical industries is also increasing steadily. Total number of user experiments carried out at Indus beamlines in the reported period was 524.

Machine studies: Experiments for machine studies and improvements were carried out on days specifically reserved for this purpose (total 17 days). Some of the important experiments carried out in Indus-2 are: (a) Broadband impedance measurement experiment, (b) Calculation of alignment offsets of beam position indicators (BPIs) using beam based alignment (BBA) technique, (c) Exercises to address the temperature rise issue of dipole vacuum chambers, and (d) Operation of machine in the orbit having minimized closed orbit distortion (COD).

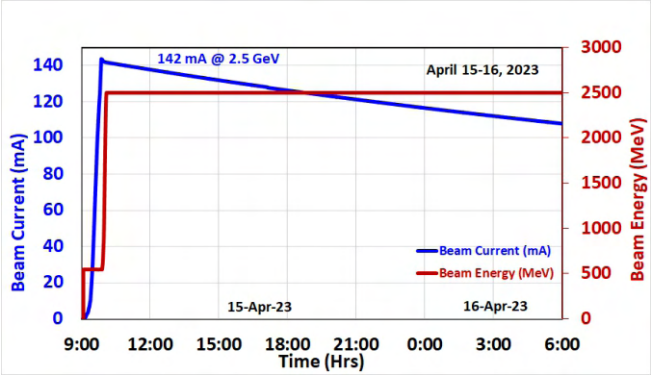

Fig. A.1.2: Typical user mode operation of Indus-2.

Upgradation of vacuum system of TL-2 and other maintenance activities: Upgradation of 25.5 m long vacuum system of TL-2, connecting booster synchrotron to Indus-1 storage ring, was carried out during shutdown taken from 18th to 28th February 2023. The aging effect on the 25 year old vacuum system of TL-2 had started affecting its reliable performance. New vacuum chambers and sputter ion pumps having ConFlat (CF) demountable joints, were installed replacing old ones aimed at reliable operation in years ahead and standardization. More details about this major upgradation work is given separately in report A.8 at page no. 8. Beam injection and filling into Indus-1 was successful on very first day of restart after shutdown due to proper installation and maintaining the working position and orientation of TL-2.

Other major activities carried out during this shutdown were: (a) Upgradation of Motor Control Centre and replacement of electrical panels, both at Indus-2 low conductivity water (LCW) plant, and (b) Upgradation of CAP sub-station.

The above activities were accomplished by the respective teams by working for extended hours due to tight shutdown schedule.

Training qualification and licensing (TQL) programme: The training of 5th batch of operators under TQL programme was completed successfully in the month of April. Under this programme, a total of 39 personnel have been trained and qualified for operation of Indus facility at qualifying levels 3, 4 and 5. The newly trained personnel along with 24 personnel from previous batch have taken over round the clock operation of Indus accelerators with effect from 1st July 2023.

Reported by:
T. A. Puntambekar (tushar@rrcat.gov.in)

A.2 Activities at Indus beamlines

Beamlines at Indus-1 and Indus-2 are national facilities that have a total of 18 operational beamlines. These beamlines have been in regular use by the scientists, researchers and students from the Indian academia and Indian industry. The total number of user experiments that have been carried out at Indus beamlines in the period of January 2023 to June 2023 were 524.

During this period, the total number of papers published in peer reviewed international journals exceeded 90. Work on diverse topics based on the experiments that have been carried out at the Indus beamlines, which include: materials science, biology, chemistry, physics, etc., have been published. Some of the published works are highlighted below:

Different groups have worked on several problems related to energy materials. The understanding of structural changes in $LiNi_xMn_yCo_zO_2$ cathodes of Li ion batteries during charging and discharging has been reported (Ref.: N. Abharana et al., Solid State Ionics, Vol. 398, p 116270 (2023)). Results related to the development of a high-rate-capable O3-structured 'layered' Na transition metal oxide by tuning the cation–oxygen bond covalency for electrodes in Na ion batteries has been published (Ref.: Ishita Biswas et al., Chem. Commun., Vol. 59, p 4332 (2023)). By carrying out in-operando synchrotron X-ray diffraction and stress measurements, the process of degradation of the metal electrodes of Li ion batteries has been analysed and published (Ref.: Ankur Sharma et al., ACS Appl. Mater. Inter., Vol. 15, p 782 (2023)). In a related work on characterization of carbon containing shale rocks, the pore anisotropy in shale, its dependence on thermal maturity and its organic carbon content was studied and published (Ref.: J. Bahadur et al., Int. J. Coal Geo., Vol. 273, p 104268 (2023)).

Several interesting materials science problems aimed at development of devices in the future, have been studied and published. These include the following: Enhanced temperature coefficient of resistance in nanostructured $Nd_{0.6}Sr_{0.4}MnO_3$ thin films for spintronic applications has been reported (Ref.: Mrinaleni R. S. et al., Thin Solid Films, Vol. 779, p 139933 (2023)). Magneto-strain effects in 2D ferromagnetic van der Waal material $CrGeTe_3$ for spintronic device applications has been published (Ref.: Kritika Vijay et al., Sci. Rep., Vol. 13, p 8579 (2023)). Piezoelectric properties and structural evolution in La- and Al- modified $K_{0.5}Bi_{0.5}TiO_3$ ceramics for lead free ferroelectric applications has been reported (Ref.: Manish Badole et al., J. of Alloys & Comp., Vol. 944, p 169204 (2023)). Tunable magnetoresistance driven by electronic structure in Kagome semimetal $Co_{1-x}Fe_xSn$ was published (Ref.: Kritika Vijay et al., Appl. Phys. Lett., Vol. 122, p 233103 (2023)). Ultrafast carrier relaxation and second harmonic generation in higher-fold Weyl Fermionic system PtAl for high-speed device applications has been reported (Ref.: Vikas Saini et al., Adv. Phys. Res., Art. No. 2300063 (1 of 8) (2023)). Enhanced magneto-dielectric properties of Pr-doped polycrystalline $Gd_{0.55}Pr_{0.45}MnO_3$ at low temperatures for applications as multiferroics has been reported (Ref.: Pooja Pant et al., J. Mag. Magnetic Mat., Vol. 572, p 170621 (2023)). Chemical in-homogeneity and amorphous to crystalline transformation in CoFeB/MgO based magnetic tunnel junctions has been reported (Ref.: Pramod Vishwakarma et al., Mat. Res. Bull., Vol. 161, p 112150 (2023)).

In the area of basic materials science, some of the work published include: the structural evolution in $GdVO_4$ under extreme pressure (Ref.: Ankit Bhoriya et al., J. Solid State Chem., Vol. 324, p 124072 (2023)), and crystallographic structural variations in nano-crystalline Sc_2O_3 under pressure (Ref.: D. Yadav et al., Phys. Scr., Vol. 98, p 045707 (2023)).

Regarding applications in the nuclear industry, the following works are reported. A novel gamma ray shielding block developed using alumina industry waste has been reported (Ref.: Rahul Arya et al., Const. & Building Mat., Vol. 373, p 130895 (2023)). Studies of defects generated in neutron-irradiated austenitic stainless steels at low displacement damage levels has been published (Ref.: Shreevalli M. et al., J. of Nucl. Mat., Vol. 577, p 154338 (2023)). Understanding the process of microstructure and defect evolution in oxygen ion-irradiated pure nickel, for applications in high temperature and other extreme environment is reported (Ref.: U. Saha et al.. Mat. Chem. & Phys, Vol. 305, p 127916 (2023)).

Several results on biological problems that have been carried out and published have been summarized below, A detailed insight into the inhibitory mechanism of new Ebselen derivatives against main protease (Mpro) of severe acute respiratory syndrome coronavirus-2 (SARS-CoV-2) has been reported (Ref.: P Sahoo et al., ACS Pharmacol. Transl. Sci., Vol. 6, p 171 (2023)). New insights into the antimalarial mechanism of Chloroquine, the most common malarial drug, has been published (Ref.: Rahul Singh et al., ACS Infect. Dis., Vol. 9, p 1647 (2023)).

Reported by:
Tapas Ganguli (tapas@rrcat.gov.in)

A.3: Expansion of commercial E-beam irradiation services at ARPF

Electron Beam Radiation Processing Facility (ARPF) began its commercial operation in second half of 2022 and made its first shipment of electron beam sterilized Risk Class-B medical devices in October 2022. The E-beam irradiation services at ARPF are being provided as per the process control requirements of ISO 11137 and Quality Management System (QMS) requirements of Medical Device Rules (MDR) 2017, ISO 13485:2016 and ISO 9001:2015 certifications.

Sterilization of the IV cannula (used for transfusion of blood or liquids in patient body) manufactured by M/s Becton Dickinson (BD) is being carried out on regular basis after signing of irradiation agreement between RRCAT Incubation Centre and Becton Dickinson in 2022. Figure 3.1 shows progressive growth in the sterilization of medical devices (IV cannula) at ARPF till June 2023.

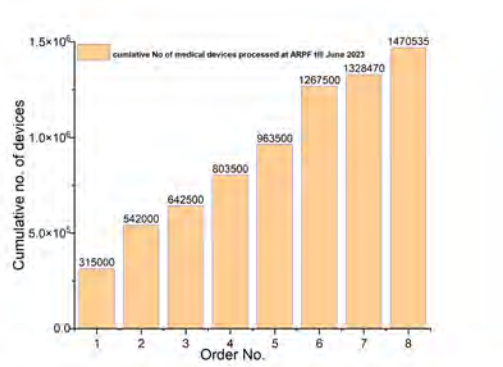

Fig. 3.1: Cumulative sterilization of medical devices at ARPF.

To expand the user base for electron beam applications, outreach activities were carried out through e-mails/ presentation and webinar. As a result, a large number of medical device manufacturers from across the country have started exploring, qualifying and validating the electron beam facility for electron beam sterilization process development and to generate the baseline data for radiation compatibility of various products. Some of the products irradiated with electron beam are listed in Table 3.1 and shown in Figure 3.2.

Table 3.1: Products irradiated with electron beam.

Product name	Usage	Dose (kGy)
Silvasorb	Wounds dressing	18 - 28
IV blood bags	Filling of drug and blood	25 - 45
Skin Temp AG	Burn healing	27 -32
Butyl rubber stopper	Drug packaging	25 – 40
Blood collection tubes	Blood sample collection	7 – 9
EPDM sheet	Crosslinking	120 - 145

Making improvements in the process performance, the conveyor control system has been upgraded for reliable and efficient process operations. Firmware of PLC and drives have been updated. New PLC, HMI and SCADA programs for "Batch mode" "Performance Qualification (PQ) mode", "Manual mode" has been developed.

Blood collection tubes

Blood transfusion bags

Antimicrobial dressing

Butyl rubber stopper

Fig. 3.2: Medical devices irradiated for process development.

These modes can be operated for one as well as two sets of trolley trains. In case of two sets of trolley trains, empty trolleys can be transferred from unloading station to loading station while irradiation process of one batch is going on. This permits loading of next batch of products on the second trolley train while first batch is being irradiated. Thus, irradiation of next batch can be started immediately after process completion of the previous batch. A customized system for process speed measurement, irradiation pass counting, box identification (in case of process trip) and jamming detection has been developed and implemented. The PLC based conveyor control system has been integrated with main control system (MCS) in such a way that all the operations can be executed from main control system, data of critical parameters (process speed, number of pass and location of box at trip time) is transferred for data logging. Figure 3.3 shows the mimic of conveyor control panel for two sets of trollies.

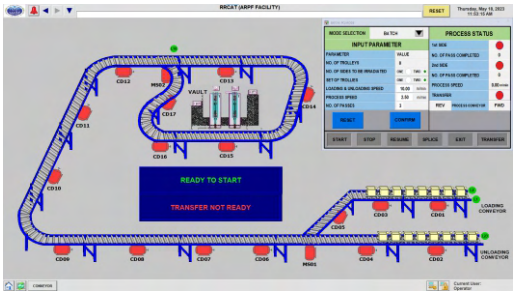

Fig. 3.3: Mimic control panel for upgraded conveyor.

Additionally, gem industry is availing ARPF services for color modification of their products.

Reported by:
V. C. Petwal (vikash@rrcat.gov.in)

A.4: Power converters for sextupole coils in combined function corrector magnets in Indus-1

Due to the space limitation in the Indus-1 ring, a set of eight combined function multipole magnets are being developed to facilitate closed orbit distortion (COD) correction. Each magnet will produce four required magnetic field components, namely; sextupole component to correct the chromaticity, skew quadrupole component to reduce the coupling (between the horizontal and vertical planes), and vertical & horizontal dipole components for steering the beam in both the planes. Each skew quadrupole coil, horizontal corrector coil and the vertical corrector coil will be energized independently by separate true-bipolar power converter, whereas for chromaticity correction, sextupole coils of four magnets will be connected in series and energized by one unipolar power converter. Therefore, two unipolar power converters of maximum output rating 125 A/25 V and output current stability of ± 100 ppm are required to energize the two series circuits of sextupole coils. A brief account of the design and development of 125 A/25 V unipolar power converters is reported here.

The power converters are developed based on switch-mode, two-switch forward converter topology. The converter is operating at 25 kHz switching frequency. IGBTs are used as switching devices. The main features of the design are: high efficiency, smaller size, less cooling requirement, low audible noise, high stability, better maintainability, etc. The power converters are designed and developed in modular fashion. Each module, namely, power module, breaker panel and control rack are developed and tested separately.

It was important to design the system of power converter keeping in mind the available space in Magnet Power Supply Hall in Indus-1, as well as the utilization of existing load cables for facilitating their installation. With this constraint, the mechanical assembly of power converters was planned in two 38 U cabinets with footprint of 0.8 m x 0.8 m, each housing one125 A/25 V unipolar power at the bottom in 17 U height. The remaining 21 U space in each cabinet was left to house the bipolar power converters. Figure A.4.1 shows photograph of one cabinet with the 125 A power converter assembly at the bottom. The inset of the figure shows assembly of power module and breaker panel inside the cabinet.

Rigorous testing has been performed on the power converters. Open and closed loop testing at low and high power has been carried out. Apart from various functional tests, heat run test and special endurance tests, such as current cycling tests, periodic on-off cycles, etc., have been carried out. Stability for eight hours of continuous operation has been recorded to be well within the specification of ± 100 ppm, as shown in Figure A.4.2.

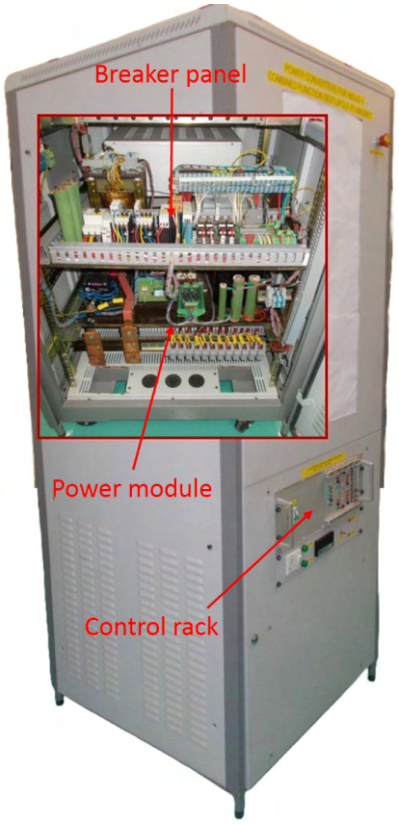

Fig. A.4.1: A view of one power converter cabinet showing 125 A / 25 V power converter at the bottom and inset shows the inside assembly.

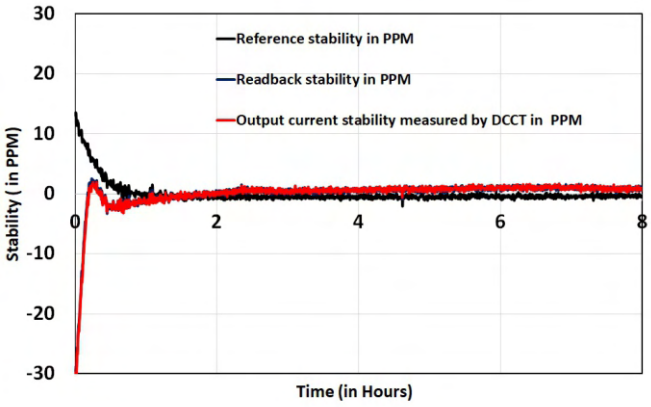

Fig. A.4.2: Output current stability for eight hours of continuous operation.

Reported by:
Vineet Kumar Dwivedi (vineet@rrcat.gov.in)

A.5: Processing of a field emission free nitrogen-doped high-β single-cell 650 MHz superconducting RF cavity

High-β (HB) superconducting radio frequency (SRF) cavities processed with nitrogen (N) doping technique are known to demonstrate better performance than non-doped cavities. As a result, HB cavity deliverables to Fermilab, under IIFC collaboration, mandates N-doping to be included in the processing recipe. Moreover, successful adoption of such technique in the processing cycle at RRCAT, holds significance for future accelerator programs of DAE. In this technique, the cavity is subjected to standard degassing at 800 °C for 3 hrs. in high vacuum furnace followed by a "2/6 recipe" (2 min. at ~25 mtorr N_2 partial pressure followed by 6 min. soak under high vacuum at 800 °C) and thereafter cool down.

To augment its benefits, efforts at RRCAT were initiated, which included setting up of a nitrogen (N_2) gas bleeding attachment to the furnace; N-doping studies on Niobium (Nb) samples followed by trial on HB cavities and its testing. The performances were however, limited by the maximum accelerating gradient (E_{max}) at ~ 14.5 MV/m, quality factor (Q_o) < 1 x 10^{10} at E_{max} along with high field emission (FE) (x-rays > 500 µSv/h).

As a result, modifications to nitrogen gas bleeding set-up were adopted, followed by detailed evaluation of the gas purity using a residual gas analyzer (RGA) fitted on furnace chamber such that no traces of O_2, Ar, CO_2 and moisture was observed during testing of the line with high purity nitrogen gas. Based on the above upgradations and another round of sample studies, a single-cell cavity (HB92-RRCAT-104) was processed. This cavity had previously underwent four rounds of processing and testing with E_{max} limited to 12.8 MV/m and Q_o < 1 x 10^{10} at E_{max} and high field emission. Hence, the RF surface of this cavity was first reset by 50 µm electropolishing (EP) followed by ultrasonic cleaning (UC) and high pressure rinsing (HPR) to prepare pristine surface for N-doping. The cavity along with niobium samples were then loaded in the furnace as shown in Figure A.5.1 and doped using above mentioned recipe. Secondary electron (SE) imaging of the representative niobium samples revealed star shaped niobium-nitride precipitates on surface, which are a characteristic of proper doping procedure (see Fig. A.5.2). Compositional depth profiling also revealed contamination free nitrogen-diffusion at majority of locations. The cavity was then light electropolished for ~7 µm, under cold conditions, followed by ultrasonic cleaning and 3+5 pass high pressure rinsing with ultra-pure water, drying and assembly in an ISO Class-4 cleanroom. Stringent quality control during assembly was followed along with few procedural modifications.

Fig. A.5.1: Single-cell cavity loaded in furnace.

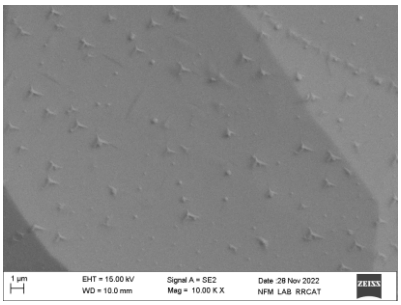

Fig. A.5.2: Secondary electron image of Nb-nitride precipitates.

Subsequently, the cavity was evacuated with upgraded slow pumping set up followed by high vacuum pumping, leak testing and sealing at vacuum < 1.0 x 10^{-6} mbar. Low power RF testing of this cavity at 2K revealed excellent field emission free (x-rays < 0.2 µSv/h) gradient up to 24.7 MV/m with an improved Q_o of 3 x 10^{10} at 18.8 MV/m (see Fig. A.5.3).

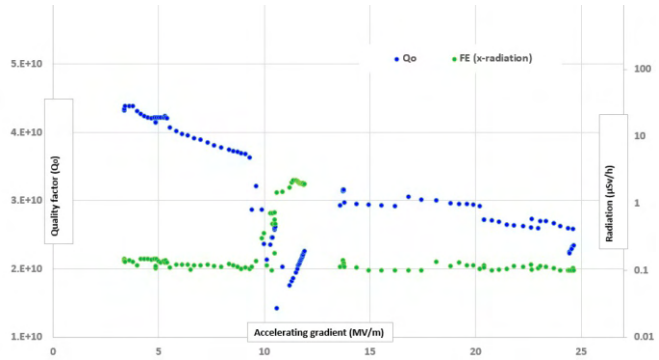

Fig. A.5.3: RF performance of N-doped HB92-RRCAT-104 single cell cavity at 2K.

The results show improvement in cleanroom operational procedures and understanding of N-doping treatment, resulting in the first field emission free and high gradient cavity to be processed successfully at RRCAT. This expertise shall be immensely beneficial for future accelerator programs of DAE.

Reported by:
Aniruddha Bose (aniruddha@rrcat.gov.in)

A.6: Soft x-ray absorption measurement on Indus-2 soft x-ray reflectivity beamline using x-ray fluorescence signal

Soft x-ray absorption spectroscopy (SXAS) is a powerful tool to analyze the chemical and electronic properties of materials. For the absorption measurements, one needs the ratio of transmitted beam to the incident photon beam intensity. In the soft x-ray region (< 2000 eV), the transmission measurements are very challenging because they require ultrathin freestanding samples (< 50 nm thickness), which are difficult to produce. Therefore, the SXAS measurements in the soft x-ray region are performed in indirect mode by measuring the total electron yield (TEY) or x-ray fluorescence signal. The TEY technique is surface sensitive, as the electron signal is collected from the top within few nanometer thickness (2-3 nm). The resultant absorption data are affected by surface contamination, if any. The SXAS signal collected in fluorescence mode has higher depth sensitivity (> 100 nm) as the penetration depth of the soft x-ray photons is relatively large, and therefore the fluorescence based technique is useful to probe the bulk properties. Charge neutrality is another major advantage of the fluorescence based x-ray absorption measurement technique. Thus, non-conducting samples can also be measured easily.

At Indus-2 soft x-ray reflectivity beamline, BL-03, a soft x-ray fluorescence (SXF) based x-ray absorption measurement setup is designed, installed, and commissioned. A separate vacuum chamber is installed in downstream of the existing reflectometer station with a vacuum isolation valve. A separate vacuum pumping arrangement is made for the SXF chamber. At a time four samples of ~10×10 mm^2 size can be mounted. The SXF chamber operates in ~1×10^{-6} mbar vacuum. A vacuum compatible energy dispersive silicon drift detector (SDD) is used for soft x-ray fluorescence measurement.

In order to protect the detector from the exposure to ambient while sample loading/unloading, the detector is mounted on a retractable linear movement feedthrough and kept in a detector vessel, isolated with a vacuum valve. The detector can be brought close to the sample during the measurement. Along with mechanical vacuum assembly, a LabView based instrument control and data acquisition software is also developed. The software is used to control the detector and the beamline monochromator together so that the energy dependent x-ray absorption measurements can be performed. The SXAS measurements in the fluorescence mode are successfully performed on various samples. Figure A.6.1 shows the SDD detector based SXAS setup installed in downstream of the reflectometer station. Figure A.6.2 shows a measured SXAS spectra of CrN and Cr thin film sample using the nitrogen *K* emission line. The setup can be used for elemental identification of different low *Z* elements, e.g., carbon, nitrogen, oxygen, etc., which are otherwise not feasible in the hard x-ray based fluorescence measurement setup operating in air environment.

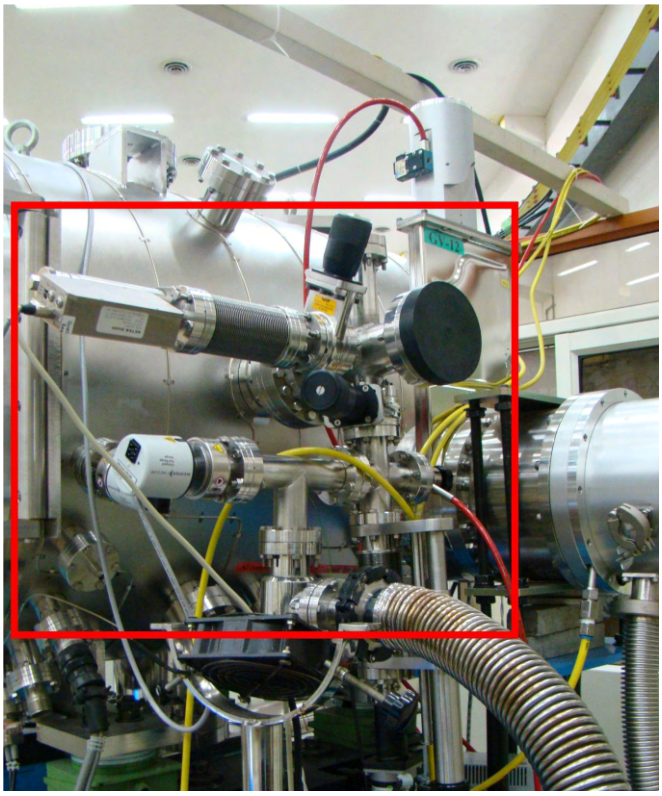

Fig. A.6.1: Soft x-ray fluorescence based absorption measurement setup shown in the red marked area is installed in the downstream of the reflectometer station.

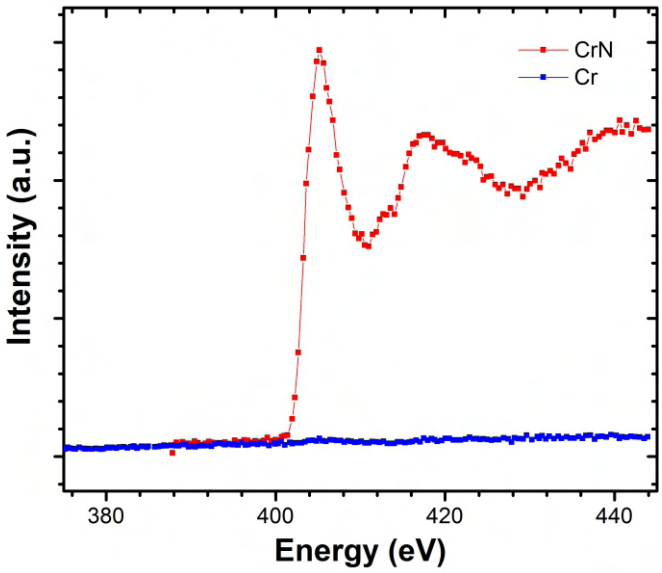

Fig. A.6.2: SXAS spectra of CrN and Cr thin film samples measured using the nitrogen K fluorescence signal.

Reported by:
R. K. Gupta (rkg@rrcat.gov.in)

A.7: Low jitter FPGA based VME delay generator board

A four layer Versa Module Euro (VME) delay generator board has been designed and developed for future accelerators. This is a field programmable gate array (FPGA) based delay board. It gives multiple delayed trigger outputs (O/P) with low timing jitter (10s of ps).

Board features: Main features of the board are: Standard VME bus interface (A24:D16), Form factor: 6U & single slot, both external & on-board clock interface, pin programmable clock selection, delay resolution is 10 ps and jitter is ~ 10s of ps, one external trigger input (I/P) & 5 trigger O/P, I/P trigger is fed with optical isolation, each O/P gives delayed trigger pulse with respect to I/P trigger pulse, delay of each O/P is remotely adjustable in coarse and fine time scale, coarse scale - as per the clock frequency, fine scale - 10 ps, trigger O/Ps are in two forms- electrical form: low voltage transistor-transistor logic (LVTTL), fibre optic (FO) form: FO transmitter O/P is for plastic optical fibre (POF) interfacing, board supports RS-485 based interfacing also for standalone operation.

Description: The board is shown in Figure A.7.1. It is designed with high speed logic circuits for handling high frequency differential clock and O/P trigger pulse signals. External high frequency RF clock is handled via differential 50 ohm lines, high speed logic circuits for its scaling and direct interfacing to Spartan-3 FPGA clock I/Ps. 125 MHz on-board oscillator is also interfaced to FPGA. It has selectable clock feature. The O/P trigger pulse is generated at the specific delayed instant as per the set data. Delay data of each channel is stored in particular register. This can be set via VME as well as by RS-485 interface. Coarse delay of each O/P is generated by the synchronous counter within FPGA. Coarse delay resolution is governed by the external/on-board clock frequency, being used for counter. Delayed trigger pulses from FPGA are available at coarse delay time scale. These signals are handled via LVPECL logic circuits for interfacing with external precision delay line ICs, which gives delay in fine time scale of few nano seconds range with delay step in 10 ps. Differential O/P from fine delay IC is converted into 1:2 fanout single ended O/Ps. One of these is electrical O/P of LVTTL level. Other one is converted into fibre optic based output for plastic optical fibre interface. Isolated RS-485 serial interface is provided for its access in standalone mode to select particular channel and set delay data.

Testing: High frequency external RF signal is provided to the board from RF generator. 1 Hz I/P trigger is fed from function generator. Presently external RF signal of 505 MHz (like Indus-2 RF) is applied. Five trigger O/Ps are observed at both electrical and FO version. Existing FO receiver card is used for checking the performance. Coarse, fine delays of each trigger O/P, delay resolution of each channel & timing jitter are checked. Timing jitter between two channels at the electrical O/P is < 40 ps (Fig. A.7.2). The same is observed between two FO receivers O/Ps. It is < 80 ps. (Fig. A.7.3). Board has been tested successfully in laboratory with both VME and RS-485 interfaces. This board may be used for low timing jitter application in future accelerators.

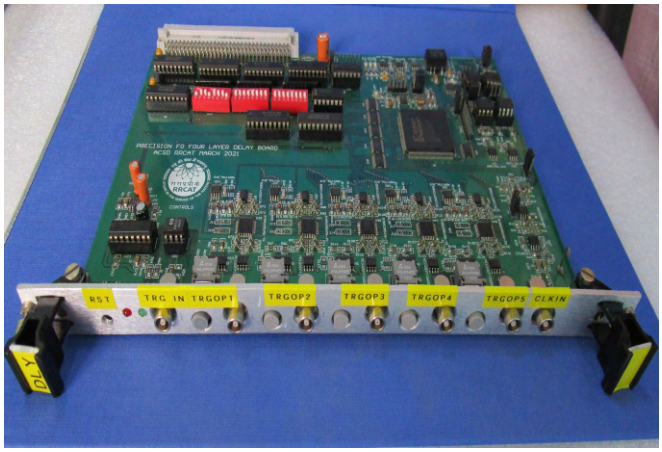

Fig. A.7.1: Low jitter VME delay generator board.

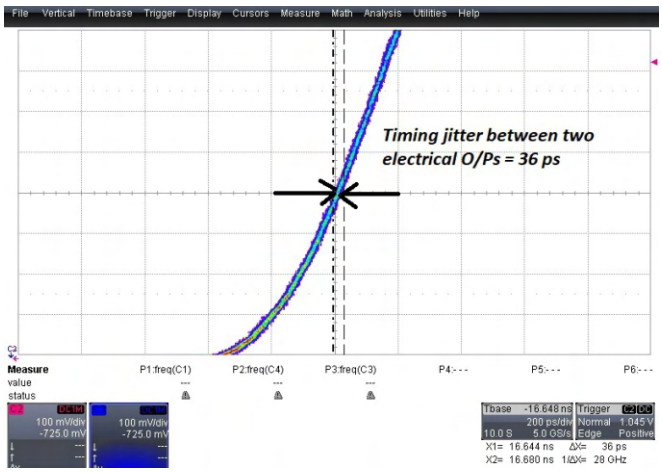

Fig. A.7.2: Timing jitter between electrical O/Ps.

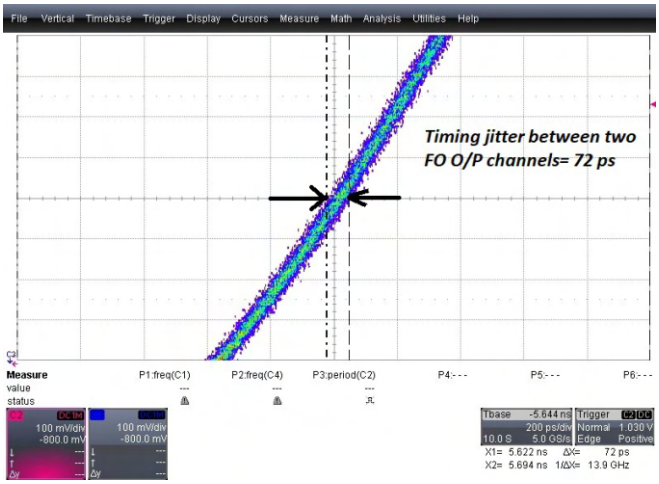

Fig. A.7.3: Timing jitter between FO receiver O/Ps.

Reported by:
Sampa Gangopadhyay (sampa@rrcat.gov.in)

A.8: Upgradation of vacuum system of Transport line-2

Upgradation of 23.5 m long vacuum system of Transport Line-2 (TL-2), connecting Booster to Indus-1 storage ring, was carried out during machine shutdown period from 18th to 26th Feb. 2023. Ageing of aluminium wire sealed demountable joints of ~ 25 year old vacuum system was affecting its reliable performance. New vacuum chambers and sputter ion pumps (SIP), having ConFlat (CF) demountable joints, were installed replacing old ones for reliable operation in years ahead. This activity was accomplished by the entire team working extended hours due to very tight shutdown schedule.

New vacuum components installed replacing old ones during the stated shutdown period are: 02 numbers of bending magnet (BM) chambers of 28º and 35º angles respectively, 11 numbers of straight section chambers, 04 numbers of bellow sub-assemblies, 10 numbers of sputter ion pumps and 02 numbers of Bayard Alpert gauges (along with new cables). Aged beam diagnostic devices namely wall current monitor (WCM) and 2-π monitor were also replaced with new ones. One manually operated ultra-high vacuum (UHV) gate valve of size DN-63-CF was installed in central portion for facilitating the maintenance on either side. New compatible supports were installed at several locations to obtain better alignment accuracies.

The new vacuum chambers along with diagnostic devices with upgraded features were designed, fabricated, tested for its vacuum performance in lab prior to their installation at TL-2 site. Flange design of all the new chambers and associated components are based on CF sealing technology replacing wire seal design in old components for enhanced reliable performance. New straight section chambers were designed with longer length thereby reducing number of demountable joints and incorporating pumping ports having larger diameter offering higher conductance for SIP's compared to old design. Salient features of BM chambers are listed in Table A.8.1 below.

Table A.8.1: Salient features of BM chamber.

Sr. No.	Parameter	Value
1.	Material of construction	SS316L
2.	Bending angles and radius	28° and 35°/ 2000 mm
3.	Internal aperture	30 mm (V) x 55 mm (H)
4.	Profile cutting method	Water jet cutting
5.	Welding method	GTAW

28° BM is at upstream end of TL-2, after extraction chamber of booster. 35° BM, also known as switching magnet, is located in central portion of TL-2. Switching magnet chamber (35º chamber) is having two ports: zero degree port connecting to TL-3 leading to Indus-2 storage ring and 35º port connecting to downstream part of TL-2 leading to Indus-1 storage ring. The switching magnet is energised for beam injection into Indus-1 ring, whereas during beam filing in Indus-2, through TL-3, it remains un-energised. Photograph of newly installed vacuum system of TL-2 is shown in Figure A.8.1.

Fig. A.8.1: Photograph of newly installed vacuum system of TL-2 (Indus-1 hall).

New vacuum components were fabricated and leak tested for helium leak tightness $<1x10^{-10}$ mbar.l/s using helium mass spectrometer leak detector (MSLD). All the components were tested for its UHV performance after chemical treatment as per UHV requirements in lab prior to their deployment in ring. The chambers were assembled in lab with their vacuum system evacuated, baked at 250 °C for 48 hours and ultimate vacuum of $<1x10^{-9}$ mbar was achieved after baking.

Old vacuum system was dismantled and removed from TL-2 after opening the upper halves of quadrupole magnets followed by placing new vacuum chambers at their respective locations and finally re-assembling the magnets upper halves. Subsequently all the newly installed vacuum system was integrated with Booster ring, Indus-1 ring and TL-3 successfully. Leak detection was carried out after assembly for leak tightness of $<1x10^{-10}$ mbar.l/s with MSLD. Complete vacuum system of TL-2 was baked for short duration at 150 °C for 8 hrs. and vacuum level of $3.3x10^{-8}$ at Booster end and $6.2x10^{-10}$ mbar at Indus-1 side was attained.

Installation of vacuum components, vacuum conditioning and recovery of required vacuum in TL-2 was accomplished well within the scheduled shutdown period and handed over for resumption of regular operation of the machine.

Reported by:
B. K. Sindal (bksindal@rrcat.gov.in)

A.9: Upgradation in Indus-2 low conductivity water cooling system

Cooling water system in Indus complex provides cooling for Indus-2, transfer line-3 (TL-3), magnet coils, magnet power supply racks, RF cavities & their power supply racks, etc. It circulates the low conductivity water (LCW) at 29 ^{0}C in the closed primary loop. A plate type heat exchanger (PHE) transfers the heat to a secondary side cooling loop, which finally dissipates its heat into the atmosphere through cooling tower units. The achievable cold-water temperature and performance of this evaporative cooling system is highly dependent on relative humidity of the atmospheric air throughout the year.

To meet the supply water temperature of 26±0.5 ^{0}C in place of 29±1 ^{0}C as per the new requirement, it was decided to install and commission a refrigeration based new secondary cooling system in the upgraded chiller plant area as shown in Figure A.9.1.

Fig. A.9.1: Developed water cooled chiller plant area with automatic tube cleaning system.

Fig. A.9.2: Three numbers of 180 TR water cooled chillers with electrical panel, instrumentation & controls.

Hence, a new water-cooled, refrigeration based chiller plant was developed and commissioned along with three water-cooled chiller units having flooded type evaporator devices, pumping system, pipelines, heat exchangers, instrumentation & control system as shown in Figures A.9.1 and A.9.2. This provides very fast cooling response for required demand of accelerator machine components. The chiller has shown to achieve 0 to 100% RLA (rated load amps) within 12 minutes. Another aspect of the operational behaviour, achieving temperature control and stability within 26±0.5 ^{0}C is shown for one of these chillers in Figure A.9.3.

The chiller unit condenser tubes are made of Cu-Ni, which will provide long operational life. Moreover, for reliable performance, an automatic tube cleaning system (ATC) has also been installed, which caters the requirement of condenser cleaning for online removal of the scale deposits and maintains the heat transfer effects of the condenser tubes, internally.

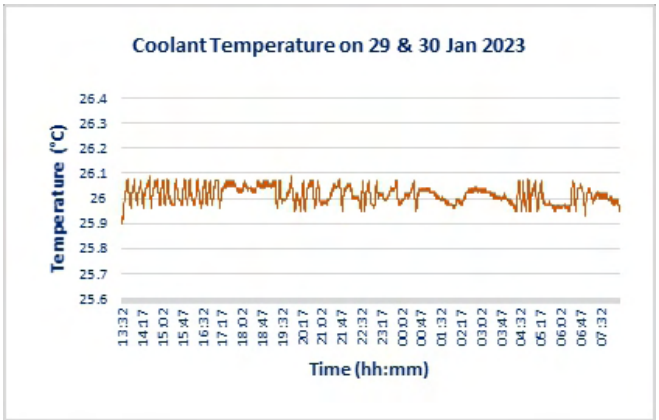

Fig. A.9.3: Operational performance of upgraded Indus-2 cooling water system providing temperature stability of 26±0.5 ^{0}C with integrated chiller system.

These chiller units were tested on site to ensure trouble free operation by operating continuously for 72 hours with available thermal load before putting into service.

Now, with the upgraded cooling system in place, the LCW water is being provided at 26±0.5 ^{0}C to TL-3 magnet coils, magnet power supply racks, RF cavities & their power supply racks in 24x7 mode, which will increase the operational life of the subsystem components. For more details, please refer to: *M. K. Singh, R. M. Pandey, Rakesh Kumar, Yogesh Kumar, Ravi Parkash, Jimmy James, T. A. Puntambekar, "Improvement in Indus-2 coolant temperature stability during beam energy ramp-up with Flooded Evaporator Type Chiller System", 11th DAE–BRNS Indian Particle Accelerator Conference, 13-16 March 2023, BARC, Mumbai.*

Reported by:
Manitosh Kumar Singh (manitosh@rrcat.gov.in)

L.1: Development of cold atom gravimeter for the measurement of gravitational acceleration

The value of earth's gravitational acceleration *(g)* changes from place to place depending upon structure of earth underneath. The accurate measurement of *g* on the earth's surface, using an accurate gravimeter, has applications in mineral explorations, study of geophysics, monitoring of seismic activities, space missions, etc. The accuracy of a gravimeter depends upon the fundamental method used for developing a gravimeter. Matter wave interferometry-based gravimeter, such as cold atom gravimeter (CAG), is an absolute gravimeter with high sensitivity, accuracy, and long-term stability.

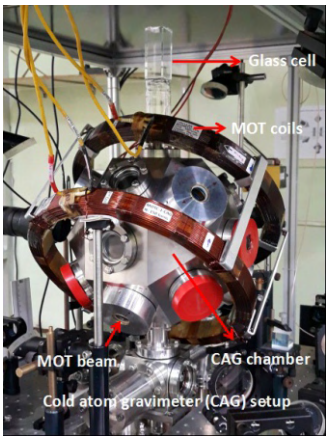

Fig. L.1.1: Photograph of the cold atom gravimeter at RRCAT.

At RRCAT, a cold atom gravimeter has been developed. The Doppler sensitive two-photon Raman transition based internal state atom interferometry is used for the measurement of *g,* when atoms are moving under influence of gravitational acceleration.

The cold atom gravimeter setup (Fig. L.1.1) has a magneto-optical trap (MOT) to cool and trap ^{87}Rb atoms. This is in [111] configuration of laser beam such that three pairs of counter propagating MOT beams are oriented in vertical direction with three-fold symmetry (Fig. L.1.2). Cold atoms from MOT are launched in the vertical direction to make a fountain. After the launch of atoms in fountain, the interferometric measurements are done by two-photon Raman excitation of ^{87}Rb atoms from hyperfine state F=2 to hyperfine state F=1 in the ground state. It is a Doppler sensitive technique that can sense the changing speed of atoms due to deceleration of *g.* When atoms are moving under influence of gravity *g,* and atoms undergo to a Raman pulse sequence of π/2-*T*-π-*T*-π/2, the population in F=2 after the pulse sequence is given as,

$$P_{|F=2\rangle} = \frac{1}{2}\left[1+\cos\left(\Delta\phi\right)\right]$$

where, $\Delta\phi = k_{eff}gT^2 - 2\pi\alpha T^2$ is net phase in the interferometer, with $k_{eff} \sim 2k$ as the effective wave-vector magnitude of two Raman beams, k is wave vector magnitude of each beam, T is separation between Raman pulses, and α is frequency chirp rate applied to Raman beam for compensating the changing Doppler shift due to gravitational acceleration.

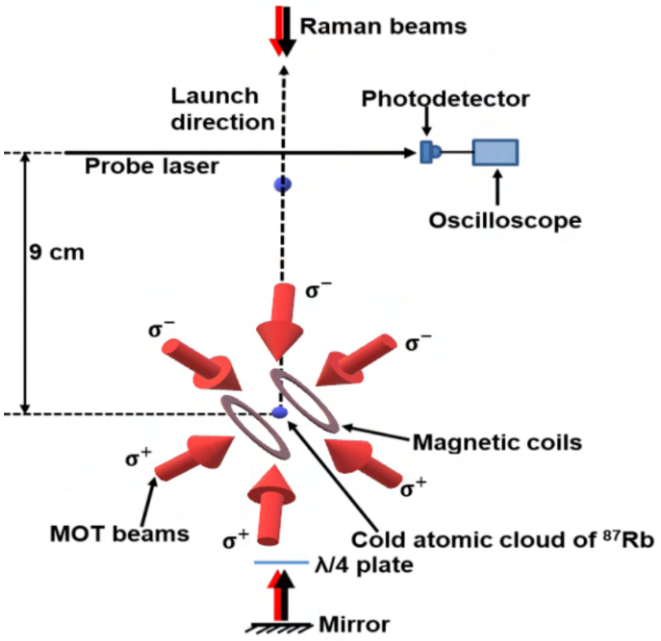

Fig. L.1.2. Schematic of cold atom gravimeter at RRCAT. Upper circle and dotted arrow shows launched cloud in upward direction.

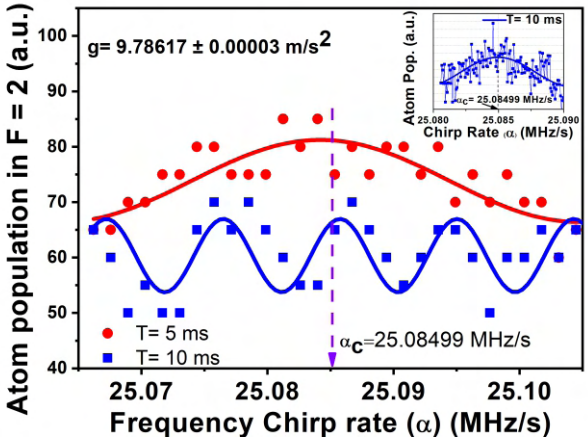

Fig. L.1.3: Interferometric fringes for different values of T.

Fig. L.1.3 shows the measured oscillations, i.e., interferometric fringes in the population in state F=2 with chirp rate α. By measuring the chirp rate for common peak to all values of *T,* we can measure the central chirp rate α_c, for which $\Delta\phi$=0 and g=πα_c/k. We measured α_c = 25.08499±0.000069 MHz/s, which gives the value of g as 9.78617±0.00003 m/s^2. The work is in progress to further improve the accuracy of the gravimeter.

The electronics and control support was provided by Laser Controls & Instrumentation Division, RRCAT.

Reported by:
S. R. Mishra (srm@rrcat.gov.in)

L.2: Setting up a Nitride Molecular Beam Epitaxy facility

Gallium nitride and its alloys with Aluminium and Indium are important due to their numerous applications in light emitters and detectors. Compared to Silicon and GaAs-based devices, GaN-based devices are more radiation tolerant owing to their wider bandgap. It makes GaN-based materials an attractive candidate for applications in high radiation environments like nuclear reactors, particle accelerators, and spacecraft. Keeping this in mind, a Nitride Molecular Beam Epitaxy (MBE) facility has been set up at RRCAT. The system can be used to grow high crystalline quality layers of nitride materials e.g., GaN, AlGaN, InGaN, InAlN, and their quaternary alloys with high compositional/thickness uniformity. It has a triple chamber configuration, and the sample is transferred across the three chambers under ultra-high vacuum conditions with the help of a magnetic transfer rod as shown in Figure L.2.1.

The system was recently commissioned, where an ultimate vacuum of $1x10^{-11}$ ($2x10^{-10}$) Torr was achieved in the growth (buffer) chamber. MBE Growth of GaN epitaxial layer (3923000) and GaN/AlGaN multi-quantum well (3923001) was carried out and the pictures of two samples are shown in the inset of Figure L.2.1.

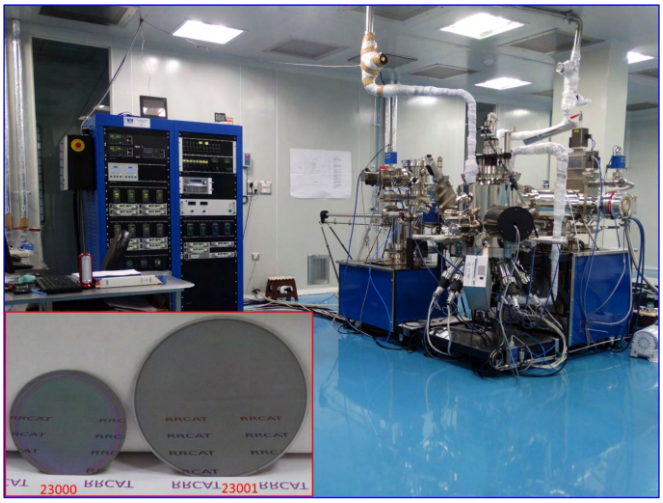

Fig. L.2.1: Photograph of a Nitride MBE facility at RRCAT, inset shows the image of GaN (2" dia.) and GaN/AlGaN multi-quantum well (3"dia.) samples.

The nitride MBE facility has been in regular use since its commissioning where several GaN epitaxial layers are grown on Sapphire under different conditions. In order to reduce the dislocations density, ~30 nm thick AlN buffer layer is first grown subsequent to the nitridation of the substrate. MBE growth conditions like growth temperature, III/V flux ratio, growth rate, buffer layer thickness, etc. are currently being optimized. It is also known that the density of dislocations reduces with the thickness of GaN layer. In view of this layer, thickness of GaN epitaxial layers is also varied. Photoluminescence (PL) spectrum of a GaN sample with 6.7 μm thickness is shown in Figure L.2.2. An intense PL peak at 363 nm with a narrow full width at half maximum (FWHM) is clearly seen. Further, defect feature, which is seen in the visible range is considerably suppressed indicating a low density of defects in the layer. HRXRD pattern of the same sample is shown in the inset of Fig. L.2.2, where a FWHM of ~350 arcsec is observed. It confirms a good crystalline quality of the GaN layer grown by MBE.

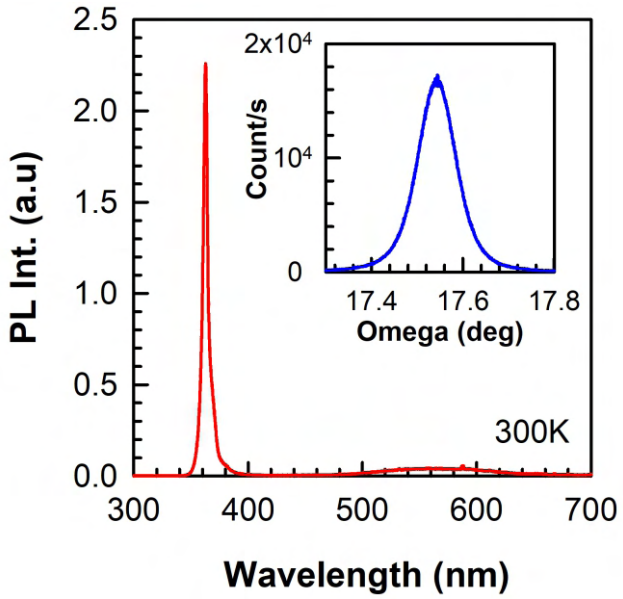

Fig. L.2.2: PL spectrum of 6.7 μm thick GaN layer, inset shows HRXRD pattern of the same sample.

Another important characteristic of the MBE facility is associated with the uniformity of grown layer. GaN epilayer (6.7 μm thick) was grown under optimized conditions and a plot of thickness non-uniformity across full 3" diameter wafer is shown in Fig. L.2.3. It is seen that the thickness non-uniformity lies below ±1%, which confirms an excellent control on the MBE growth process.

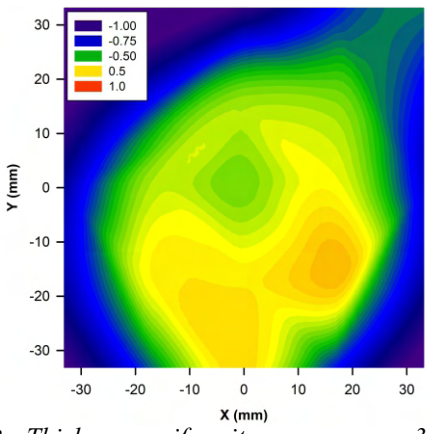

Fig. L.2.3: Thickness uniformity map across 3" diameter GaN/Sapphire sample grown by MBE.

Reported by:
T. K. Sharma (tarun@rrcat.gov.in)

L.3: Setting up a low-temperature Fourier transform infrared spectroscopy system

Fourier Transform Infrared (FTIR) spectroscopy is a widely used characterization tool in various fields such as material science, pharmaceuticals, biology, and geology. It has a high signal-to-noise ratio and faster data acquisition capability, which makes it suitable for characterizing semiconductor material systems whose optical/vibrational transitions lie in the infrared (IR) region. However, the FTIR signal becomes quite sensitive to thermal variations in the IR range. To obtain a high signal-to-noise ratio by minimizing thermal broadening, a low-temperature FTIR is required, especially for narrow energy bandgap material systems. Keeping this in mind, a low temperature Fourier transform infrared spectroscopy system has been setup at RRCAT. In this setup, a low-vibrational table is designed to mount the closed cycle refrigerator (CCR) with 1-dimensional/linear axis motion, as shown in Figure L.3.1. Other components, such as the CCR, turbo-molecular pump (TMP) station, temperature controller, and water chiller are suitably located to vary the sample temperature from 8 to 325 K.

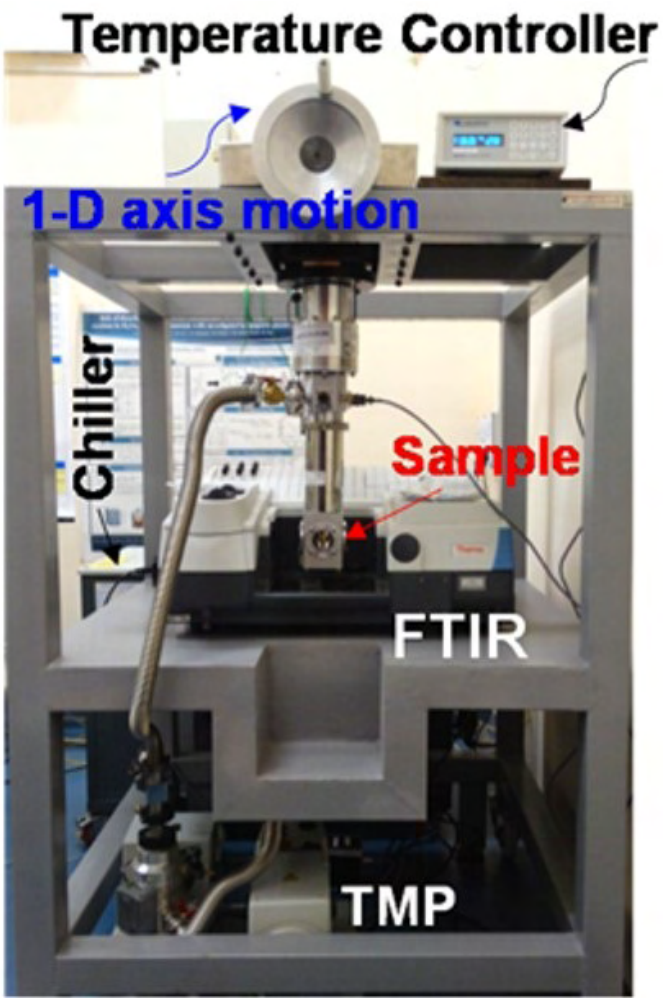

Fig. L.3.1: Photograph of the setup for low temperature FTIR measurements.

Among the group III-V semiconductors, Indium arsenide (InAs) is the most suitable material for electronic, photonic, and quantum computation applications. This is due to its small electron-effective mass (~$0.023m_0$), making it an ideal choice for high electron mobility transistor devices. Additionally, InAs is a low energy band gap direct semiconductor, which makes it the most promising material for photonic devices operating in the mid-IR region. The large electron Lande *g*-factor value (g_e ~ -15) makes it an ideal platform for integrating InAs on Si for long-term quantum-secured qubit-based quantum computing applications.

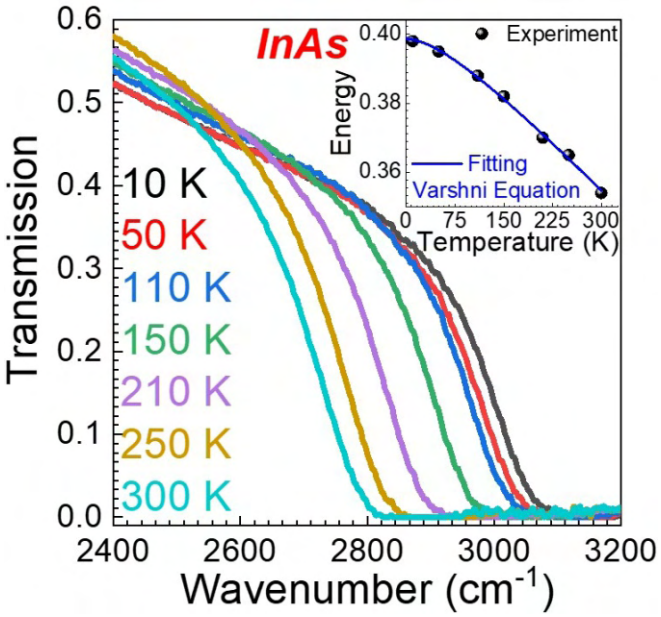

Fig. L.3.2: Temperature-dependent FTIR spectra of InAs semiconductor. The inset shows the fitting of the experimental energy bandgap data measured at different temperatures.

The band gap of InAs bulk is measured at different temperatures using the FTIR setup shown in Figure L.3.2. A sharp transition in the transmission spectra is associated with the valance band to conduction band electronic transition feature of the InAs semiconductor. The inset of the figure shows the energy band gap variation with temperature, where the Varshni equation $\left[E_g(T) = E_g(0) - \frac{\alpha T^2}{\beta + T}\right]$ is used to fit the experimental data points. The extracted values of $E_g(0)$, which is the energy band gap value of InAs at zero kelvin, is around 0.4 eV. The parameters $\alpha \sim 2\times10^{-4}$ eVK^{-1} and $\beta \sim 105$ K correspond to the entropy and Debye temperature associated with the InAs material system, respectively. The experimentally obtained values are found very close to the theoretically estimated values. Therefore, this facility can be used to characterize any semiconductor material system whose electronic/vibrational transitions occur in the IR region. Its temperature variation capability with very low vibrations at the IR region is of utmost importance. Further work is in progress to measure electronic/vibrational transitions from semiconductor quantum structures at low temperature.

Reported by:
Geetanjali Vashisht (geetanjali@rrcat.gov.in)

L.4: Development of high energy nanosecond acousto-optic Q-switched Yb-doped fiber laser

High energy and short pulse fiber lasers are attractive for many applications such as marking, cleaning, decontamination, nonlinear frequency conversion, range finding, remote sensing, medical, and industrial processing. Compact nanosecond duration fiber lasers with pulse energy of a few millijoules are preferred for such applications. Yb-doped fiber lasers in master-oscillator power-amplifier (MOPA) configuration can deliver pulse energy in the range of a few millijoules to hundreds of millijoule. In such configurations, one or more power amplifier stages separated by optical isolators are used to amplify the low-energy pulses derived from master oscillator. In this direction, a 3.3 mJ pulse energy and 100 W average power acousto-optic (AO) Q-switched Yb-doped fiber laser operating at 1064 nm has been developed.

Figure L.4.1 shows the schematic of the experimental set-up of 100 W average power AO Q-switched fiber laser, which consists of three stages. The first stage is an oscillator, which contains an acousto-optic Q-switch for loss modulation in the resonator to generate Q-switched pulses and this stage works as a seed source for the next stage. The second and third stages are amplifier stages, which amplify the signal pulse from the seed source. Oscillator stage consists of a 2.5 m long octagonal inner clad Yb-doped fiber (YDF) as the gain medium having a core/inner clad diameter of 15/125 µm with NAs of 0.075/0.46, respectively. Two 10 W fiber pig-tailed diode lasers at 976 nm with fiber core/clad diameter of 100/125 µm and NA of 0.22 have been used to pump Yb-doped fiber. For pumping of YDF, a multimode pump combiner has been used, which has two pump input ports, one input signal port, and one output port. Two fiber Bragg gratings (FBG), one having 99.8% reflectivity and another having 10% reflectivity at the center wavelength of 1064 nm have been used to form the linear cavity for master oscillator. At the output port of the pump combiner, YDF has been spliced, which is further spliced with a compatible fiber optic AOM. The 10% OC FBG has been spliced with the output end of the AOM. The pulse repetition rate of this AO Q-switched oscillator has been controlled using a 20 MHz signal generator, which modulates the radio frequency applied on the AO Q-switch. From the oscillator stage, 1 W of average power at 30 kHz of repetition rate with 175 ns pulse duration was achieved, which was fed to the first amplifier stage. In order to separate the oscillator stage/seed source from the amplifier stages, polarization insensitive in-line isolators have also been spliced in series to prevent any backward propagating signal causing any damage to the other fiber components in the oscillator stage. For the pumping of 1st amplifier stage, 10 W fiber coupled laser diodes at 915 nm were used. Such six pump diodes of the same power were spliced with pump input ports of (6+1)x1 pump combiner. The output of the pump combiner was then spliced with another 4 m long YDF. This fiber has a core/inner clad diameter of 20/125 µm with NAs of 0.075/0.46, respectively. From this stage, an average output power of 16 W was achieved. Further, the output signal was fed to the second amplifier stage. For the pumping of second amplifier stage, fiber coupled laser diodes at 975 nm having a maximum of 70 W of CW output power have been used. Such three pump diodes of the same power were spliced with three pump input ports of (6+1)x1 pump combiner. The output of the pump combiner was then spliced with another 1.5 m long YDF having a core/inner clad diameter of 48/400 µm with NAs of 0.075/0.46, respectively. At a repetition rate of 30 kHz, an average output power of 100 W, 3.3 mJ of pulse energy with 175 ns pulse duration and an optical to optical conversion efficiency of 54% was achieved. This resulted in a peak power of ~ 19 kW. Figure L.4.2 shows an oscilloscope trace of the laser pulse at the maximum average output power of 100 W. Output spectrum is peaked at 1064 nm with a FWHM linewidth of 1.5 nm. Due to larger core size of gain fiber in the 2nd amplifier stage, output is multi-moded. This laser is being engineered for cleaning and decontamination applications.

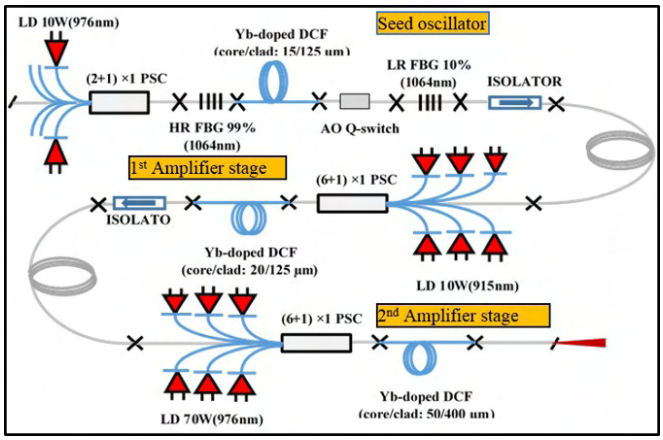

Fig. L.4.1: Schematic of 100 W average power AO Q-switched fiber laser.

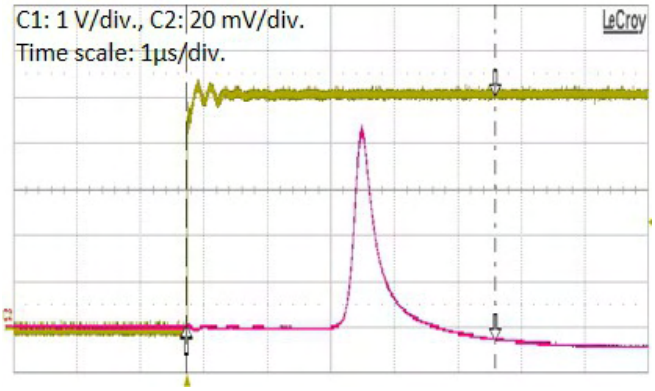

Fig. L.4.2: Oscilloscope trace of laser output pulse at 100 W of average output power (laser pulse (pink), modulation signal (green)).

Reported by:
B. N. Upadhyaya (bnand@rrcat. gov.in)

L.5: Development of ultrafast Mamyshev fiber oscillator

During the last two decades, ultrafast fiber oscillator has evolved from all-anomalous dispersion configuration generating soliton-like pulses to all normal dispersion (ANDi) configuration generating dissipative soliton (DS) pulses in a quest to scale-up the pulse energy directly from the oscillator with ultrashort duration. However, even in ANDi configuration pules energy is limited to 10s of nJ and pulses exhibit significant side-lobes after compression in external grating pair. In recent time, there is a considerable interest in fiber Mamyshev oscillator (MO), which can potentially overcome the challenges involved in ANDi configuration. In its simplest form MO consists of two gain media and two offset band pass filters (BPFs) of appropriate bandwidths, which are spectrally blind to each other. In fiber MO, the gain media and the BPFs are arranged alternately in a linear or ring cavity configuration. Depending on the offset between filters, a strong modulation depth of the saturable absorber can be obtained by strong self-phase modulation (SPM) induced self-amplitude modulation. The major difficulty in fiber MO setup is the self-starting of mode-locking from noise due to the presence of offset filters, which inhibits CW lasing. Hence, an external seed source is usually injected in fiber MO to initiate the mode-locking process. The seed source is then blocked after realizing the stable mode-locked operation in MO and the oscillator continues to operate steadily.

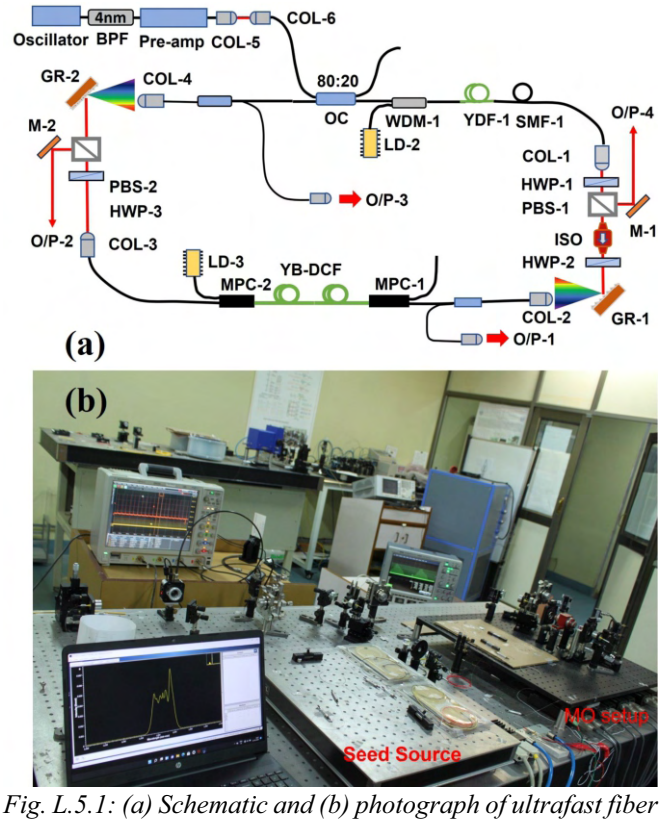

Fig. L.5.1: (a) Schematic and (b) photograph of ultrafast fiber Mamyshev oscillator setup.

Recently, we have constructed ultrafast fiber MO setup driven by conventional mode-locked laser in ANDi configuration as shown schematically in Figure L.5.1(a). The MO consists of two gain media (YDF-1 and Yb-DCF) and two tunable offset band pass filters (BPF1 and BPF2) made using the combination of diffraction gratings (GR1 and GR2) and in-fiber collimators (Col-2 and Col-4), respectively. Both BPF1 and BPF2 have a transmission bandwidth of ~2 nm, and the separation of the peak transmission wavelength of the filters is adjusted to ~5 nm, so that their combination acts like an ideal saturable absorber based on SPM induced strong self-amplitude modulation. Due to the presence of spectrally blind filters, the MO is not self-starting and pulses (5 ps, 40 MHz) from a specially designed seed source in ANDi configuration is injected to MO via an optical coupler (OC) to drive the MO as shown in the schematic. With appropriate pumping levels in the gain fibers in MO, the injected pulses drive the MO in mode-locking state and it remains in the mode-locking state even after blocking of seed pulses from injecting to MO (Fig. L.5.2(b)).

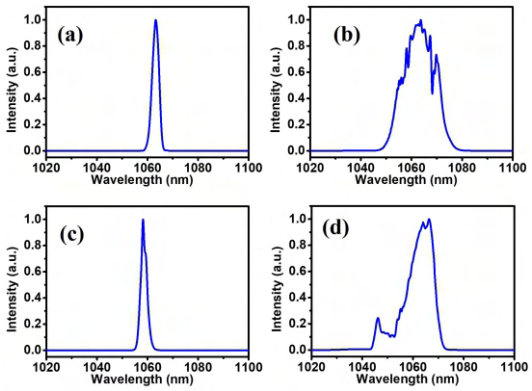

Fig. L.5.2: Recorded spectra at various locations of fiber MO (a) O/P-1, (b) O/P-2, (c) O/P-3, and (d) O/P-4.

The pulses from MO are highly stable (SNR~65 dB) with a repetition rate of 9.6 MHz. To study the spectral shaping dynamics in MO, the pulse spectra are recorded at several locations in the setup and are shown in Figure L.5.2. It can be seen that just after the BPF1 (O/P-1), the spectra is narrow with spectral bandwidth (FWHM) of ~3.2 nm and peak centred at 1063.2 nm. The spectrum broadens considerably to ~16.7 nm (O/P-2, Fig. L.5.2(b)) as it propagates through the fiber due to SPM, while the central wavelength is maintained at ~1063.2 nm. The BPF-2 again reduces the spectral width to ~2.6 nm (O/P-3, Fig. L.5.2(c)), but with peak at ~1058.3 nm clearly indicating the filter offset. The spectrum again broadens to ~11 nm (O/P-4, Fig. L.5.2(d)) as it propagates through the fiber before it is shortened again at BPF1. From O/P-4 around 112 mW of average power is obtained corresponding to pulse energy of ~12 nJ signifying the energy scalability feature of MO. The pulses from the MO are highly chirped with a measured duration of 9.53 ps and was compressed to ~200 fs duration with a clean smooth profile using a grating pair. Further work is in progress to scale-up the pulse energy from the setup.

Reported by:
P. K. Mukhopadhyay (pkm@rrcat.gov.in)

L.6: Nonlocal probing of amplitude mode dynamics in $EuTe_4$ using time-resolved X-ray diffraction

$EuTe_4$ is a quasi-two-dimensional metallic compound that shows semiconducting behaviour (~ 0.2 eV bandgap) in the charge-density-wave (CDW) state. In the CDW state below T_{CDW} ~726 K, amplitude mode emerges from the collective excitation of frozen lattice distortions. Here, we present the nonlocal probing of amplitude mode dynamics far beyond the optically excited depth of ~150 nm in the CDW state of ~10 μm thick single-crystal $EuTe_4$ using time-resolved X-ray diffraction (TXRD) in the transmission geometry. 'Nonlocal' refers to the effect of laser pumping propagation far beyond the photoexcited region.

The experiment was performed using a 1 kHz, 50 fs, ~ 5.7 mJ Ti:sapphire laser system. A beam splitter reflects ~10% energy, which acts as a pump pulse to excite the sample. The remaining (90%) beam was focused on a moving Cu wire target to create ultra-short laser plasma copper K_α X-ray source, which acts as a probe pulse. These X-rays were focused on the sample (spot size ~ 330 μm) using a polycapillary lens. Both the pump and probe pulses collinearly overlap at the sample. The $EuTe_4$ sample was a single crystal of dimension ~ 0.7 mm (W) × 1.0 mm (H) × 10 μm (T). A combination of a DRZ phosphor screen and an EMCCD camera was used to detect the XRD from $EuTe_4$ sample in transmission geometry. The TXRD pattern of $\boldsymbol{Q}_{CDW}$ = (2,2,0)−$\boldsymbol{q}_{CDW}$ peak ($\boldsymbol{q}_{CDW}$ = (0,0.643,0) r.l.u.) was recorded with 300 fs temporal resolution, which is limited by the pulse duration of the probe. To detect low-intensity signals of CDW peak, the path between the X-ray source and DRZ phosphor was shielded by a 30 mm thick lead sheet. A small shift in the diffracted angle of the (2,0,0) Bragg peak due to heat deposition by the pump beam was detected by an X-ray CCD.

Figure L.6.1(a) shows the underdamped oscillations of the CDW peak intensity for 2 mJ/cm^2 fluence. The oscillations in the CDW peak intensity are fitted with the dominant frequency (black line), corresponding to the peak observed in a Fast Fourier Transform (FFT) of the data (Fig. L.6.1(b)). The observed oscillations are found to occur at the amplitude mode frequency. Figure L.6.1(c) shows the decrease in oscillation frequency with increasing excitation fluence, which is rationalized by sample heating by comparing with polarized Raman scattering measurements performed at different temperatures. The temperature rise on laser excitation is measured from the peak shift of (2,0,0) Bragg peak, as shown in Figure L.6.1(d). The constant peak shift after the first delay point indicates the rise in the equilibrium sample temperature. The underdamped oscillation amplitude is at odds with the observed overdamped nature of the amplitude mode measured using meV resolution inelastic X-ray scattering and polarized Raman scattering.

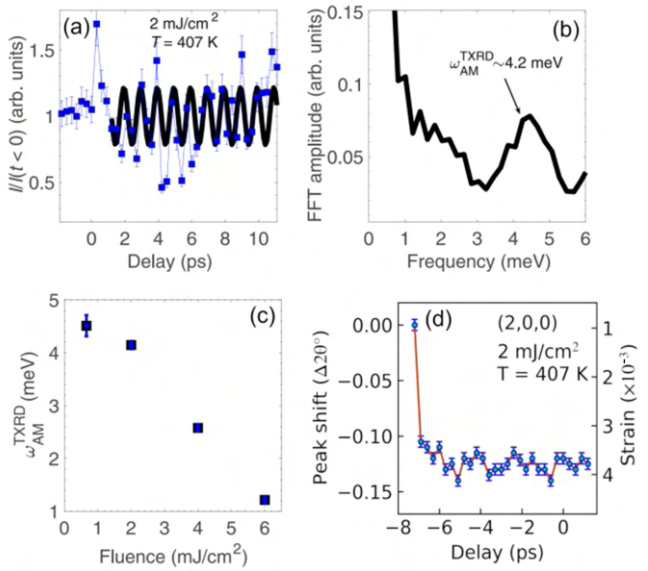

Fig. L.6.1: (a) TXRD intensity (I/I(t<0)) at $\boldsymbol{Q}_{CDW}$ (blue square markers) for 2 mJ/cm^2 fluence. The solid black line shows the fit with the dominant oscillation frequency, (b) FFT amplitude versus frequency of intensity reported in (a), (c) variation in oscillation frequency with excitation fluence, and (d) peak shift (strain) of the (2,0,0) Bragg peak as a function of delay for 2 mJ/cm^2 fluence. The rise in the equilibrium sample temperature is indicated in the panel.

We propose the nonlocal behaviour and underdamped nature of the oscillation amplitude are possibly due to the generation of either of the two quasi-particles, viz., phonon-polariton or exciton-polariton, which propagates with light-like speed beyond the optically excited depth. The observations cannot conclusively confirm or rule out one, but it is proposed that the measured oscillations are likely from propagating phonon-polariton.

In conclusion, the observed nonlocal behaviour and underdamped oscillations in the TXRD signal of the CDW peak can be rationalized by coupling of the polar amplitude mode with incident IR photons to form a phonon-polariton quasiparticle. The decrease in oscillation frequency with increasing excitation fluence is rationalized by the sample heating. The observed nonlocal behaviour of amplitude mode provides an opportunity to engineer material properties at a significantly faster time scale with optical pulses. For more details, please refer to: *R. Rathore, H. Singhal, V. Dwij*, M. K. Gupta*, A. Pathak*, J. A. Chakera, R. Mittal*, A. P. Roy*, A. Babu*, R. Kulkarni*, A. Thamizhavel*, A. H. Said*, and D. Bansal*, Ultrafast Science - A Science Partner Journal (AAAS), 3, 041 (2023).*

Reported by:
R. Rathore (ranjana@rrcat.gov.in)

L.7: Development of a microscopic mechanical exfoliation setup for monolayer preparation of 2-D materials

Monolayers of two-dimensional (2D) semiconductors are potential candidates for optoelectronic and flexible devices. Two-dimensional semiconductor materials such as molybdenum disulfide (MoS_2) are van der Waals materials that are strongly bonded in two dimensions and are weakly bound in the third dimension. Due to this weak bonding in the third dimension, it is possible to prepare monolayers and a few layers of these materials. It actually transforms from indirect to direct bandgap when it is reduced to single layer. Such direct bandgap monolayer 2D materials have high carrier mobility, broadband optical absorption, and a large surface area, resulting in strong light-matter interaction. These materials make an attractive system for fundamental physics studies and optoelectronic applications.

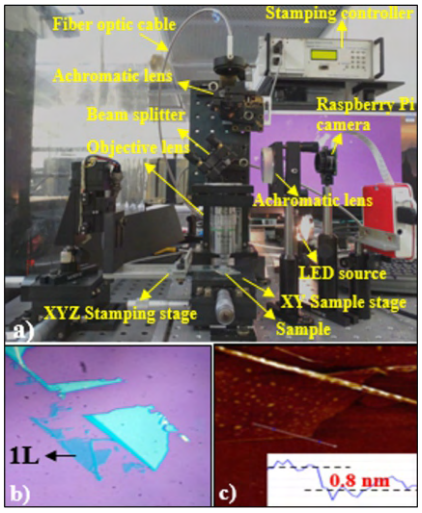

Fig. L.7.1: (a) An in-house developed microscope along with stamping mechanism to prepare monolayer, (b) optical microscope image of prepared monolayer, and (c) the AFM measurement on the prepared monolayer.

One of the critical challenges in harnessing the potential of monolayer MoS_2 lies in its synthesis and fabrication. Various methodologies have been developed to produce monolayer MoS_2, with mechanical exfoliation standing out as a technique that allows for the creation of high-quality, atomically thin layers. Mechanical exfoliation along with PDMS-gel dry transfer stamping method is developed to prepare monolayer MoS_2. In-house built optical microscope along with stamping stage is used to transfer monolayer MoS_2 on SiO_2/Si substrate by identifying the optical contrast (Fig. L.7.1). AFM analysis confirmed the height of monolayer MoS_2 to be 0.8 nm. Raman analysis also showed distinct peaks at E_{2g}^{1} (383.7 cm^{-1}) and A_{1g} (403.9 cm^{-1}) modes and peak difference of 20.2 cm^{-1} confirms the pristine monolayer nature of MoS_2 flake (Fig. L.7.2).

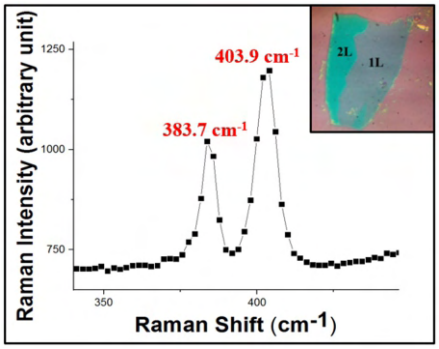

Fig. L.7.2: Raman measurement on large sized MoS_2 monolayer prepared by gold assisted mechanical exfoliation, inset shows the optical image of the sample.

For preparing much larger size flakes, gold assisted exfoliation is also performed. Gold-assisted exfoliation is an effective method to produce large-area monolayers, since sulphur is said to have a very strong affinity for gold. The exfoliated MoS_2 flakes is stacked with 150 nm gold. Thermal release tape (TRT) is pressed onto Au/MoS_2 stack and transferred onto SiO_2/Si substrate. TRT is released by heating at 90 °C and gold is etched away. This resulted in a few hundred microns in the size of the MoS_2 monolayer.

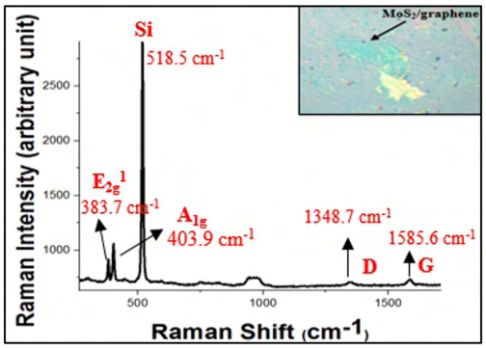

Fig. L.7.3: Raman measurement on MoS_2/graphene monolayer heterostructure prepared using stamping process. The inset shows the optical image of the sample.

Further, MoS_2/graphene heterostructure was prepared using stamping process. Commercial graphene monolayer on copper substrate was transferred to SiO_2/Si substrate and mechanically exfoliated monolayer of MoS_2 identified by optical contrast on PDMS-gel was stamped on top of Graphene monolayer on SiO_2/Si substrate. Raman analysis confirmed the presence of monolayer MoS_2 at E_{2g}^{1} (383.7 cm^{-1}) and A_{1g} (403.9 cm^{-1}). Graphene peaks were also seen at *D* (1348.7 cm^{-1}) and *G* bands (1585.6 cm^{-1}) (Fig. L.7.3). The observed broadening and enhanced defect states in the MoS_2/graphene heterostructure provided compelling evidence of interaction between the MoS_2 and graphene, which alters its optical and electronic properties.

Reported by:
Salahuddin Khan (skhan@rrcat.gov.in)

I.1: Commissioning of "e-Office" setup at RRCAT

DAE has mandated usage of "e-Office" solution for efficient collaboration among various stake holders in units of DAE. To comply with the mandate, "e-Office-Lite", "A Digital Work Place Solution" software system developed by National Informatics Center (NIC), India has been commissioned.

The complete "e-Office" suite comprises of six modules namely: EFILE, MIS, PIMS, MDM, KMS and WAW portal, catering to various requirements of e-governance. In the first phase necessary setup for enabling "eFile lite" module has been commissioned. "eFile lite" is a workflow-based system that extends the features of existing manual handling of files in addition to more efficient electronic system.

The system comprises of different sub-modules that are interlinked to manage official workflow of entire life cycle of a document/DAK from the moment it is received by the organization till the time it is disposed off with proper set of actions. It involves all stages of working in a file, including the scanning, electronic diarization, file creation, noting creation, digital signing on noting and drafts, dispatch, faster processing and movement of files and receipts, closing of files and receipts, and finally archival of records.

The need for 24 x 7 operation of "e-Office" solution necessitated setup to be commissioned in disaster recovery (DR) mode. To facilitate DR mode operations, two set of servers have been commissioned at Data Center Hall in IT-Building-A (DCH-A) and one server has been commissioned at Data Center Hall in IT-Building-B (DCH-B). Figure I.1.1 shows the logical layout of the complete setup of "e-Office".

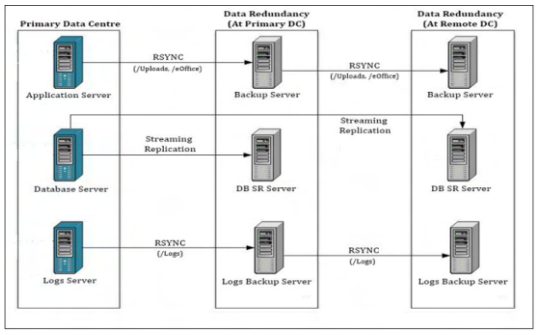

Fig. I.1.1: Logical layout of redundant setup of e-Office servers at DCH-A and DCH-B.

Complete setup of the "e-Office" solution comprises of three physical servers with virtualization of different services running on each server. Each server has 2.4 GHz processor with 12 cores, 128 GB RAM, 1 TB solid state drive (SSD), 12 TB hard disk drive (HDD), 2x10 Gbps, 2x1 Gbps network connectivity. Two numbers of 960 GB SSD have been configured in level 1 of redundant array of inexpensive disks (RAID-1) and six numbers of 2.2 TB HDD have been configured in RAID-5. Actual photograph of the setup in DCH-A is shown in Figure I.1.2.

Fig. I.1.2: Photograph of e-Office servers commissioned in DCH-A.

For effective collaboration, the "e-Office" solution has been integrated successfully with the existing software services at RRCAT like centralized lightweight directory access protocol (LDAP) authentication, email, short messaging service (SMS), digital signatures, etc., which are developed and operated by RRCAT, as shown in Figure I.1.3.

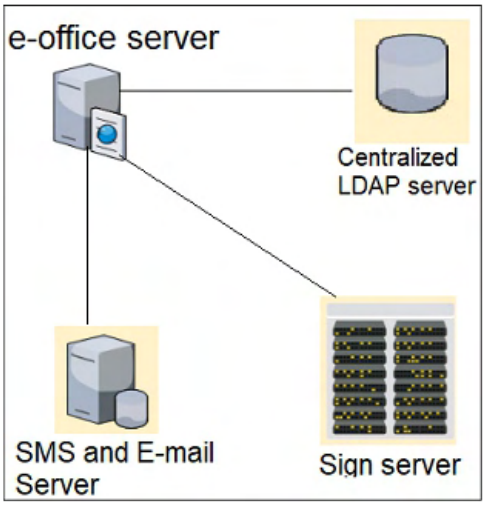

Fig. I.1.2: Block diagram showing integration of e-office with various software services of RRCAT.

Commissioning of e-Office setup at RRCAT will help in achieving simplified, responsive, effective and transparent working in various departments of the organization. Contributions of NIC officials and colleagues from other divisions of RRCAT who have worked along with Computer Division in commissioning of the e-Office setup at RRCAT are acknowledged.

Reported by:
Alpana Rajan (alpana@rrcat.gov.in)

I.2: Development of electrical feedthroughs

Non-magnetic, ultra-high vacuum (UHV) compatible and special purpose electrical feedthroughs are required for transmission of electric current into or out of a vacuum chamber. Three different types of feedthroughs have been developed to serve specific purposes:

1. Electrical feedthrough with alumina as insulator: The developed feedthrough has molybdenum conductor, alumina insulator and SS316L CF flange for mounting. Niobium has been chosen as the interface metal with alumina due to its proximity of its expansion coefficient with that of alumina, non-magnetic nature, low Young's modulus and low yield strength. Use of active braze filler metal with niobium interface metal has successfully eliminated the need of metallized ceramic. The brazing process has been done under high vacuum environment, copper silver active braze alloy (CuSIL-ABA) has been used as braze filler metal (BFM) between alumina and niobium as well as between niobium and molybdenum. Copper-silver eutectic has been used as BFM between nickel coated SS316L and niobium. The design incorporates flexible geometrical features to accommodate the stress due to large differential thermal expansion of niobium and SS316L, as shown in Figure I.2.1. The feedthrough has been successfully qualified for its electrical connectivity and ultra-high vacuum performance

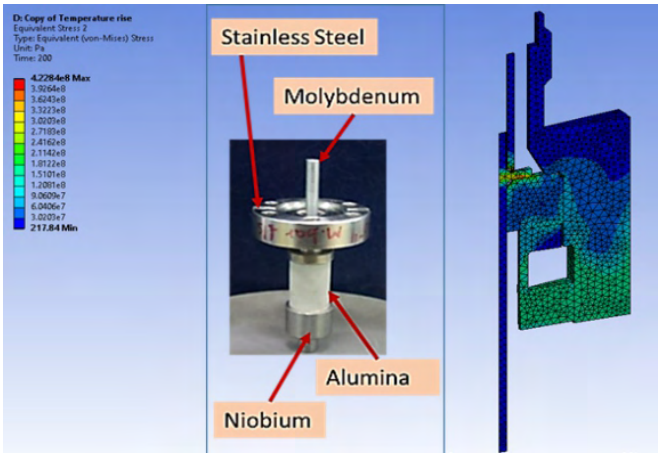

Fig. I.2.1: Electrical feedthrough with alumina as insulator (FEA for compliance feature optimization)

2. Sub miniature version A (SMA) feedthrough with alumina as insulator: A prototype SMA feedthrough for 50 Ω coaxial structures, incorporating two numbers of ceramic to metal joints, has been developed using the aforementioned design philosophy as shown in Figure I.2.2. Compliance feature for stress free joining, single brazing cycle with precisely calculated amount of active precious braze filler metal to avoid short-circuiting are the key highlights of the development. Electrical continuity test has been carried out and it does not show any short path in its coaxial structure. To verify its UHV compatibility, SMA feedthrough was baked up to 150^{0}C for 48 hours (five thermal cycles), and then cooled down to the room temperature followed by helium leak testing. No leak was detected up to a helium background of 1.2x10^{-10} mbar.l/s. The residual gas analyser (RGA) spectrum was also found satisfactory.

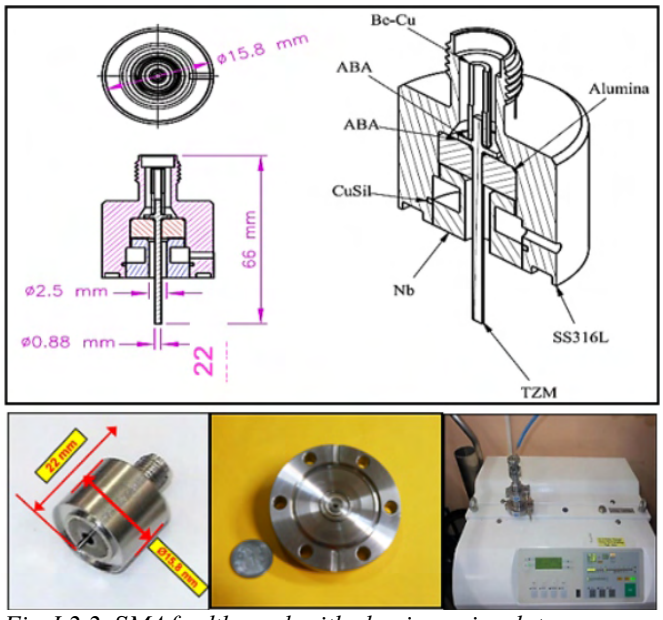

Fig. I.2.2: SMA feedthrough with alumina as insulator.

3. Electrical feedthrough with modified polytetrafluroethylene (PTFE) as insulator: A hermetically sealed modified PTFE insulator-based vacuum feedthrough has also been developed as shown in Figure I.2.3. The feedthrough has three main components namely: nickel-coated copper conductor, SS316L flange, and modified PTFE insulator. Push fit creep resistant joints have been deployed for assembling the components. The design offers low cost and customizable solution that is also suitable for swift production cycles. No leak was detected up to a helium background of 1.2x10^{-10} mbar.l/s.

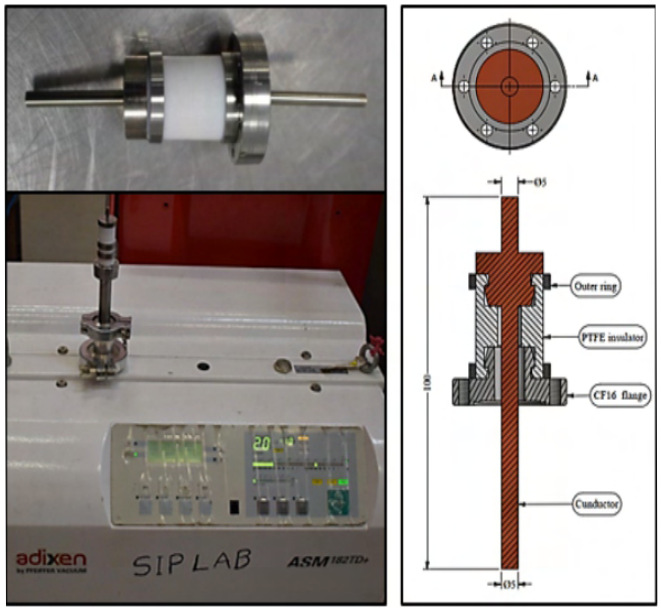

Fig. I.2.3: Feedthrough with modified PTFE as insulator.

Reported by:
Abhay Kumar (abhay@rrcat.gov.in)

T.1: Recent advances in materials joining at RRCAT

P. Ganesh[1*], A. P. Singh[2], A. Bhardwaj[2], Saranjeet Singh[2], Abhay Kumar[2] and Rakesh Kaul[1]
[1]*Laser Materials Processing Division*
[2]*Design & Manufacturing Technology Division*
[*]*Email: ganesh@rrcat.gov.in*

Abstract:
Materials joining is an ever emerging field to cater the specific needs of growing industry. Well established joining processes like fusion welding, diffusion bonding, tungsten inert gas brazing, etc. are continuously evolving with certain modifications in the form of fixturing and process modifications to tailor the weld metal properties compatible to various applications including low-magnetic-permeability, use in ultra-high vacuum applications, dissimilar joints, etc. The ease of implementation of new techniques at the shop floor and the economic aspect play an important role in acceptance of the new methodologies in the industry. The techniques developed at RRCAT Include new joint design, use of passive fixtures, minor modifications to existing welding and joining practices followed in the shop floor and have strong potential for deployment in industry. Present article summarizes the recent developments related to materials joining in the authors's lab, which essentially address the requirements of ongoing and future requirements related to particle accelerators at RRCAT.

1. Introduction

Construction of particle accelerators involve use of various types of materials for their specific properties. These materials must be joined to their conventional counterparts such as austenitic stainless steels to build the ultra-high vacuum (UHV) envelope. Joining of austenitic stainless steels also pose some very specific type of challenges from the perspective of particle accelerators. Other similar material joining challenges involve active metals like titanium, niobium, aluminium and their alloys due to the requirement of specified hygiene levels and environmental specification of cleanliness and humidity. These challenges must be met in order to build products that are compatible with general requirement of UHV and specific requirements coming from particle accelerator side.

Relative magnetic permeability (μ_r) is an important factor governing the choice of material for construction of vacuum chambers for particle accelerators; particularly those components that are either enclosed inside magnets or are placed in the vicinity of magnets. Austenitic stainless steel AISI 316L SS is a strong candidate for construction material of such vacuum chambers due to low values of μ_r (<1.05), ease of fabrication, ease of availability and competitive pricing. It is also a candidate for construction of helium vessels of superconducting radiofrequency (SRF) cavities for high-energy, high-power particle accelerators due to the possibility of meeting the requirements of ASME B&PV Code Section VIII Division-1 for operation at 2 K temperature [1]. There are challenges in joining of austenitic stainless steels as welding must produce ferromagnetic delta-ferrite phase to avoid deleterious phenomenon of hot cracking and micro-fissuring. The ferromagnetic phase can attract the magnetic lines of forces while in operation and distort the charged particle's trajectory. This article presents the results of an experimental study, which attempted to limit the μ_r of weld metal to that of the base metal by introducing nitrogen-argon binary shield gas during gas tungsten arc welding (GTAW) of AISI 316L SS using bare ER 316L stainless steel filler metal [2]. An indigenous binary gas mixing system has been developed at RRCAT for reliable and economical deployment of the technology at particle accelerator laboratories.

Nitrogen-argon mixed shield gas requires two adaptations in the existing GTAW process usually deployed for GTAW of AISI 316L SS as nitrogen is a noble gas but not inert. The first one is to use gases of 5N purity and second one is to use gas lens system in the welding torch to avoid intermixing of environmental air with the shield gas flow. Gas lens system efficiently prevents the ingress of air into the stream of shield gas, which is due to Kelvin-Helmholtz instability at the interface of static air envelope and the shield gas. The instability is more pronounced in the turbulent flow regime as eddies formed at the interface lead to quick intermixing. The turbulence in shield gas due to Kelvin-Helmholtz instability can be delayed if the shield gas flow is maintained in laminar flow regime for longer distances [3]. The addition of gas lens improves the weld quality and reduces the gas consumption [4]. This article presents the results of studies carried out at author's laboratory involving use of gas lens and 5N purity shield gas.

Groundwork to build a mega-science project "Laser Interferometer Gravitational-Wave Observatory" – India (LIGO-India) is under progress as a part of the international network of gravitational wave observatories [5]. LIGO-India needs an 8 km long, ultra-high vacuum (UHV) compatible AISI 304L SS beam pipe. Each pipe is of 20 m length, 1239 mm outer diameter (OD), 3.2 mm thickness and straightness of 160 µm/m length. These non-standard precision pipes need to be manufactured specifically using an automated continuous spiral welding pipe mill. Single pass and full penetration Activated-TIG (A-TIG) welding appears to be more suitable in this case due to its ease of deployment, minimal edge preparation and low distortion [6-9]. The study reported here essentially focuses on evaluation of the A-TIG welds of AISI 304L SS for UHV compatibility, which is not explored in earlier reports of A-TIG welding. The activating flux containing a mixture of five metal oxides was obtained from IGCAR, Kalpakkam [6].

Aluminium alloys of 5000 and 6000 series are popular materials for vacuum chambers of particle accelerators due to their paramagnetic nature and excellent UHV compatibility.

The Indus-2 (RRCAT) synchrotron radiation source's vacuum chambers are entirely made of aluminium alloys [10,11]. However, majority of gauges, pumps and piping connected to vacuum chambers are made of stainless-steel (SS). This necessitates deployment of aluminium alloys to SS bimetallic transition joints. Other than vacuum chambers, aluminium alloys-to-SS transition joints are also required for stray electron absorbers for industrial linear accelerators, cryogenic heat exchangers and components of irradiation capsules in nuclear reactors [12,13]. Such joints also find a lot of application in other industries as well [14]. The Al-SS joints are required for a variety of in-house applications like vacuum chambers, beam scrapper assembly, cryogenic heat exchangers, cryo-module of superconducting radio frequency (SCRF) cavity, aluminium irradiation capsules, neutron sensitive ion chambers and ion chambers for environmental monitoring. Formation of brittle inter-metallic (IMC) phases at the weld interface during fusion welding of aluminium alloys and SS prohibits application of such processes [14-20]. Many of the friction welded aluminium alloy-to-SS transition joints of Indus-2 have failed after multiple baking cycles. In view of this, there is a need to develop an alternate way of joining aluminium alloys and SS. A study has been initiated at RRCAT to develop Al-SS joints through diffusion bonding, vacuum brazing and TIG brazing. The article presents some of the interesting results of these investigations.

Tantalum being a heavy metal (Z=73), is extensively deployed as an x-ray target material in electron beam based radiation processing facilities because of its refractoriness (T_m: ~3000 °C), excellent corrosion resistance, ductility and electrical and thermal conductivities. X-ray target assembly of Agricultural Radiation Processing Facility (ARPF) [21], requires dissimilar metal joining of 1.4 mm thick tantalum (Ta) sheet with an AISI 304L SS flange. Large difference in coefficient of thermal expansion (CTE) of materials being joined poses a problem in conventional vacuum brazing of 1.2 m long x-ray target component. Braze joining by using a TIG torch using a suitable filler without melting the parent materials is termed as TIG-brazing. TIG-Brazing due to localized heating and inherent control of heat input can be used as an alternate joining technique for a wide range of applications where normal braze joining or vacuum brazing methods fail due to large difference in CTE of materials being joined. An in-house study was undertaken with an objective of fabrication of x-ray target assembly of ARPF. The article presents the details of this study and successful demonstration of fabrication of first build (Ta-SS TIG braze joint) of the sub-size structure of x-ray target [22]. Exploring the use of titanium as a structural material for tantalum based x-ray target applications presents a promising solution. Open literature on joints of Ta with Grade-2 titanium reports tensile strength of 353 MPa. The metallurgical compatibility of both metals Ta and Ti with mutual solid solubility of *bcc* Ta in both forms of Ti (*hcp alpha* phase up to 882 °C as well as high temperature *bcc beta* phase) enables formation of a sound joint. Notably, CTE for titanium (9.9 µm/m.K) and tantalum (6.5 µm/m.K) exhibits tolerable disparity with respect to other combinations, resulting in reduced thermal stress in the resultant joints. Other methods of joining such as laser welding [23] and diffusion bonding [24] of tantalum to titanium have been reported with a tensile strength of about 260 MPa. However, certain limitations like joint fit-up requirements in laser welding, joint configuration in diffusion bonding and overall economic viability restrict their use. GTAW has a clear advantage over existing joining methods. The article presents the results of preliminary investigations of Ta-Ti joining using GTAW.

SCRF cavities will form important part of the upcoming high energy, high current proton accelerators. The high beta 650 MHz SCRF cavity would be enclosed in a cylindrical vessel to hold liquid helium (LHe). Titanium (Ti) is being considered as the material of construction of helium vessel. The LHe inlet supply line and return helium gas pipe line of the helium vessel would be made of AISI 316L SS. This requires a bi-metallic tubular transition joint between Ti and AISI 316L SS, operating at LHe temperature. Vacuum brazing and explosive welding are potential processes for joining these two dissimilar metals, as fusion welding leads to extensive cracking [25]. Explosive welded joint suffers from excessive shear stresses at the bond interface during subsequent fusion welding and cool down to 2 K temperature. The article presents the results of experimental study carried out at author's laboratory for vacuum brazing of Ti-pipe/316LSS flange with BVAg-8 braze filler metal (BFM) [26]. These joints remain under compression by design and have features that prohibit excessive heating during subsequent welding at both the ends.

Diffusion bonding, in spite of its many unique capabilities, has not been widely used for the joining process in fabrication of components due to high set-up cost, complex shape and size of the required joints for industrial applications [27]. An experimental study has been carried out at RRCAT with the aim of joining pipes of SS and Ti using passive fixtures with suitable CTE to generate required compressive stress between mating surfaces at elevated temperature to obtain diffusion bonding between titanium and austenitic SS tubes, without the use of a press. The article presents the new design of tube-to-tube joint assembly and results of microscopic examination of joints [28]. The new simplified approach will be useful in fabricating diffusion bonded joints in the vacuum furnaces using appropriate fixtures.

2. Materials and methods

2.1 Development of low-magnetic-permeability GTA welds

GTA welds were produced using 12 mm and 6 mm thick 316L SS with double and single V-grooves, employing a binary gas mixture of argon and nitrogen as shielding gas. Introduction of 1.5% nitrogen in the argon shielding gas resulted in nitrogen concentrations of about 0.15–0.2 wt% in the welds, compared to 0.04 wt% in welds without nitrogen. The resulting weld metal (WM) exhibited magnetic permeability (μ_r) of 1.033–1.035 close to μ_r of base metal, typically 1.02 to 1.05 (see Fig. T.1.1). Ferrite number (FN) values decreased significantly from 4.53 in WM to about 0.22–0.59 with 1.5% nitrogen addition. These welds met strength, ductility, and

impact test requirements of the ASME Boiler & Pressure Vessel Code (BPVC) for operation at room temperature and liquid helium temperature of 4 K (see Fig. T.1.2) [1]. This technique holds promise for fabricating BPVC-compliant 316L SS vacuum chambers and pressure vessels for particle accelerators, including helium vessels for SCRF cavities. Typically, pre-mix gas cylinders are employed for GTA applications due to the advantages of specific gas mixtures, such as achieving low magnetic permeability as in the case mentioned above. However, pre-mix binary gas cylinders face challenges in maintaining the consistency of the desired proportion of gases over time. This inconsistency occurs because the gases tend to stratify due to their density differences and associated buoyancy effects. Therefore, the authors have designed and developed an affordable binary gas mixer (see Fig. T.1.3) calibrated with standard binary gas analyzers. This system ensures cost-effectiveness and yields consistent weld joints.

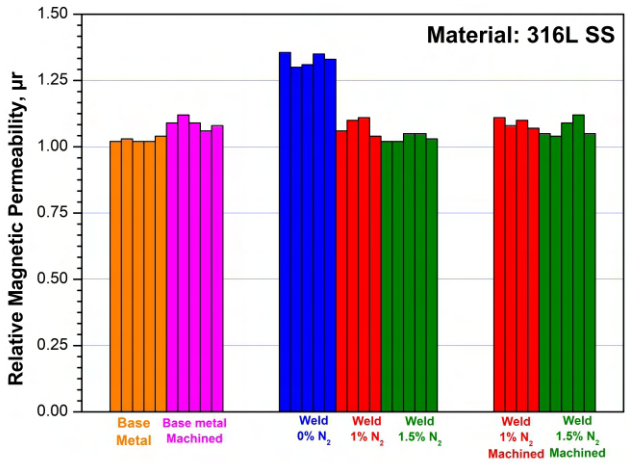

Fig. T.1.1: Relative magnetic permeability (μ_r) of base metal, machined base metal (left), weld metal with different nitrogen wt% (center) and weld metal after machining (right).

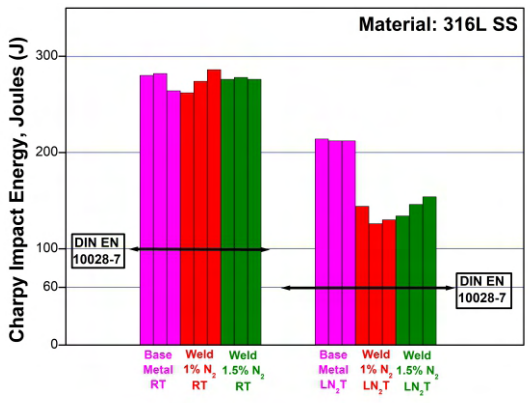

Fig. T.1.2: Charpy impact test results of base metal and weld metal at room temperature and liquid nitrogen temperature with different nitrogen (wt%) in shield gas. The black line represents the minimum required energy for failure at the respective temperatures. (DIN EN 10028-7:2008-02, pp17-21).

Fig. T.1.3: In-house developed binary gas mixer (Ar, N_2) calibrated with standard binary gas analyzer.

2.2 Deployment of gas lens for superior weld quality

TIG torch when incorporated with a gas lens generates a laminar flow of shielding gas. Figure T.1.4 depicts the gas flow image along the flow direction from torch orifice. It is evident that the laminar flow is limited only to 10-15 mm as compared to about 40-45 mm after incorporating gas lens. The waviness at the center of the image (Fig T.1.4(a)) is indicative of the turbulence whereas the straight edge in Fig. T.1.4(b) represents the laminar gas flow. As a result, a spatter-free, smooth weld bead without oxidation effects was achieved even with low shield gas flow rate (~6 lpm).

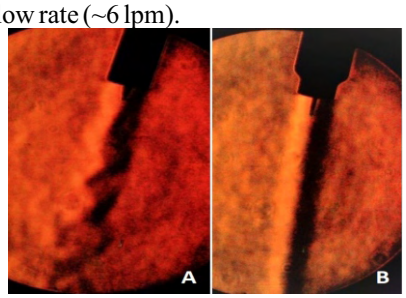

Fig. T.1.4: Gas flow of shielding gas as captured by Schlieren imaging technique: (a) turbulent flow without the gas lens & diffuser and (b) laminar gas flow with the gas lens & diffuser.

Additionally, an extra layer of gas diffuser was introduced (see Fig.T.1.5), enhancing performance while safeguarding the gas lens from potential damage as well. Gas diffusers, being cost-effective consumables, minimally impact welding expenses. These nozzles, typically made of ceramic or transparent quartz glass, can be reused multiple times and are replaced only if damaged by mishandling (see Fig. T.1.5). The integration of the gas lens system effectively addressed weld spatter issues, resulting in sound weld surfaces devoid of defects.

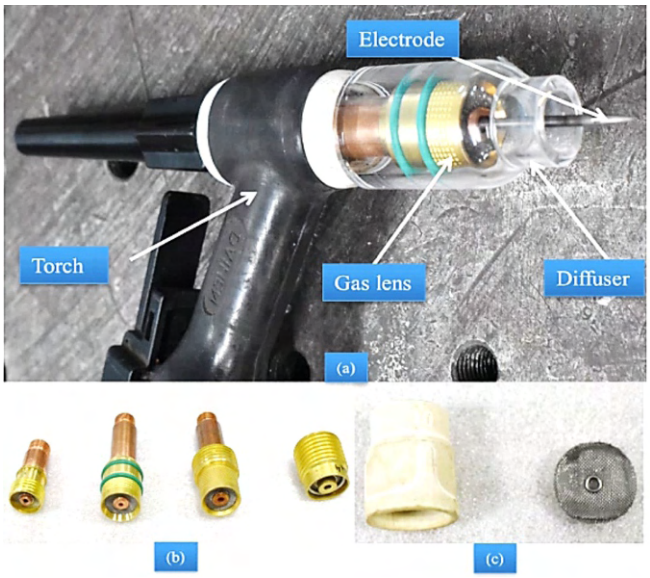

Fig. T.1.5: (a) Gas lens with diffuser mounted on welding torch, (b) various gas lens assemblies, and (c) diffuser.

2.3 Activated GTA welding for ultra-high vacuum applications

Investigations to explore autogenous activated GTA welding (A-TIG) for fabricating austenitic steel components for UHV applications has yielded promising results. Figure T.1.6 depicts the macro-structures of weld cross-section of normal TIG welded and A-TIG welded 3.2 mm thick sheet of 304L.

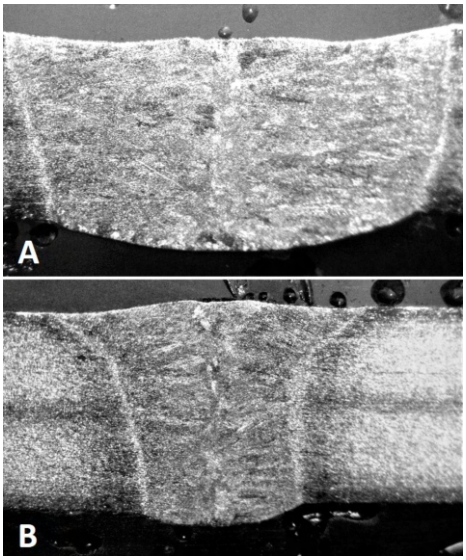

Fig. T.1.6: (a) Macro-structure of weld cross-section of normal GTA welded 3.2 mm thick sheet of 304L with slight concavity at the weld face and (b) macro-structure of weld cross-section of active GTA (A-TIG) welded 3.2 mm thick sheet of 304L with narrow fusion zone and heat affected zone without any concavity at weld face.

SEM analysis revealed that A-TIG welding did not introduce any deleterious inclusions due the use of activated flux. Residual gas analysis (RGA) findings provide conclusive evidence supporting the reliability of single-pass autogenous activated GTA welding for fabricating long tubular UHV compatible structures (see Fig. T.1.7) for LIGO application where stringent cleanliness and UHV are essential [8]. With respect to unbaked condition the RGA results show significant reduction of residual gases like H_2, O_2, N_2 and Ar after baking at 250 ^{0}C. A-TIG welding of 3.2 mm thick SS 304L sheets demonstrates that this process can be used for fabrication of austenitic steel components for UHV applications without any risk of encountering the deleterious constituents in the weld metal. Further, 316L SS sheets of higher thickness of up to 6 mm were welded using A-TIG process in 100% argon gas shield using bottom plate and gas lens in an autogenous mode in the butt configuration. This is in view of the fact that majority of the other in-house requirements fall in this thickness range. The resultant welds were completely free of any concavity and other defects in the fusion zone.

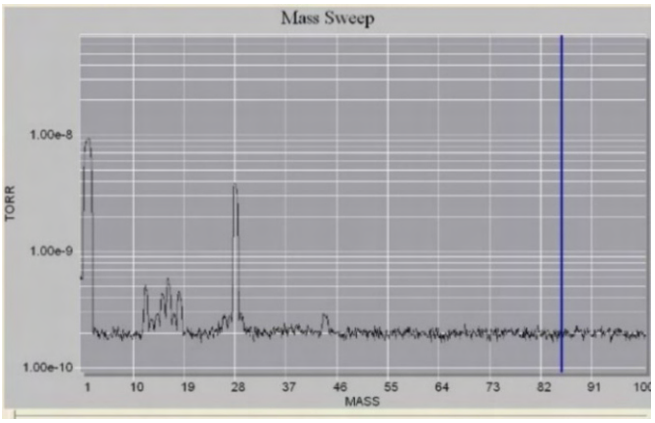

(a)

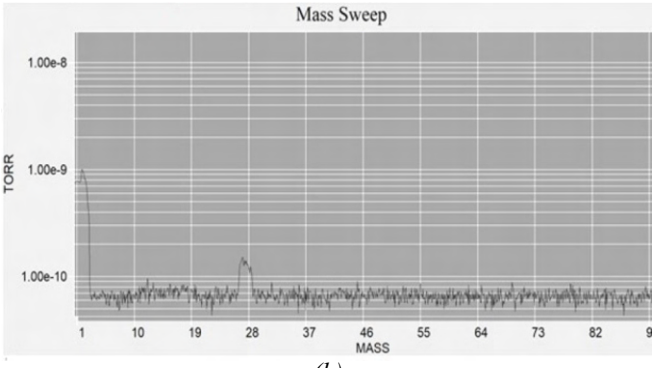

(b)

Fig. T.1.7: RGA plots during UHV qualification for (a) unbaked condition and (b) after 250 ^{0}C baking cycle. RGA tests confirm the leak tightness and a hydrocarbon free environment.

2.4 Development of aluminium to stainless-steel transition joints for ultra-high vacuum applications

Various methods of joining aluminum-to-stainless steel joints

are being investigated at DMTD, RRCAT. The aim is to develop robust joints suitable for diverse applications, including UHV and high temperature. Successful development of diffusion-bonded joints exhibiting vacuum compatibility has been achieved. Initially, diffusion bonding was conducted for fabrication of tensile test specimens using a specially designed fixture (see Fig. T.1.8), which generated the required compressive stress due to differential thermal expansion of materials involved. Joining was achieved at a temperature of 560 °C in a vacuum furnace with a heating duration of 10 minutes. The diffusion-bonded joints exhibited tensile strength of 50 Mpa.

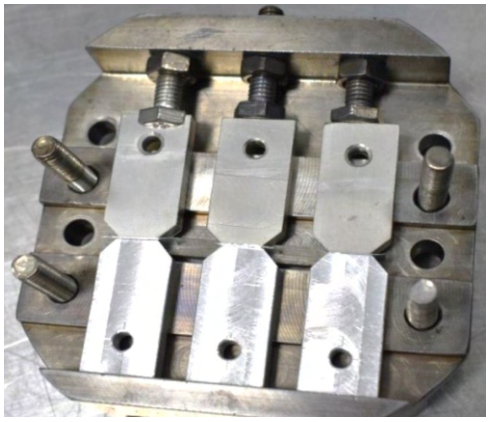

Fig. T.1.8: Diffusion bonded tensile test samples along with the fixture used for joining.

Subsequently, tubular joints were fabricated (see Fig. T.1.9) with a specific design to accommodate differential thermal expansion. Additionally, threads are incorporated to enhance strength. Aluminum, which has higher coefficient of thermal expansion is placed inside compression ring of low CTE to prevent differential radial expansion and generate compressive stress on the threaded portion. To reduce longitudinal expansion, force is applied to the assembly using a high strength steel bolt of low CTE with respect to Al joining. The joints demonstrated no leaks under a helium background of $1x10^{-10}$ mbar.l/s.

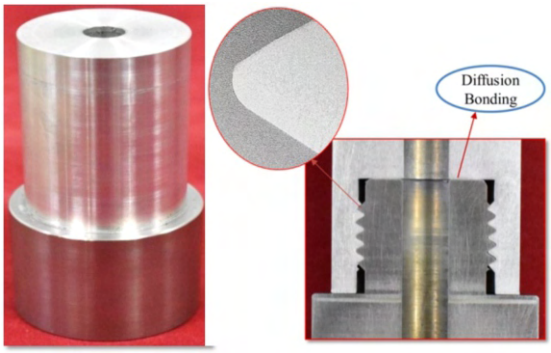

Fig. T.1.9: Tubular joint with a specific design to accommodate differential thermal expansion. Additionally, threads are incorporated to enhance strength.

2.5 Development of transition joints for x-ray target for Agricultural Radiation Processing Facility

2.5.1 Joining tantalum to stainless-steel through TIG brazing

X-ray targets used in the Agricultural Radiation Processing Facility (ARPF) are made of tantalum. However, for various other components, SS is utilized as the structural material. Consequently, tantalum-to-stainless-steel transition joints are necessary. Among the different braze fillers investigated for joining tantalum to SS; oxygen-free electronic (OFE) copper emerged as the most suitable filler. However, vacuum brazing of an actual component (1.2 m long) with OFE copper filler resulted in a vacuum leak of $1x10^{-3}$ mbar.l/sec due to thermal stresses developed during cool down. To mitigate the challenge posed by the difference in thermal expansion, an alternative joining method was explored, involving manual GTA weld braze in a controlled Ar atmosphere with the OFE copper filler. A sub-size model (110 mm x 55 mm x 12 mm) of the x-ray target assembly of ARPF was fabricated (see Fig. T.1.10). The joint sustained hydro testing of up to 6 bar and demonstrated vacuum leak tightness better than $1x10^{-10}$ mbar.l/s. Tensile strength of the joint made by GTA braze is about 90 MPa and the failure is ductile in nature.

Optical microscopy examinations reveal complete penetration of the braze filler into the joint, resulting in the formation of a sound joint without defects such as cracks and porosity (see Fig. T.1.11). Scanning electron microscopy (SEM) and energy dispersion spectroscopy (EDS) analysis indicate no melting of tantalum and SS or intermixing in the braze zone (see Fig. T.1.12). EDS analysis of the joint cross-section displayed the formation of a thin layer of ~5 µm consisting of Ta-Fe/Cr/Cu intermetallic compounds in areas where there was excessive filler deposition and associated higher heat input. Therefore, controlled heat input, appropriate gas shielding, and filler compatibility with both parts to be joined are crucial for achieving sound joints through GTA brazing. Another method involving TIG-braze joining of Ta-SS using eutectic filler (BVAg-8) is attempted in open atmosphere. The use of BVAg-8 has an added advantage of good wetting with Ta and SS, lower melting temperature (780^{0}C) and scope for better control of manual TIG brazing operation. The fabricated joints (sheet to sheet) were free from melting of Ta and SS and other defects like lack of filling or cracks and the tensile strength is 250 MPa. Further work is under progress to qualify these joints for end use requirements.

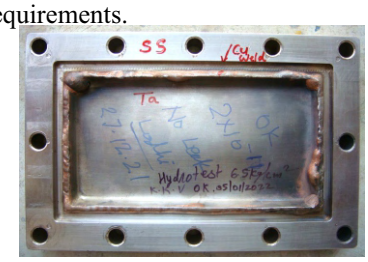

Fig. T.1.10: Tantalum brazed to 316L SS using GTA braze, employing OFE copper filler in a controlled argon atmosphere. The brazing involved a 1 mm thick tantalum sheet centrally positioned and joined along its rectangular perimeter.

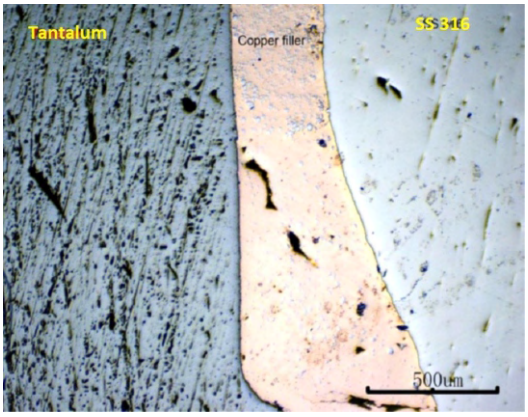

Fig. T.1.11: Optical micrograph of the cross-section of the tantalum-SS GTA brazed joint reveals complete penetration of the OFE copper filler into the joint gap, with no evidence of melting at the edges of the SS and tantalum.

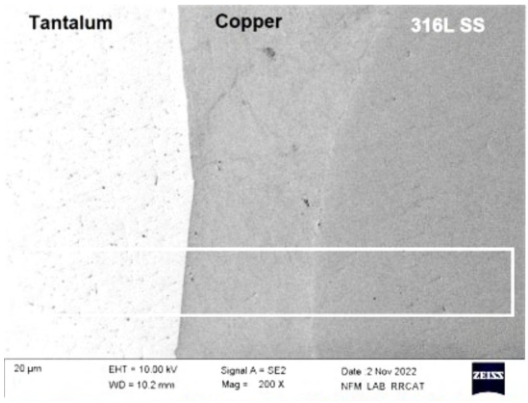

(a)

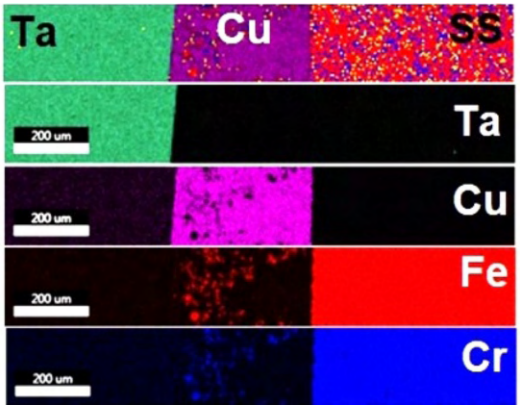

(b)

Fig. T.1.12.: (a) SEM image of joint cross-section with distinct interfaces of tantalum-copper and copper-SS without any intermixing and (b) EDS elemental mapping depicting the distribution of various elements in zone marked in the SEM image.

2.5.2 Joining tantalum to titanium through TIG welding

Continuing from previous developments, the project now focuses on joining tantalum to titanium sheet material (1.6 mm thick) using autogenous GTA welding with pure titanium filler. Special welding equipment such as gas lens, gas diffuser, back purging box, and trailing shield are utilized without the need for a glove box. Effective positioning of the tungsten electrode minimizes tantalum melting, resolving liquation cracking issues stemming from the significant difference in melting points.

Optical macrograph of GTA welded sample (1.6 mm thick) (see Fig. T.1.13) of tantalum to titanium alloy revealed complete penetration without any porosity or other defects. Tantalum exhibited minimal/no melting due to its high melting point, while titanium sheet has completely melted, forming a clean interaction layer in the weld joint. Elemental mapping of the cross-section (see Fig. T.1.14) indicates no melting of tantalum. There is no evidence of any deleterious second phase/ intermetallic layer. The ultimate strength of the joints is found to be in the range of 352-406 MPa, which is more than the strength of tantalum. The tensile specimen also showed signs of necking and ductile fracture in the weld region. The welded flange to sheet joint has been inspected for hermeticity and high pressure test. The joint exhibited an impressive hermeticity with a leak rate of 9.7×10^{-11} mbar.l/sec. The welded job passed the hydrostatic pressure test at 6 bar, which is more than the operating working pressure of 4 bar.

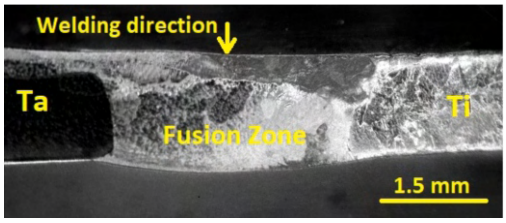

Fig. T.1.13: Cross-section of weld macro-structure of GTA weld of Ta and Ti with Ti filler.

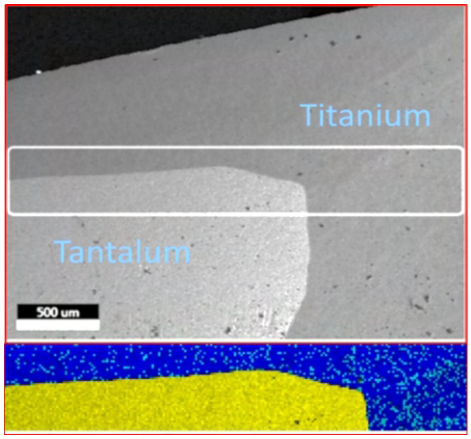

Fig. T.1.14: SEM image of joint cross-section along with the elemental distribution in the marked rectangular zone at Ta-weld interface of weld cross-section (yellow: Ta; blue: Ti).

2.6 Vacuum brazing of titanium and stainless steel

The present experimental study was carried out to address the in-house requirements related to SCRF cavity structural components. The challenge is joint design to accommodate the differential thermal expansion (Ti and SS) and braze gap control during brazing. Vacuum brazing was performed to join titanium pipe and 316L SS flange with BVAg-8 braze filler metal (BFM). Figure T.1.15 depicts the final joint of titanium tube to SS flange. Figure T.1.16 shows the microstructure of the joint cross-section with a thin layer of reaction bonded Cu-Ti intermetallic layer at the Ti- braze interface. Notable features of the process include (i) 5-10 µm nickel electro-plating as a diffusion barrier on SS faying surface for preventing possible iron migration towards titanium and improving surface wettability for BFM and (ii) use of 304 SS plug, shrunk fit into Ti-pipe, for achieving dimensional and profile accuracy of Ti-pipe during machining and controlling joint gap during brazing process. The brazed joint displayed uniform joint thickness and acceptable level of hermeticity (helium leak rate less than $2x10^{-10}$ mbar.l/sec) and sustained six thermal cycles between 293 K and 77 K. Shear strength of Ti-SS brazed specimens, made in sandwich configuration, was found to be in the range of 50-60 MPa, with failure occurring at Ti/braze interface [22].

The results of the present study have demonstrated that vacuum brazing of titanium pipe to nickel-plated 316LSS flange with BVAg8 filler resulted in sound transition joint with satisfactory shear strength of about 50-60 MPa and uniform joint thickness of about 50 +/- 10 µm. Vacuum brazed component displayed helium leak tightness better than $5x10^{-10}$ mbar.l/s and also withstood six numbers of thermal cycles between 300 K and 77 K without any degradation in joint's hermeticity; thereby establishing its suitability to withstand service-induced low cycle fatigue conditions.

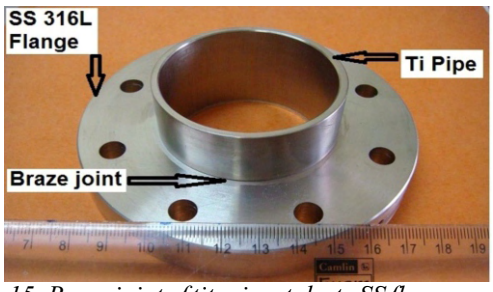

Fig. T.1.15: Braze joint of titanium tube to SS flange.

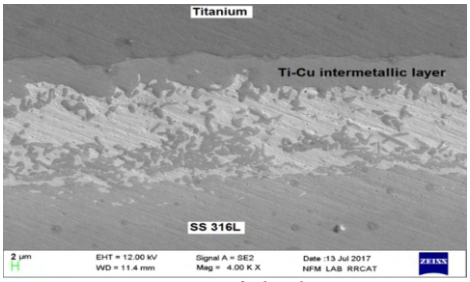

Fig. T.1.16: Microstructure of the braze cross-section with titanium-copper intermetallic layer at titanium braze interface.

2.7 Diffusion bonding of Ti & SS tubes

The study involved diffusion bonding between titanium and type 316L SS tubes in a lap configuration, utilizing fixtures such as a densimet sleeve on the outer diameter and a 304 SS plug on the inner diameter (see Fig. T.1.17). This setup generated the necessary compressive stress at the mating interface. Heating the assembly in a vacuum furnace at 900 ^{0}C for 120 minutes followed by furnace cooling resulted in diffusion bonded joints. Joints were prepared with titanium tubes of varying wall thicknesses (1.2-1.8 mm). All joints exhibited helium leak rates better than $2x10^{-10}$ mbar.l/sec and shear strength of 45-50 MPa. Microscopic examination revealed sound joints with an interdiffusion zone of 3-5 µm.

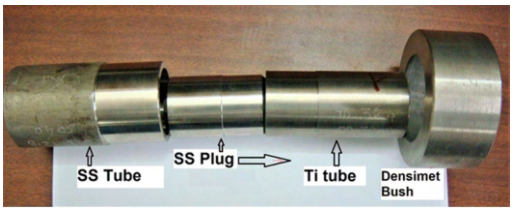

(a)

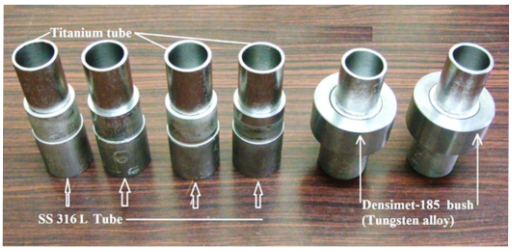

(b)

Fig. T.1.17: (a) Machined components set before assembly and (b) diffusion bonded titanium-SS tubular joints.

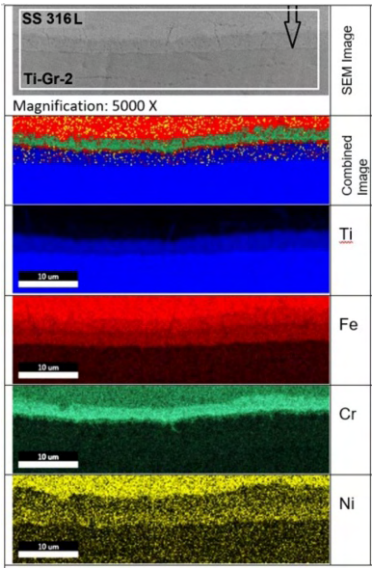

Fig. T.1.18: SEM image of the joint cross-section and the EDS mapping of elements in the region marked in the SEM image shown at top with segregation of titanium, chromium and iron at the joint interface.

Intermetallic compounds, specifically Ti-Fe/Cr, formed at the joint interface through reaction bonding at 900 °C are responsible for the joining (see Fig. T.1.18). Despite a shear strength of approximately 50 MPa, the SS-Ti tube-tube joint exhibits a high load-carrying ability of over 40 kN due to the compressive stress developed at the joint interface. Enhancements in joint strength can be achieved by controlling dimensional tolerances and reducing associated eccentricity. This study demonstrates successful diffusion bonding of titanium and austenitic stainless steel tubes using passive fixtures without the need for pressing [28]. This technique shows significant promise for joining dissimilar metallic materials, particularly tubes with wide differences in coefficient of thermal expansion, suitable for applications in the chemical and nuclear industries.

3. Conclusions

This article presents a brief summary of the recent developments in the domain of materials joining at RRCAT. The highlights include successful development/demonstration of:

(i) Low-magnetic-permeability welds of 316L SS using nitrogen alloying (using an in-house made binary gas mixture) targeted for use in critical applications in particle accelerator structural components.
(ii) Use of gas lens and diffuser with TIG torch for obtaining superior welds in the open atmosphere which otherwise necessitate controlled atmosphere for handling active metal welding.
(iii) Active-TIG welding of AISI 304L for LIGO-India application and development of aluminium to stainless-steel transition joints for ultra-high vacuum applications.
(iv) Joining tantalum to 316L stainless steel using TIG-brazing and Ta –Ti joining by TIG welding in open atmosphere using gas lens for targeted x-ray target application of an electron accelerator.
(vi) Diffusion bonding of Al-SS and tube to tube diffusion bonding of Ti–SS using passive fixtures without the use of press.

The above developmental activities and the ongoing research will provide a strong knowledge base for the present and future joining requirements of RRCAT/DAE in particular and joining industry in general.

Acknowledgements

Authors sincerely acknowledge the contribution of all the colleagues of UHVTS and LMPD for conducting these studies. Special thanks are due to Shri Vineet Kumar Lal and staff members of vacuum brazing furnace for their unconditional support for carrying our various experiments. Authors gratefully acknowledge the colleagues from LFMD (Smt Rashmi Singh and Shri M. K. Singh) for their help in conducting the SEM and EDS analysis. Dr. P. Ram Sankar, Head, Chemical Treatment Lab and his team members have provided valuable contributions for electroplating related to these developmental studies. The valuable contribution of colleagues from LMPD, Shri Ram Nihal Ram, Shri Abhijit Chowdhury, Shri Dinesh Nagpure and Shri Ram Kishor Gupta is gratefully acknowledged.

References:

[1] ASME Boiler & Pressure Vessel Code, Section VIII Division-1, The American Society of Mechanical Engineers, 2019 Edition. New York: Table ULT-23, p265; UHA-51(a)(3).

[2] A Kumar, P Ganesh, V. K. Sharma, M. Manekar, R. K. Gupta, R. Singh et al., "Development of Low-Magnetic-Permeability Welds of 316L Stainless Steel", Welding Journal, Research supplement, Vol. 100, 323-s 337-s, (2021). *https://doi.org/ 10.29391/2021.100.029.*

[3] URL: *https://sea.itwwelding.com/Article/11/Article-Using-a-Gas-Lens-for-TIG-Welding-Applications* (Visited on 12 March 2024).

[4] URL: *https://weldingweb.com/vbb/threads/38318-Noob-Gas-Lens-Basics-for-TIG-Applications* (Visited on 12 March 2024).

[5] *https://www.ligo-india.in/* (Visited on 12 March 2024).

[6] Penetration enhancing Activated Flux for TIG welding of Stainless Steels – Bhabha Atomic Research Centre (BARC); *https://www.barc.gov.in/technologies/ch44igcar/index.html.*

[7] M. Vasudevan, "Effect of A-TIG welding process on the weld attributes of type 304LN and 316LN stainless steels", Journal of Materials Engineering and Performance 26(3), 25-36 (2017).

[8] Hemant Kumar, Singh N. K., "Performance of activated TIG welding in 304 austenitic stainless steel welds", Materials Today: Proceedings, 4:9914–9918 (2017).

[9] Ashutosh Pratap Singh et al., "Characterisation of A-TIG welding of AISI 304Lfor ultra-high vacuum application", National Welding Seminar (NWS) 2022, 19-21 January 2023, Chennai, Tamilnadu, India: C-023

[10] D. D. Bhawalkar, G. Singh and R. V. Nandedkar, "Synchrotron Radiation Sources Indus-1 and Indus-2", PRAMANA- J. Phys. Indian Acad. Sci., 50(6), p 467–484 (1998).

[11] S. K. Sharma, Honey Gupta, Vikas Jain et al., "Investigation of Ultra-High Vacuum Compatible Weld Joints of AA5083 and AA6061 Materials for Synchrotron Radiation Source", J. Mater. Eng. Perform. Vol. 31, 4795–4810(2022). *https://doi.org/10.1007/s11665-022-06589-8.*

[12] D. Popov, K. Fikiin, B. Stankov, G. Alvarez, M. Youbi-idrissi, A. Damas, J. Evans, T. Brown, "Cryogenic heat exchangers for process cooling and renewable energy storage : A review", Appl. Therm. Eng. 153, 275–290 (2019). *https://doi.org/10.1016/j.applthermaleng.2019.02.106.*

[13] Szontagh, Endre, Eva, Andras, Koevari, Tiborne,

"Application of aluminium in nuclear power plants; the role of corrosion under breakdown conditions within the hermetic zone", Magy. Alum. 24 153–159 (1987).

[14] M. Zhao, X. Wang, S. Tang, Zhigang Lin, H. Chen, "Determination and characterization of heat input, microstructure and performance in cold metal transfer welding-brazing of dissimilar AA6061-T6 to SS304 sheets", Trans. Indian Inst. Met. (2023).

[15] T. Murakami, K. Nakata, H. Tong, M. Ushio, "Dissimilar Metal Joining of Aluminum to Steel by MIG Arc Brazing Using Flux Cored Wire", ISIJ Int. 43 1596–1602 (2003).

[16] J. L. Song, S. B. Lin, C. L. Yang, C. L. Fan, G. C. Ma, "Analysis of intermetallic layer in dissimilar TIG welding – brazing butt joint of aluminium alloy to stainless steel", Sci. Technol. Weld. Join. 15, 213–219 (2010). *https://doi.org/10.1179/136217110X12665048207610.*

[17] H. T. Zhang, J. C. Feng, P. He, H. Hackl, "Interfacial microstructure and mechanical properties of aluminium–zinc-coated steel joints made by a modified metal inert gas welding– brazing process", Mater. Charact. 58, 588–592 (2007). *https://doi.org/10.1016/j.matchar.2006.07.008.*

[18] C. Muralimohan, B. Srinivas, N. Abhishek, T. Ramachandraiah, S. Karna, D. Venkateswarlu, "Dissimilar Joining of Stainless Steel and 5083 Aluminum Alloy Sheets by Gas Tungsten Arc Welding-Brazing Process Dissimilar Joining of Stainless Steel and 5083 Aluminum Alloy Sheets by Gas Tungsten Arc Welding-Brazing Process", Mater. Sci. Eng. 330, 1–7 (2018). *https://doi.org/10.1088/1757-899X/330/1/012048.*

[19] H. He, S. Lin, C. Yang, "Weld Brazing a Joint of Aluminum to Stainless Steel", Weld. J. 365–378 (2019). *https://doi.org/10.29391/2019.98.030.*

[20] S. Babu, S. K. Panigrahi, G. D. J. Ram, P. V. Venkitakrishnan, R. S. Kumar, "Cold metal transfer welding of aluminum alloy AA 2219 to austenitic stainless steel", J. Mater. Process. Tech. 266 (2018). *https://doi.org/10.1016/j.jmatprotec.2018.10.034.*

[21] URL: *https://www.rrcat.gov.in/newsletter/NL/nl2019/issue2/pdf/T1.pdf* (visited on 12 March 2024).

[22] P. Ganesh, et al., "Joining tantalum and type 316l stainless steelusing TIG-brazing for application in x-ray targetassembly of agriculture radiation processing facility", Proc. National Welding Seminar 2022, 19-21 January 2023, Chennai, Tamilnadu, India. Article No.: C008.

[23] D. Grevey, V. Vignal, Issam Bendaoud, P. Erazmus-Vignal, I. Tomashchuk, et al., "Microstructural and micro-electrochemical study of a tantalum-titanium weld interface", Materials & Design 87, 974-985 (2015). *10.1016/j.matdes.2015.08.074.*

[24] K. Nishio, H. Masumoto, H. Matsuda, H. Ikeda, "Diffusion bonding of tantalum to titanium", Quart. J. Jpn. Weld. Soc. 21 302–309 (2003).

[25] A. Winiowski, "Mechanical and structural properties of joints of stainless steel and titanium brazed with silverfiller metals containing tin", Archives of metallurgy and materials 55(4), 2010, *DOI: 10.2478/v10172-010-0001-9.*

[26] P. Ganesh et al., "Vacuum brazing of titanium/316L stainless steel transition joint for application in helium vessel of superconducting RF cavities", Proc. Indian Institute of Welding International Congress (IIW-IC), 7-9 Dec. 2017, Chennai, Tamilnadu India; Paper ID C066.

[27] T. Vigraman, D. Ravindran and R.Narayanasamy, "Effect of phase transformation and intermetallic compounds on the microstructure and tensile strength properties of diffusion bonded joints between Ti-6Al-4V and AISI 304L", Materials and Design 36, 714–727 (2012).

[28] P. Ganesh et al., "A new approach of diffusion bonding for joining titanium and austenitic stainless steel tubes", National Welding Seminar (NWS) 2022, 19-21 January 2023, Chennai, India. Article ID: C-007.

T.2: Optical thin film coatings and characterization facility at RRCAT

C. Mukherjee[1,2*], K. Rajiv[1], V. V. V. Subrahmanyam[1] and N. S. Benerji[1]

[1]High Energy Laser & Optics Section, RRCAT, [2]Homi Bhabha National Institute, Mumbai
[*]Email: cmukh@rrcat.gov.in

Abstract

Ever since the advent of lasers, applications of lasers in various diversified fields have increased by many fold and lasers have been used in innovative ways. The development of laser systems and laser application setups require a wide range of optical components with high-performance optical thin film coatings e.g., high reflection (HR) coatings and antireflection (AR) coatings on lenses, windows, crystals, laser rods and polarizing optical components. The rapid developments in laser technology have put enormous technological challenges on thin film coatings. RRCAT is involved in the design, development, and applications of various lasers. With a view to cater to these requirements, specialized optical coatings, state-of-the-art technology to produce multilayer optical thin film coatings with excellent spectral performance, laser damage threshold, durability, and thin film characterization facilities have been established. The very basis of these coatings is nano-metric thin film layers of dielectrics with defined microstructures, or their stacking as multilayers that utilize the principle of interference, governing the amplitude, phase, and polarization of the electromagnetic radiation. Both material and geometric parameters are equally important in the description of optical coatings. In this article, the thin film deposition facilities, the process development for fabrication of important optical components and different characterization techniques are discussed. An overview of various specialized and challenging optical coatings developed in Optical Coating Laboratory (OCL), RRCAT and their characteristics is presented in this article.

1. Introduction

Optical thin film coatings are all around us - on Earth and in Space - working in innumerous essential products that better our lives. Technological and scientific applications linked to interference coatings especially lasers are enormous and are continuing to grow. The very basis of these coatings is nanometric or sub-nanometric thin film layers of metals, ceramics, dielectrics, composites with defined microstructures or their stacking as multilayers that utilize the principle of interference governing amplitude, phase and polarization of the electromagnetic radiation.The beautiful natural phenomena and vivid spectral colorful creations of the nature are the outcome of the optical interference and are fascinating over the ages. The rainbow, the colorful birds, insects, bugs, sun light-lit waterfall are the prominent examples as shown in Figure T.2.1.

Fig. T.2.1: Natural optical interference phenomena [1].

Optics and optical components with specialized optical coatings are important for laser based R&D and spectroscopic studies and also help in considerably enhancing the efficiency of various industrial and high power laser systems being developed at RRCAT. These components are very expensive, not readily available as and when required and are mostly being imported. Development of large area optical coatings with high performance uniformity and high damage threshold is required for the development of high energy lasers.

It is well known that a stack of thin layers of optical materials can preciously control the flow of light through the surface of a transparent solid on which layers are deposited. The behavior of the coating depends on the optical properties of the material together with interference effects, which vary with wavelength, angle of incidence and polarization. Only specular component of light is considered. As the incident light enters the system of optical thin film coatings, it suffers multiple internal reflections at each interface. All the reflected/transmitted component waves having a distinct amplitude and phase as decided by the multilayer stack interfere either constructively or destructively to produce the resultant reflected/transmitted wave as desired [2]. Such calculation is well organized and understood. However, the inverse problem is rather complicated with no unique solution. The success depends equally on powerful theoretical tools, experience and skill. Design has to be finalized based on the practical problems faced in depositing and the limitations of the deposition and monitoring systems. The problem is compounded by the fact that properties of materials in thin film form vary on their own and also in the vicinity of another material.

2. Antireflection coating- Destructive interference

To understand the performance of thin film coating we need to accept following statements. First is that the amplitude reflectance of light at any boundary between two media (e.g., air and glass) at normal incidence is given by $(1- n_2)/(1+n_2)$, where n_2 is the refractive index of glass. The second is that there is a phase shift of π (i.e. $\lambda/2$) when the reflection is backed by a denser medium. The third is that light splits into two components, one at the top and the other from the bottom surface of a thin film. The incident ray is shown in black color. The thickness and refractive index of the film (blue) are such that the reflected beams (blue and red) from the 1st and 2nd interfaces have a phase difference of π and also their amplitudes are almost equal. Therefore, they recombine

destructively producing low reflection and is known as antireflection (AR) coating [2]. This is described in Figure

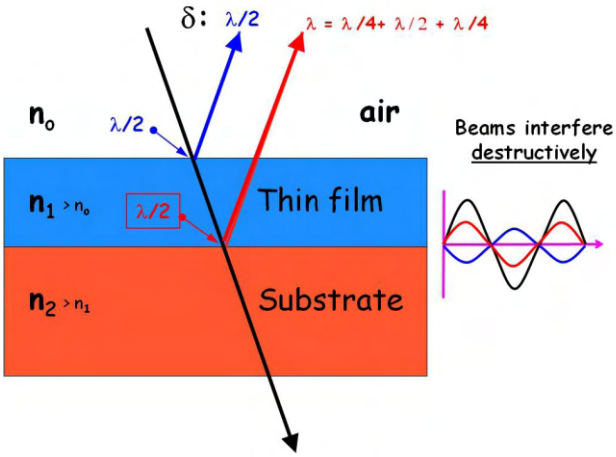

Fig. T.2.2: Principle of antireflection (AR) coating.

3. High reflection coating- Constructive interference

The basic high reflectance (HR) thin film structure consists of a stack of alternate high and low refractive index layers, starting and ending with high index layers and all the layers are one quarter wave thick at the centre of the desired wavelength range. Under such condition all the reflected rays meet constructively and result in high reflectance. The reflectivity can be made very high simply by increasing the number of layers. One of the most important requirements of all these coatings is that the films have very low absorption in the wavelength range of interest. Figure T.2.3 shows the principle of such a stack.

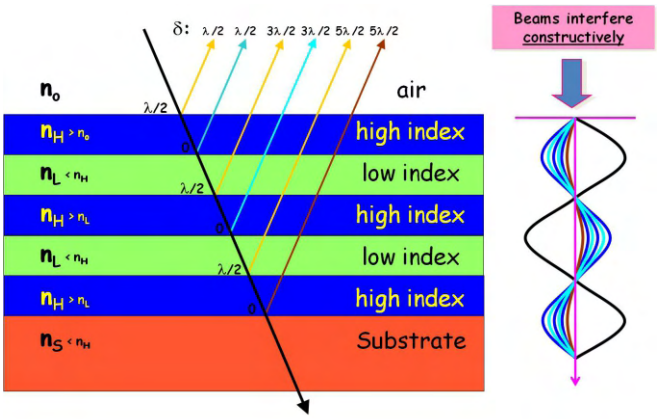

Fig. T.2.3: Principle of high reflection (HR) coating.

4. Multilayer coatings: Design & optimization

The computation of multilayer assembly, with large number of layers, is a complex task. One possibility is to use matrix formalism. This is based on the fact that tangential component of electric and magnetic fields are continuous across a boundary between two layers of different refractive indices. In this approach each layer is represented by a 2x2 characteristics matrix and multiplication of large number of such matrices provide the final equivalent layer matrix (2x2). Often the practical requirements are more demanding, complex and difficult to attain by a conventional design approach. Hence, there has been an extensive role of computer-aided-design for such multilayer stack. A giant step in coating design was taken by P. Baumeister [3,4]. He introduced the merit function for estimating the closeness between designed and target spectral performance. An automatic process that involves an element of design construction is usually known as synthesis. An automatic computing/numerical process that makes adjustments to an already existing design without making major changes is known as refinement. The term optimization simply means improving performance and includes both refinement and synthesis. A good starting design is important for this. In 1982, the needle optimization technique was invented and is used in all commercial thin film softwares [1].

5. Optical thin film materials- Dielectric materials

A typical transmission characteristic of an optical thin film material is presented in Figure T.2.4. Every material, because of its structure, has a characteristic transmission spectrum that can be split into three parts: (i) the high-frequency electronic absorption region, (ii) a transparent region, and (iii) a region dominated by the low-frequency lattice vibration. The transparent region, merely the region in between the electronic absorption and the lattice vibration, and as such is particularly influenced by impurity and free-carrier absorption [5].

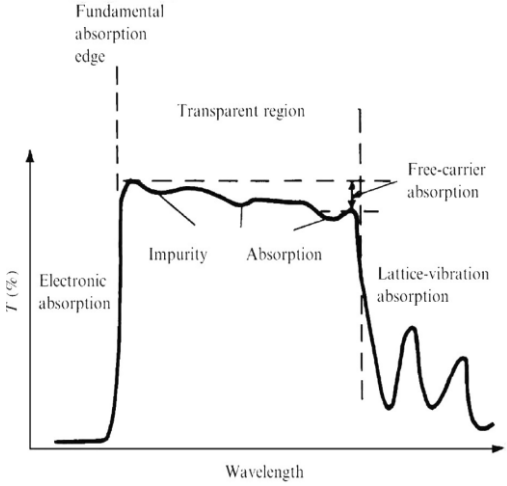

Fig. T.2.4: Wavelength dependent characteristic of a typical optical material used for interference coating [5].

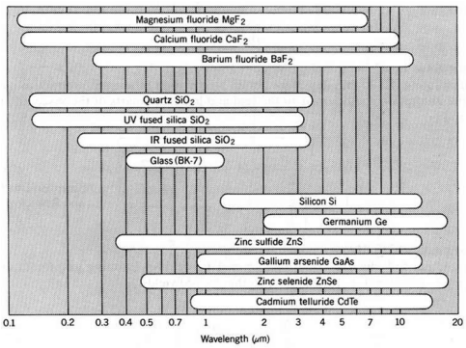

Fig. T.2.5: The spectral band in which optical substrate materials are transparent [6].

As it can be seen in Figure T.2.5, there are a very limited number of substrate materials available for optical coating applications. Out of these, a handful of materials are available for UV lasers such as excimer lasers. Refractory oxides are the most favourable materials for multilayer laser coatings and a list of popularly used coating materials is presented in Table T.2.1.

Table T.2.1: Refractory oxides for multilayer laser coatings.

Metal Oxide	Refractive index at 550 nm	Transparency range (nm)	Melting point (°C)
TiO_2	2.31	450 – 10000 nm	1850
Nb_2O_5	2.25	400 – 10000 nm	1460
Nd_2O_3	1.79 – 2.15	400 – 2000 nm	2300
HfO_2	1.93 – 1.97	250 – 10000 nm	2800
ZrO_2	2.05	270 – 7000 nm	2700
Sc_2O_3	1.85 – 1.90	220 – 10000 nm	2300
Ta_2O_5	2.05 – 2.10	400 – 10000 nm	1800
SiO_2	1.40 – 1.45	185 – 5000 nm	1710

6. The coating process

Modern thin film multilayer optical coatings are usually fabricated by physical vapour deposition techniques in a vacuum chamber. Prior to deposition, necessary substrates are polished and thoroughly cleaned by multi-frequency ultrasonic cleaning, which is followed by hot air drying [7]. The vacuum chamber is also cleaned from residues of previous deposition runs. The substrates on which the thin films are to be deposited are mounted on a flat or a hemispherical plate called calotte. Deposition chamber is evacuated to a low pressure of 10^{-7} to 10^{-8} mbar. A small amount of oxygen is added into the chamber during deposition of refractory oxide materials. The substrates may be at room temperature or they may be heated say upto 300 °C. To ensure uniformity of the deposited film thickness over the coated area, the calotte is usually rotated about a central vertical axis, and the relative geometry of the source and substrates is carefully chosen [1,2,8]. Various coating processes include: (i) Ion-assisted e-beam evaporation, (ii) Magnetron sputtering, (iii) Ion beam sputtering and so on.

6.1. Deposition by electron-beam evaporation

Traditional electron-beam (e-beam) evaporation is one of the most widely employed methods for producing thin films. Here, a coating material is heated through electron beam bombardment (for dielectrics) within a high vacuum chamber until it vaporizes. This method of evaporation is a relatively low energy process, and as a result, the dielectric films it produces are porous, of relatively low density, and exhibit a columnar structure [9]. Typically, the substrate is heated to several hundred degrees Celsius during coating to mitigate this effect, but it is by no means eliminated. The problem with these porous films is that they can subsequently absorb moisture, which changes the refractive index of the layers.

6.2. Ion Assisted e-beam deposition (IAD)

IAD is a variant of the e-beam evaporation process, which adds a high energy ion beam that is directed at the part to be coated. These ions act almost like an atomic sized hammer, producing a higher film density than evaporation alone. The ion beam can also be used to pre-clean the substrate, which can improve film adhesion. IAD results in higher coating density, improved mechanical durability, greater environmental stability and lower scatter as compared to e-beam evaporation [10]. It also enables the intrinsic stress to be modified during deposition, i.e., changing the overall film stress from tensile to compressive [11]. The deposition facility is shown in Figure T.2.6.

Fig. T.2.6: Ion-assisted e-beam deposition facility at RRCAT.

6.3 Magnetron sputtering

At present, the sputtering of metals and dielectric is carried out in the in-house developed sputtering system as shown in Figure T.2.7. The system is computer controlled. The sputtering system is established to meet many metal deposition requirements. Co-sputtering of two different targets using DC, pulsed-DC and RF plasma can be done. Film thickness monitoring can be performed with multiple quartz crystal monitors. An ion source is fitted for ion-assisted deposition. The chamber can be baked out, and elevated deposition temperatures of ~400 °C can be maintained. A provision is also made for low substrate temperature (LN_2) deposition. Flat sample rotation provides better film thickness uniformity than stationary substrate holder. Samples up to 150 mm in diameter can be coated with <5% uniformity. Many challenging coatings e.g., FEL mirrors, TMT edge sensors, mirrors for underwater reactor tube cutting, large beam splitter for sag measurement of reactor tubes, WS_2 coating on bearings for RF tuners, HR coating on large size involute reflectors have been made and are shown in Figure T.2.8.

Fig. T.2.7: Magnetron sputtering deposition system at RRCAT.

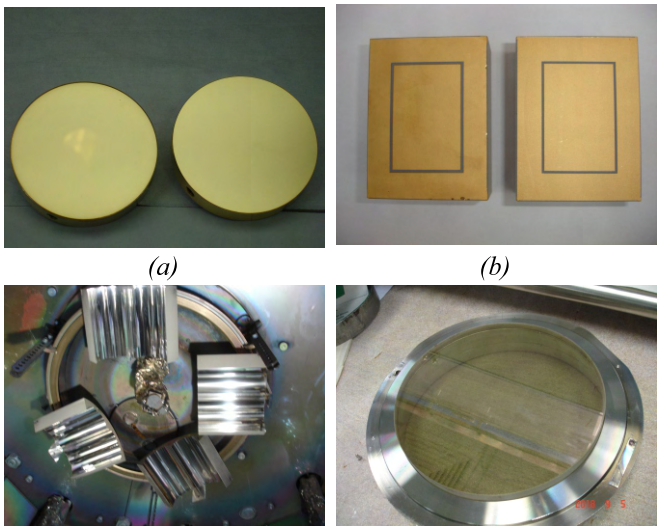

(a) (b) (c) (d)

Fig. T.2.8: (a) FEL mirrors, (b) TMT edge sensor, (c) involute reflectors, and (d) beam splitter for sag measurement of reactor tubes of KAPS reactor.

6.4. Dual ion beam sputtering

Dual ion beam sputtering (DIBS) is remarkable to deposit thin films with better compositional stoichiometry and film adhesion even for films grown at room temperature. A few other unique features of the DIBS system are high-quality growth with reduced surface roughness and increased growth uniformity on a larger substrate area, and in-situ substrate pre-cleaning before growth [12]. There are two ion sources in a DIBS system, a primary radio frequency (RF) ion source is used for sputtering of materials from a multiple target assembly. A RF secondary assist ion source had dual roles to play. Before actual film deposition, assist source was turned on for substrate pre-cleaning with Ar bombardment. During material growth, assist ion beam, composed of Ar/O_2 ions, helps in the reduction of columnar growth and thereby enhances growth uniformity and film adhesion to the substrate [12]. Moreover, the assist ion source hinders island formation and removes weak dangling bonds during the actual sputtering process [13]. Four oxide targets each of 350 mm diameter are used to grow multilayer oxide coatings. Four substrates, each of 150 mm diameter can be accommodated and are rotated at 120 rpm (max.) in a planetary configuration. The DIBS facility is shown in Figure T.2.9.

Fig. T.2.9: Dual ion beam sputtering deposition system at RRCAT.

6.5. Thickness monitoring during deposition

Precise control of film thickness (to within 1% of the desired value) and controlled film deposition rate are essential during the fabrication process. The most common method for controlling the film thickness during deposition is by the optical interference method, where a chopped beam of light is allowed to fall on a witness substrate. As the film grows on the substrate, the transmitted or reflected light intensity at a particular wavelength is monitored by the optical thickness monitor. The measured transmittance or reflectance goes through a series of maxima and minima, and extrema being reached when the optical thickness is an integral number of quarter waves of the monitoring wavelengths [14]. Alternately, the physical thickness of the film is measured by a quartz crystal monitor, where an oscillating quartz crystal is exposed to material vapour, and as the film grows on it, its oscillating frequency changes. This change in frequency is used to determine physical thickness of the deposited film.

7. Damage threshold testing of multilayer coatings

Laser induced damage threshold (LIDT) of coated optical components is a critical quality parameter for laser systems operating at high power/high energy [15]. As per ISO standard procedure (ISO-11254-1), a laser beam is directed towards optics at different locations and optics is observed carefully for any damage under microscope. This LIDT test setup consists of a pulsed Nd:YAG laser, which can give up to 0.5 J per pulse with 1-10 Hz repetition rate at 1064 nm and a typical pulse width of 5-6 ns (FWHM). Damage morphology is recorded with Nomarski DIC microscope.

If damage is not found, energy/power is increased and the exercise is repeated until damage is observed by a visible spark. This is repeated for more than 100 sites, followed by plotting the probability of damage versus fluence [16]. This is a unique facility in the country.

8. Ultra low absorption coefficient measurement

The absorption coefficient is measured by photo-thermal common path interferometer (PCI) technique. The main purpose of the system is characterization of absorption for different optical elements: coatings, substrates, crystals, interfaces, etc. The setup is of a pump/probe type, based on the thermal lensing effect. Absorption is tested at the wavelength of a "pump" laser (532 nm & 1064 nm). For better sensitivity, the pump is chopped to provide periodic heating of a tested object. The probe beam (He-Ne laser) senses the heating effect of absorbed pump. Intensity change is detected by a detector, which relies on phase distortion, which in turn relies on pump beam absorption [17]. This is a unique facility in the country and caters to the requirements of high energy laser program of RRCAT and other national institutes. The lowest absorption of 1 ppm can be measured. Figure T.2.10 shows the 2D absorption map of fused silica sample before and after prolonged exposure of laser plasma.

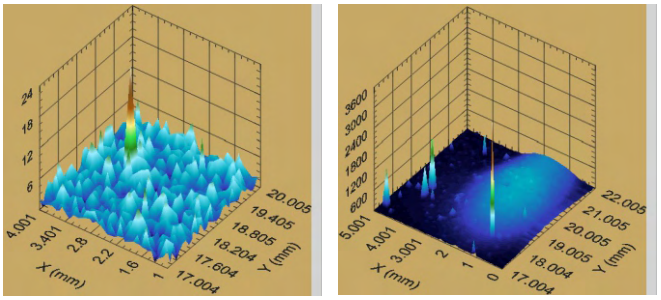

(a) *(b)*

Fig. T.2.10: 2D absorption map of fused silica sample (a) before and (b) after prolonged exposure of laser plasma.

9. Laser resistant coatings

Development of optical components for lasers operating at very high power levels (terawatt level in pulsed systems and multi-kilowatt range in CW) at various wavelengths is a challenging task. This power handling capability of optical coatings is a major limiting factor. Today thin film laser damage research continues to focus on reducing absorption and coating defects. Telecommunication optics are being limited by laser damage issues as larger number of photons are being injected into small fibers. The need of semiconductor lithography industry for short wavelength coatings requires development of low absorbing materials in deep and extreme UV region. Mega projects like inertial confinement fusion, free electron lasers, air borne lasers have extremely high energy levels over large size optics. Short pulse lasers require coatings capable of withstanding pico-second and femto-second pulses. Coating design strategies such as standing wave electric field (SWEF) reduction technique and thick silica overcoat also improve laser resistance. SWEF reduction technique have immensely helped in using materials of different refractive index by reducing the SWEF peaks in the high index materials and also by shifting the peaks away from the interfaces. Reproducible and reliable measurements of LIDT are essential for optimization of laser components [18]. Damage in ultra short pulse region has been demonstrated to be mainly driven by direct electronic interaction of the material with intensive laser radiation involving tunneling, multi-photon and avalanche mechanisms. Films with pores, cracks, columnar microstructure, multiple crystalline phases, and lack of stoichiometry leads to intrinsic defects. On the contrary extrinsic defects occur due to foreign defect seeds created during the coating process and due to surface contaminants present on the substrate. Therefore appropriate substrate and deposition system cleaning methods must be adopted to avoid such defects [5,18].

10. Development of AR coating on end faces of Nd:YAG, Ti:Sapphire and Nd:glass laser rods

10.1. For Nd:YAG laser rod, single quarter-wave (1064 nm) MgF_2 layer perfectly serves the purpose. Such a layer was deposited on both the end faces of 5-10 mm diameter and 100-150 mm long Nd:YAG rods. End faces of damaged rods were optically polished at Optical Design and Development Lab, RRCAT and subsequently AR coating was done. Rods were held vertically and rotated during deposition at 5 rpm. MgF_2 coated Nd:YAG laser rods are shown in Figure T.2.11. Optimized deposition parameters to grow dense film with the required refractive index were used. For this, special rod holder was developed. Deposition was carried out at 125 °C under Ar ion assisted environment. AR coated rods yield 300 J pulse energy (2-40 ms, 1-100 Hz rep. rate, 10 kW peak power).

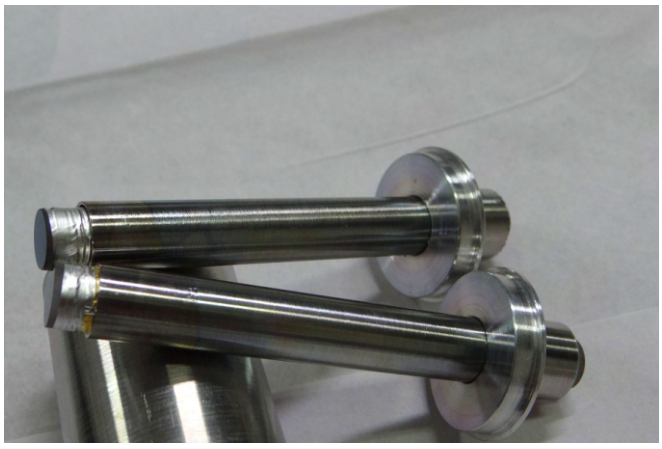

Fig. T.2.11: MgF_2 coated Nd:YAG laser rods in specialized fixtures.

AR coated rods were also tested in the amplifier cavity. Each rod was pumped up to 85 J and no lasing was observed. This shows that the quality of the coating is excellent and comparable with that of the coating, which was initially on the laser rods. Though the reflectivity of the coating was measured quantitatively on a dummy substrate and was <0.2%, it

is obvious from its performance that the coating's residual reflectivity is comparable to the original coated rods. Coating did not develop any damage and delivered 1.5 J in <10 ns [19].

10.2. For complex requirement such as Ti:Sapphire laser rod, a single layer approach is insufficient, hence multilayer thin film structure is required to achieve low reflection loss both at pump (532 nm) and lasing (800 nm) wavelengths. Non-quarter-wave layers are required for achieving such high optical performances. We have optimized a four layer structure SUB/0.25H/0.35L/2.1H/1L/AIR, where H and L represents one quarter-wave HfO_2 and SiO_2 layers, respectively. SiO_2 as low index and HfO_2 as high index material are chosen due to their very low optical absorption and high laser damage threshold. This layer structure yielded a very low residual reflection loss at 532 nm and 800 nm on a dummy sapphire substrate. Finally, this 4 layer structure was deposited on both the sides of a polished Ti:Sapphire laser rod (20 mm dia., 20 mm long). Residual loss of ~1.0% is measured at 532 nm and ~ 0.9% at 800 nm as shown in Figure T.2.12. This AR coated rod is used as a four pass amplifier in a Ti:Sapphire laser (650 mJ, 0.2 ns, 10 Hz). No coating damage is observed even at maximum laser power level [20].

10.3. High energy lasers are increasingly used in study of equation of state of materials at high temperature and pressure, high density shock, implosion physics, etc. One such laser is Nd:glass. Besides, high transmittance, high laser induced damage threshold (LIDT) and durability are important for such applications [3]. Laser induced damage in optical materials remains a limiting factor in the development of high power laser systems. Large size e.g., 300 mm long, 50 mm dia. Nd:glass rods are polished and AR coated indigenously at RRCAT. Five Nd:glass rods fitted in the deposition system is shown in Figure T.2.13.

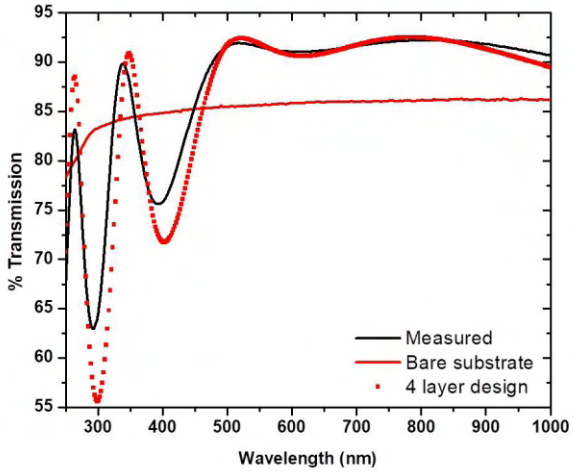

Fig. T.2.12: Transmittance of AR coated sapphire substrate.

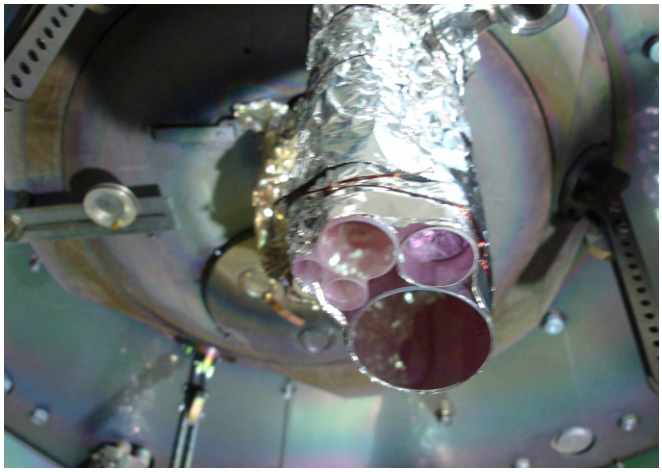

Fig. T.2.13: Five Nd:glass laser rods of different sizes fitted for coating.

We have studied two, three and four layer structures: SUB/0.5H/1.3L/AIR, SUB/2L/0.5H/1.3L/AIR and SUB/0.35H/0.3L/1.09H/1L/AIR, where H and L represent one quarter-wave HfO_2 and SiO_2 layers, respectively. The design wavelength used are 995 nm, 995 nm and 1054 nm, respectively. We have chosen HfO_2 as high-refractive index optical material with very high damage threshold. This layer structure yields a residual reflection loss nearly 0.25% per surface on a wavelength range over 165 nm, 165 nm and 325 nm, respectively. Four layer design (blue curve) is superior in its broad wavelength band. For these calculations, wavelength dispersion data of both the materials is taken into consideration. Electric field intensity profile along the depth of each multilayer is calculated and shown in Figure T.2.14. Electric field intensity profile provides insight into the laser damage phenomena. Transmission of more than 99.5% at 1054 nm is achieved. High LIDT of >21 J/cm^2 for 5.2 ns pulses is achieved in 3 layer AR coating after annealing at 450 ^{0}C for 4 hours. This is associated with 60% improvement in absorption coefficient. The large size AR coated Nd:glass laser rod delivered pulse energy of 15 J at 1.5 ns duration [21].

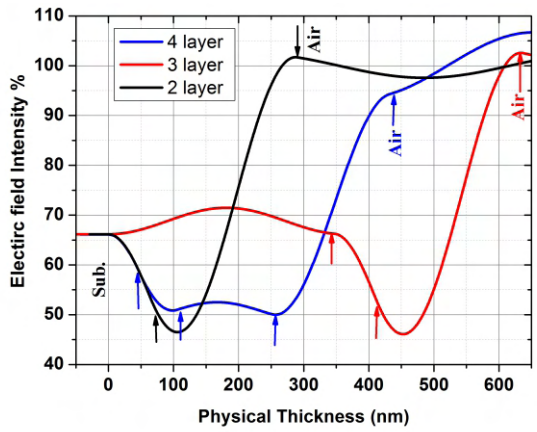

Fig. T.2.14: Calculated electric field intensity profile along depth of the multilayer for 3 different layer structures.

11. Large area AR and HR coating on super smooth fused silica optics for Nd:glass laser

Nd:glass disk laser amplifier of the high energy laser chain requires large size (150 mm) multilayer thin film coated anti-reflection and high reflectivity (HR) mirrors with high LIDT. As these large sized HR mirrors and transmission windows with high LIDT are not readily available from the OEMs, indigenous development of super-smooth substrates for these crucial optical components was taken up at RRCAT.

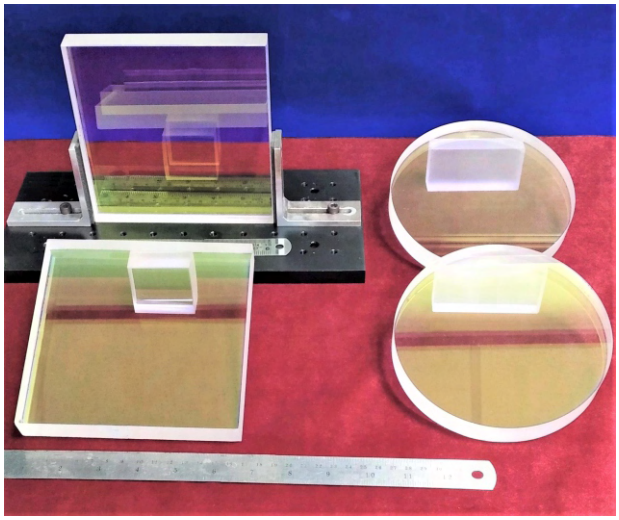

Fig. T.2.15: AR coated, 150 mm dia. & 150 x 150 mm optics.

Fused silica substrates were optically polished using bowl-feed CMP technique to generate ultra-low roughness (<5 Å) with flatness of λ/10 at 589 nm over 95% clear aperture, parallelism better than 5 arc sec and a scratch-dig of 20/40. Three layer AR coating design was optimized while using HfO_2 as high index layer.

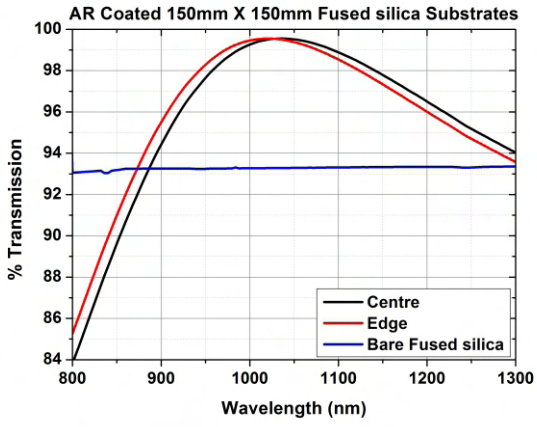

Fig. T.2.16: Transmission spectra of AR coated (red & black) and uncoated optics (blue).

Multilayer design is Sub/2L/0.46H1.26L/Air, where H & L correspond to single quarter-wave layers of HfO_2 and SiO_2, respectively.

The half-wave layer, adjacent to the substrate helps to minimize the standing wave electric field at the remaining imperfections on the substrate. AR coated optics are shown in Figure T.2.15. Transmission of 99.4% at 1054 nm, and 99.2% over wavelength band of 60 nm is achieved (Fig. T.2.16). Laser damage threshold of 13 J/cm^2 for 5.2 ns pulse at 1064 nm for un-annealed samples were recorded. Nearly 100% improvement in LIDT is noticed with respect to samples without half-wave SiO_2 layer adjacent to substrate. It is also to be noted that these substrates are having very low roughness and low scratch/dig. These two factors contributed to the improvement of LIDT [22].

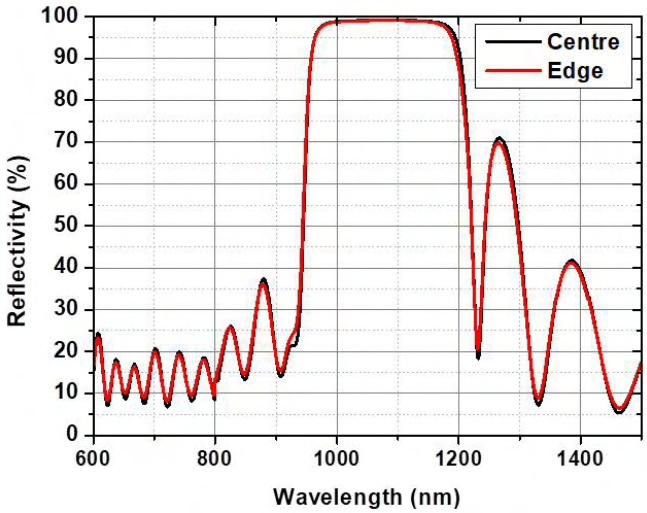

Fig. T.2.17: Reflectivity spectra of HR coated optics of size 150 x 150 mm.

The super-smooth substrates have also been coated with SiO_2/Ta_2O_5 multilayer thin-film to fabricate HR laser mirrors. 25 layers were deposited. It took 25 hrs. to grow the entire HR coating. The reflectivity of these mirrors has been measured to be 99.5% ± 0.1% over a wavelength band of 140 nm at a centre wavelength of 1054 nm, with a measured LIDT of 5.7 J/cm^2 at 5 ns as shown in Figure T.2.17 [23]. HR coated optics of sizes 150 mm x 150 mm and 90 mm x 90 mm are shown in Figure T.2.18.

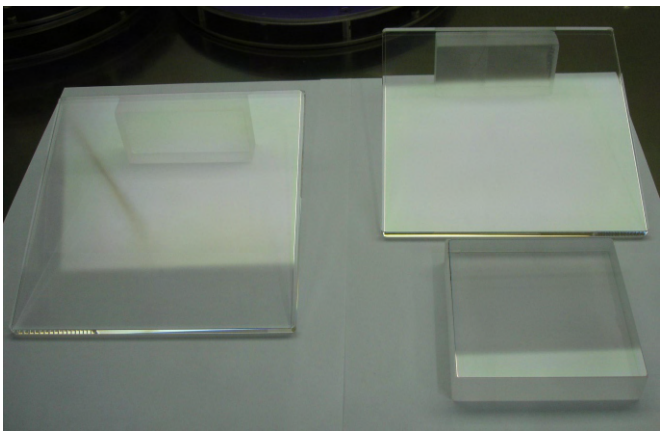

Fig. T.2.18: HR coated 150 mm x 150 mm & 90 mm x 90 mm optics.

12. Development of tunable Fabry-Perot (F-P) filter

Wavelength division multiplexer/demultiplexer (WDM/WDDM) is the key component in optical communication. Using thin film Fabry-Perot filter wavelength demultiplexing/tuning can be achieved by varying the spacer layer thickness. The spacer layer thickness was varied from 125 nm to 160 nm across a 25 mm dia. substrate. Nine channels each of FWHM = 3 nm can be placed each, 2 mm apart from the previous channel on the substrate along the direction of shutter motion. Tuning of 21 nm is achieved. Figure T.2.19. shows the transmission spectra of a 17 layer F-P filter with high refractive index spacer layer (thickness = 4*λ/4 at 465 nm plus a tapered layer varying from 0 to 33 nm) [24].

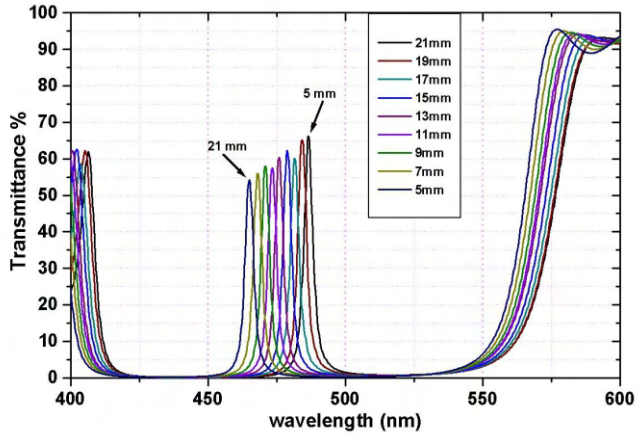

Fig. T.2.19: Transmission spectra of 17 layer F-P filter with a graded spacer thickness varying from 0 to 33 nm.

13. Recent developments in heterogeneous coatings

Any optical coating with a refractive index that depends on the spatial coordinates is considered as heterogeneous coating. Grating – waveguide structure / guided-mode resonance (GMR) filter is one such structure. A three layer GMR filter consists of top grating layer, a waveguide layer and a sub-waveguide layer coated on the substrate. The remarkable property of a grating waveguide (GWG) is that it can show a reflectivity of 100% for a given optical wavelength despite its thickness of typically less than a wavelength. This makes GWG a promising candidate for test mass coatings in gravitational wave detectors, because only a very small amount of dielectric coating material is required with a corresponding considerable reduction in coating thermal noise. Raman notch filters can also be made using such structures [25].

Meta-materials: The development of electromagnetic, artificial-lattice structured materials (photonic crystals), termed meta-materials, has led to the realization of phenomena that cannot be obtained with natural materials. The meta-material coating consists of a mesh and an electric split-ring resonator array separated by a dielectric spacer layer (~10 μm). Structured meta-materials can achieve negative refraction using nano-fabricated materials in terahertz region [26].

14. Conclusion

Specialized optical coating and characterisation facilities developed at OCL, RRCAT to meet the demands of the laser programmes at RRCAT and other institutions have been discussed. To the best of our knowledge, high damage threshold coatings, on large area optics and laser rods are being done only at RRCAT in India. State of the art characterization facilities e.g., laser damage threshold testing and ultra-low absorption measurement facilities, which are unique in the country have been established. Multilayer antireflection coatings have been designed and optimized for achieving very low reflection loss for high energy Nd:glass laser on large area super-smooth optics (150 mm x 150 mm). 99.4% transmission and LIDT of 13 J/cm^2 for AR coated optics are achieved. Such coated optical components are deployed in high energy Nd:glass laser being developed at RRCAT. 25 layer high reflection coatings have been designed and optimized for achieving very high reflectivity for Nd:glass laser. 99.5% reflectivity and 5.7 J/cm^2 LIDT have been regularly obtained for HR optics. Large size (300 mm long & 50 mm dia.) Nd:glass rods are AR coated indigenously at RRCAT. Transmission > 99.5% at 1054 nm is achieved. High LIDT of > 21 J/cm^2 at 5.2 ns is also achieved. Apart from meeting the needs of the various laboratories at RRCAT, OCL has also supported and fulfilled specialized optical coating requirements of BARC, VSSC, IIT Indore, India Security Press, Nasik, etc. and also collaborated with LEOS, VSSC, ISRO, etc. In future, it is planned to upgrade the optical coating facilities by including plasma-enhanced chemical vapour deposition (PECVD) based coating on KDP crystals, dip coating facility and develop synchrotron mirrors (500 mm x 50 mm) on super-smooth cylindrical and toroidal fused silica optics.

Acknowledgements

Authors would like to sincerely thank Dr. S. V. Nakhe, Director, RRCAT for taking keen interest in developing specialised coatings, for his continued support and guidance. Support of Dr. Suparna Pal, Dr. Neha Sharma, and all the colleagues of High Energy Lasers & Optics Section and C1-Block, RRCAT for their direct or indirect contributions is duly appreciated.

References

[1] Norbert Kaiser and H. K. Pulker, Optical Interference Coatings, Springer, (2003).
[2] H. A. Macleod, Thin-Film Optical Filters, Third Edition, IOP (2001).
[3] P. W. Baumeister, Optical Coating Technology, SPIE Press, ISBN 0-8194-5315-7 (2004).
[4] J. A. Dobrowolski, R. A. Kemp, Appl. Opt. 29, 2876 (1990).
[5] R. M. Wood, Laser damage in optical materials, Adam Hilger (1986).
[6] J. D. Rancourt, Optical thin films user handbook, SPIE (1996).
[7] T. Gischkat, D. Schachtler, B. Eiermann, Appl. Sci. 10, 8496 (2020).

[8] Ronald R. Willey, Practical Design and Production of Optical Thin Films, Second Edition (2002).
[9] H. K. Pulker, Coatings on glass, 2nd edition, Elsevier (1999).
[10] P. J. Martin, H. A. Macleod, R. P. Netterfield, C.G. Pacey and W.G. Sainty, Appl. Opt. 22, 178 (1983).
[11] W. C. Herrmann and J. R. McNeil, Proc. SPIE, Vol. 325:101 (1982).
[12] D. T. Wei, Appl. Opt. 28, 2813 (1989).
[13] S. K. Pandey, S. K. Pande, U. P. Deshpande, V. Awasthi, A. Kumar, M. Gupta, S. Mukherjee, Semicond. Sci. Technol., 28:085014 (2013).
[14] J. A. Dobrowolski, St. Browning, M. Jacobson, and M. Nada, Appl. Opt. 41, 3039 (2002).
[15] J. Shao, Ch.7, Laser Induced Damage in Optical Materials, CRC Press (2015).
[16] J. W. Arenberg, Ch.7, Laser Induced Damage in Optical Materials, CRC Press (2015).
[17] Alexi Alxandrovski et. al., Proc SPIE, Vol. 7193, 71930 D-3 (2009).
[18] C. J. Stolz and F. Y. Genin, Optical Interference Coatings, Springer (2003).
[19] C. Mukherjee, K. Rajiv, B. N. Upadhyaya, P. Misra, S. M. Oak and J. K. Mittal, 19th National Laser Symposium (NLS-19), RRCAT, Indore, Dec. 01-04, 2010.
[20] C. Mukherjee, S. Thakur, K. Rajiv, R. B. Tokas, N. K. Sahoo, L. Abhinandan, 20th National Laser Symposium (NLS-20), Chennai, Jan. 09-12, 2012.
[21] C. Mukherjee, K. Rajiv, V. V. V. Subrahmanyam, N. S. Benerji, 32nd DAE-BRNS National Laser Symposium NLS-32, RRCAT, Indore, Jan. 29- Feb. 01, 2024.
[22] C. Mukherjee, A. Biswas, K. Rajiv, D. Raghunathan, V. V. V. Subrahmanyam and N. S. Benerji, 32nd DAE-BRNS National Laser Symposium NLS-32, RRCAT, Indore, Jan. 29- Feb. 01, 2024.
[23] C. Mukherjee, K. Rajiv, V. V. V. Subrahmanyam & N. S. Benerji, 31st DAE-BRNS National Laser Symposium NLS-31, IIT Kharagpur, Kharagpur, Dec. 3-6, 2022.
[24] C. Mukherjee, A. Joseph, K. Rajiv and U. Nundy, Eighth International Conference on Optoelectronics, Fiber Optics and Photonics, Photonics-2006, Hyderabad, India, Dec. 13-16, 2006.
[25] Olaf Stenzel, Optical coatings, materials aspect in theory and practice, Springer, Vol. 54 (2014).
[26] Alexei A. Maradudin, Structured surfaces as optical metamaterials, Cambridge University Press, (2011).

T.3: High-power, ultra-short, intense laser pulse driven acceleration and transport of energetic electrons in dense plasma

Tirtha Mandal
Laser Plasma Division
Email: tirtham@rrcat.gov.in

Abstract
A comprehensive investigation on energetic fast/hot electrons (energy: 100s keV - several MeV) generation and transport through dense matter in ultra-short (tens of fs) duration laser pulse interaction with thin (few μm) metal foil targets is presented. Through direct fast electrons as well as indirect x-ray emission measurements, *JxB* mechanism of plasma electrons acceleration applicable in ultra-short intense laser pulse regime has been shown conclusively. The study addresses some important issues for the first time related to fast electrons energy, its dependence on pre-plasma scale length, demonstration of superponderomotive acceleration of electrons and counterintuitive polarization dependence for *JxB* heating. Laser to fast electrons conversion and transport processes were investigated using various x-ray emission measurements. In addition to direct relevance in generation of energetic electrons and x-ray radiation, the study is of significance for proton/ion acceleration from rear of thin foil target, warm dense matter and fusion related aspects.

1. Introduction

The invention of high-power pulsed lasers in last few decades have given us the opportunity to study the plasma in extreme condition similar to astrophysical objects [1,2]. Particularly the invention of mode-locking and chirped pulse amplification (CPA) technique by D. Strickland and G. Mourou [3] made it possible to generate ultrashort pulses of tens of femtosecond (fs) duration with peak laser power from several terawatt (TW) to petawatt (PW) levels. When such laser pulse is focused to a size of few μm using off-axis parabolic mirror, it yields an enormous intensity (I) in the range of ~10^{18}-10^{22} W/cm^2, leading to creation of plasma under extreme conditions. Due to extremely high electric field (Giga to Tera Volt per meter) created at the plasma, electrons and protons are accelerated to very high energy (~ keV to tens of MeV) from the interaction region. The study of energetic electrons generation and transport in dense solid is a subject of research investigation for various potential applications including laser driven fast ignition approach to inertial confinement fusion [4], proton and ion acceleration [5] to tens of MeV energy for practical applications including cancer therapy, creation of high brightness, ultrashort broadband x-ray sources[6] and creation of warm dense matter.

2. Ultra-short, ultra-high intensity laser plasma interaction physics

A schematic of laser matter interaction and subsequent energetic particle generation is shown in Figure T.3.1(a). Laser pulse is focused using suitable optics on thin foil targets. The tiny focal spot (few μm diameter) leads to ultra-high peak laser intensity (>10^{19} W/cm^2) on the target, leading to plasma formation by the foot of the laser pulse. In laser solid (dense plasma) interaction, different laser absorption mechanisms [2] are applicable, viz., resonance absorption, vacuum heating and *JxB* heating[7] for the generation of relativistic fast electrons. The absorption mechanisms are governed by the laser and plasma parameters and are summarized in Figure T.3.1(b). For example, at relativistic laser intensity (I >10^{18} W/cm^2), *JxB* heating is most dominant, as the electrons oscillating along the laser electric field direction get pushed by the *vxB* force along the laser propagation direction. Understanding the laser plasma coupling at such extreme condition is a unique research problem, which leads to generation of energetic electrons in the range 10s of MeV.

Next, fast electrons generated at front surface propagate through overdense medium and encounters complex transport phenomena as shown in Figure T.3.1(c). In cold solids, a strong electric field is generated, which inhibit fast electron penetration in target [2]. Further, huge magnetic field (~MG) is also generated, which tries to pinch the beam. In thin foil targets, the escape of energetic fast electrons from front and rear surfaces creates a strong sheath electric field [8] (~TV/m), which is responsible for accelerating proton. Improvement in electron flux and energy leads to the generation of energetic proton with higher energy. Next, due to the strong sheath fields, fast electrons reflux within the target, known as refluxing [9,10]. Further, this process can result in relatively higher electron energy and temperature [11-13] through 're-acceleration' of electrons by laser pulse. Next, fast electrons while propagating through solid produces bremsstrahlung and x-ray line radiations, which are used as a reliable diagnostic for fast electrons studies. Understanding the transport phenomena in solid will help in improvement of overall beam quality of electrons and proton beams apart from their importance in laser driven fusion approach.

Mostly, for fast electron generation and transport studies, metal targets are used. However, fast electron studies in transparent and dielectric mylar (polyethylene terephthalate) target also attract special attention due to their low electrical conductivity resulting in complex electron transport properties [2]. Further, with such targets, being transparent, Cherenkov radiation imaging can also be used to investigate fast electron transport. However, it has been observed that in insulator mylar target, the fast electron and K_α conversion efficiency is low as compared to metal target due to electric field inhibition inside the target material. Therefore, it is important to explore the techniques for improving the electron flux and energy in mylar target in order to use such targets for fast electron transport studies.

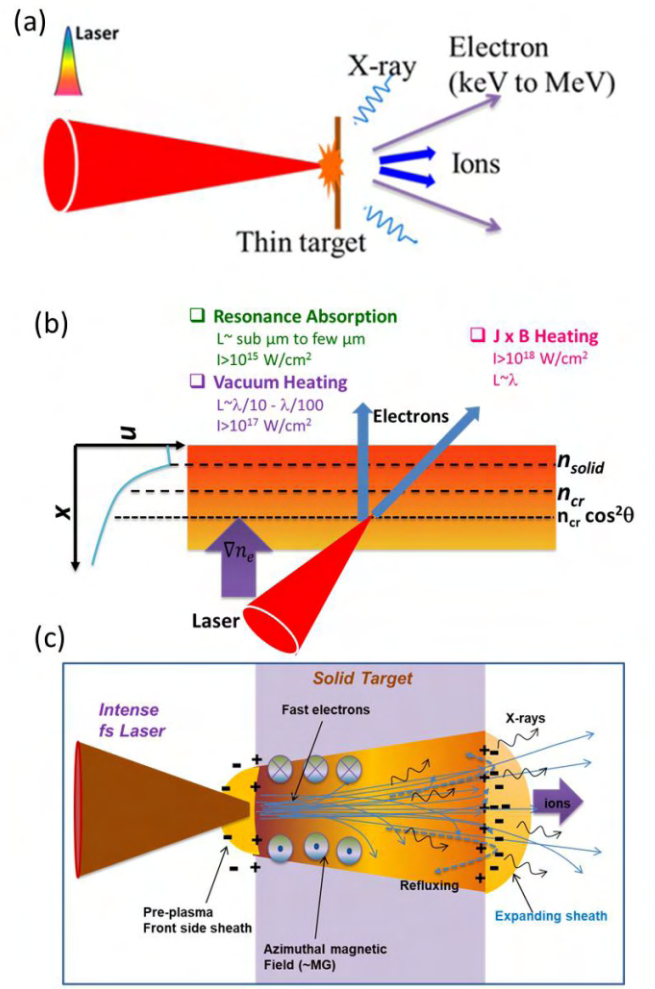

Fig. T.3.1: (a) Schematic of ultra-short ultra-high laser foil interaction and energetic particle generation, (b) different absorption mechanisms for different intensity (I) and pre-plasma density scale length (L) regime, and (c) schematic of fast electron transport through solid density matter.

3. Experimental setup

The schematic of experiment setup for fast electron angular and spectral distribution measurement is shown in Figure T.3.2(a). The ultrashort (~25 fs), high power Ti:sapphire laser (150 TW laser system) was focused using off-axis parabolic mirror to few micrometer focal spot on the thin metal foil target at oblique incidence (10°-60°) yeilding intensity of ~1 - 7x10^{19} W/cm^2. The fast electrons emitting from the interaction region were detected using DRZ setups made up from a combination of Gd_2O_2Si:Tb phosphor screen (trade name: DRZ High) and CCD cameras (14 bit PCO-Pixelfly). Three such setups (DRZ-1, DRZ-2 and DRZ-3) were used to measure the angular distribution over a wide angular range around the laser axis as shown in Figure T.3.2. The phosphor screen was shielded from ions, plasma light and low energy x-rays using Al filter. The average charge of the escaped electrons was estimated from the integrated CCD count using calibration of phosphor. Energy spectrum of the electron beam was measured using magnetic spectrograph. The spectrograph consists of a rectangular dipole magnet (length: 5 cm, pole gap: 5 cm) and a phosphor screen-CCD combination as a detector. The actual optical and mechnaical setup including the large size off-axis parabolic mirror, folding mirror, remotely controlled motorized target positioning system, etc. used inside the experimental chamber are shown in Figure T.3.2(b)

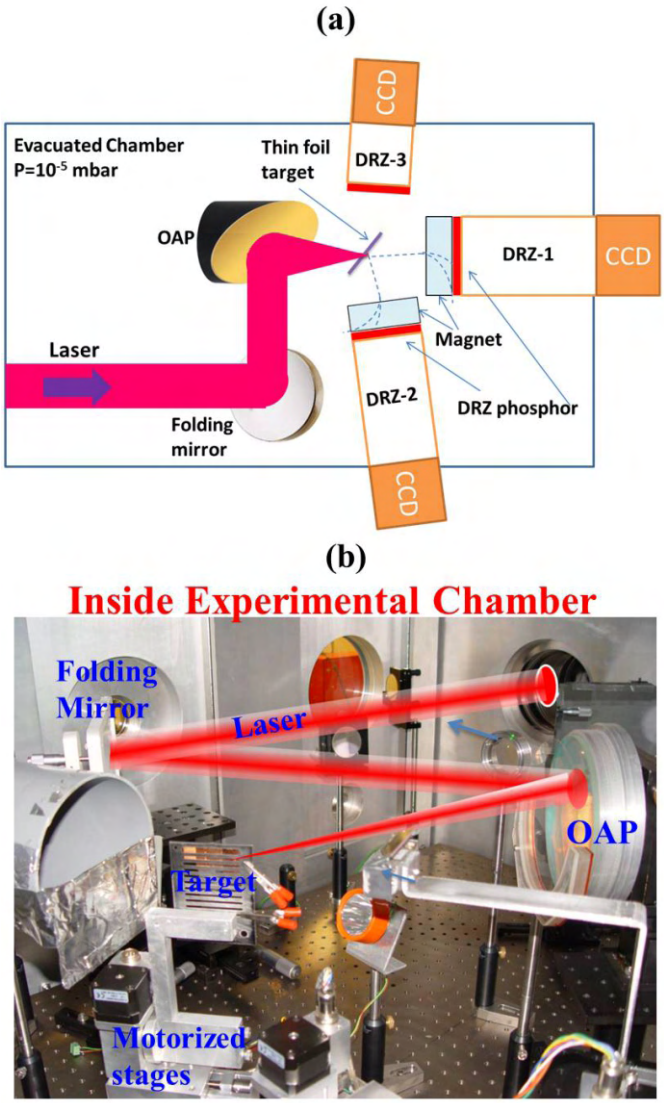

Fig. T.3.2: (a) Schematic for experimental setup for fast electron angular and spectral distribution study. Three phosphor screen-CCD camera setups were placed around the interaction region. For enegy distribution measurement, magnets were placed infront of the phosphor screens and (b) actual optical and mechnical setups inside the experimental chamber containing the off-axis parabolic mirror (OAP), target and motorized stages, etc.

Investigations were performed with peak intensity of ~1 - 7x10^{19} W/cm^2 using 150 TW Ti:sapphire laser system. The peak intensity was achieved by focusing pulse energy of ~0.16 - 2.2 J with duration of ~ 25 fs (FWHM) to small focal spot size of about few μm (FWHM). The amplified spontineous

emission (ASE) intensity contrast at 1 ns prior to fs pulse was measured to be <$2x10^{-10}$. Mostly, thin metal foils of Cu (thicknesses 2 - 100 µm) were used as target. Laser incidence angle with respect to target normal varied from ~10° to ~ 60° during the experiment by rotating the target with respect to laser axis in the incidence plane. The peak laser intensity was varied by three different methods: (i) by reducing the laser pulse energy, (ii) increasing the focal spot size, and (iii) increasing the laser pulse duration during the experiment. Laser polarization was changed from *p*- to *s*- by inserting a half wave plate in the laser beam path after the pulse compressor unit.

3.1. JxB heating and counterintuitive polarization dependence of fast electrons

First, the study of fast electron generation from thin metallic foils in oblique incidence interaction was carried out [14]. The measurements were performed for wide range of parametric variations, viz., laser intensity (~0.8 to $7x10^{19}$ W/cm^2), polarization (*p* and *s*), incidence angle (~20° - 60°), pulse duration (~ 25 fs to ~ 1300 fs), focal spot size (~ 5 µm to ~ 255 µm), pre-plasma scale length and target thickness (~ 2 µm to ~ 100 µm). Energetic electron beams (charge: ~0.3 - 2 nC, maximum energy ~ 1 to ~ 8 MeV for I ~ 1 - $7x10^{19}$ W/cm^2) were observed along laser propagation direction as shown in Figure T.3.3. Further, electron beams (charge: ~ 30 - 115 pC, maximum energy ~1 to ~3 MeV for I ~1 - $4x10^{19}$ W/cm^2) in the transverse direction was also observed (Fig. T.3.3(a)). Emission of electrons along laser direction in such high contrast condition indicates clear demonstration of *JxB* mechanism. Electron beam along laser transverse direction indicates the role of laser electric field in electron acceleration along polarization direction. Simultaneous emission of electrons in laser propagation and transverse directions has been observed for the first time due to unique interaction condition.

Energy spectra analysis (Fig. T.3.3(b)) showed that the forward electrons have less temperature (e.g., ~ 0.43 MeV at I ~$4x10^{19}$ W/cm^2) than ponderomotive scaling (~1.75 MeV), which is counterintuitive in nature. The reasons were found out to be unique interaction condition occurring at sharp density plasma and energy loss during escaping process at the rear surface [14].

Next, counterintuitive observation of strong polarization dependence of fast electrons was observed, e.g., electron flux reduced to about 4 times and maximum energy reduced from ~3 MeV to ~1 MeV on changing polarization from *p*- to *s*- at I ~$4x10^{19}$ W/cm^2 as shown in Figure T.3.3(a) and T.3.3(b). This contrary behaviour suggests role of pre-acceleration of electrons by polarization dependent mechanism in the rising part of the laser pulse [14]. The polarization dependence of electrons vanished in presence of longer scale length pre-plasma.

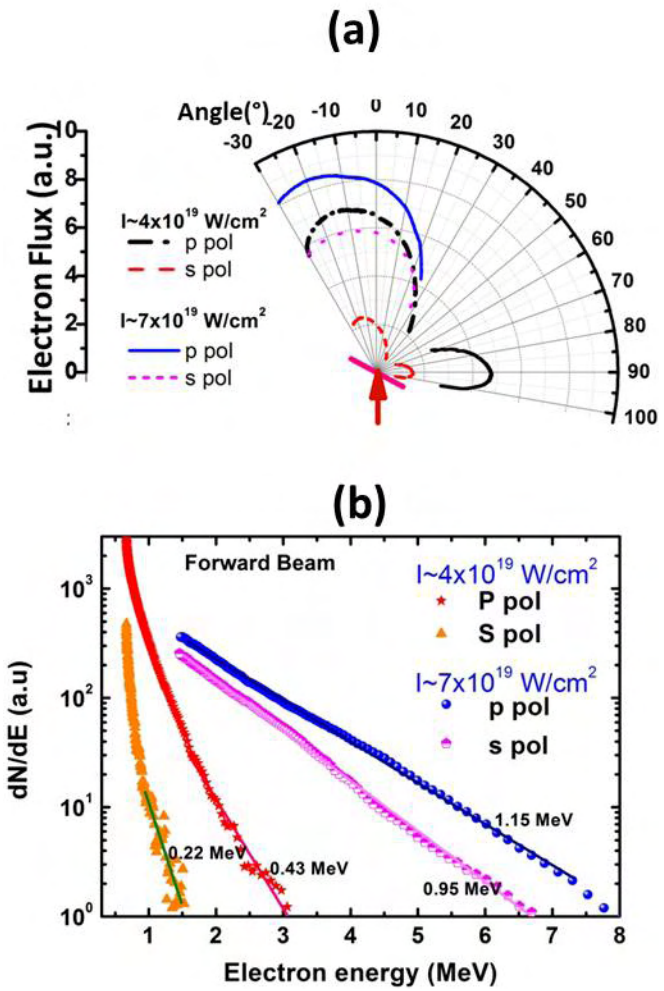

Fig. T.3.3: (a) Spatial profile of fast electrons in forward and transverse directions for p and s polarization and (b) electron energy spectrum at intensities of ~$4x10^{19}$ W/cm^2 and ~$7x10^{19}$ W/cm^2 for both the polarizations.

Further, the refluxing and reacceleration phenomena of electrons was inferred by comparing the flux of escaped electrons as a function of intensity varied by changing laser pulse energy, pulse duration and focal spot size and also from thickness variation study [15]. It was observed that in all methods of changing laser intensity, the overall charge, maximum energy and temperature reduces with decrease in laser intensity. However, the rates of decrement in three methods are different. In case of laser focal spot variation, the decrease rate is slowest whereas for pulse duration variation, the decrease rate is in between of laser pulse energy variation and focal spot variation. The propagation of fast electrons inside target foil and their escaping from targets is strongly affected by refluxing phenomena. Along with this, reacceleration of electrons can also happen, which can result in relatively higher electron energy and temperature. The condition for reacceleration is that the laser pulse duration has to be larger than twice the electron traverse time through the

target foil, so that back reflected electrons can get reaccelerated again by the laser field present at the front surface. The reacceleration of electrons was evident in the observation showing higher temperature electrons in thinner foils. Next, hard x- ray (>22 keV) angular distribution measurement and laser energy absorption measurements were also performed, which corroborates the fast electron experimental results.

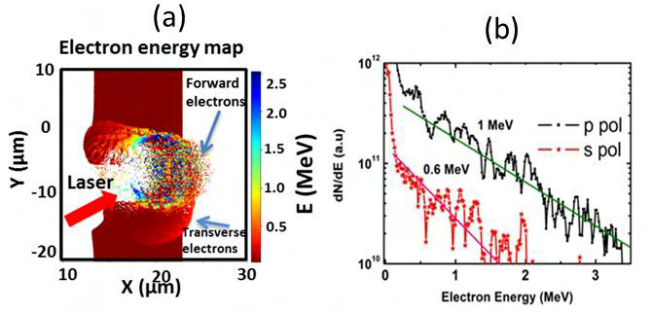

Fig. T.3.4: 2D PIC simulation results: (a) electron energy map clearly showing the forward and transverse electron emission and (b) energy spectra of the forward beam for p- and s-polarization at intensity of $2x10^{19}$ W/cm^2.

2D particle-in-cell (PIC) simulations were also performed to understand the experimental results at intensity of $2x10^{19}$ W/cm^2 as shown in Figure T.3.4. The angular distribution of electrons of different energy is shown in Figure T.3.4(a), which clearly shows the forward accelerated electrons produced from *JxB* mechanism along with the transverse low energy electrons. The strong polarization dependence of forward electrons was also replicated in simulation showing more flux and more energy for *p*- polarization (Fig. T.3.4(b)).

3.2 Superponderomotive acceleration of fast electrons

Fast electron generation in presence of larger pre-plasma scale length was investigated using an additional pre-pulse beam irradiating the target at different delays [15]. More flux and high energy electrons were obtained in longer scale length. The maximum energy (and temperature) increased from ~3 MeV (~0.35 MeV) to ~6.5 MeV (~1 MeV) with introduction of pre-pulse at 0 ns and further up to ~ 16 MeV (~2.86 MeV) for - 4 ns delay before the main pulse. Most importantly, at larger scale length (L/λ>>1, L: scale length and λ: laser wavelength) pre-plasma condition created using pre-pulse at delay of >1 ns, fast electron temperature beyond ponderomotive limit was observed (Fig. T.3.5). The temperature scales with scale length as $T \propto L^{0.59}$ and shows a saturation effect at longer scale length. The overall results indicate a gradual change in absorption mechanism from *JxB* heating at sharp density interaction to stochastic heating at large pre-plasma scale length generating super-ponderomotive electrons through efficient acceleration from the standing wave structure pattern. The experimental results were also verified through PIC simulation, where increase in electron energy with increase in scale length was observed.

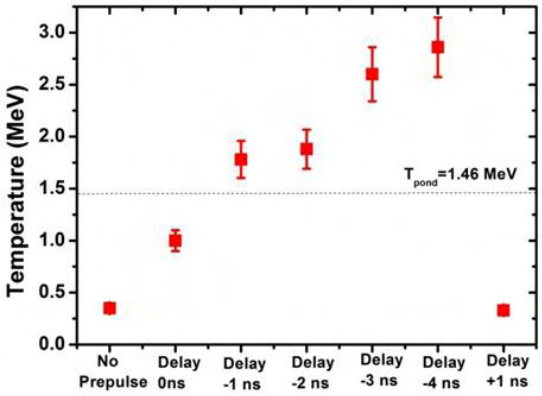

Fig. T.3.5: Fast electron temperature is plotted for different pre-pulse delay from 1-4 ns. Main pulse: energy: 1.2 J, duration: 25 fs, intensity: $3x10^{19}$ W/cm^2. pre-pulse: energy: 150 mJ, 600 ps, $1x10^{13}$ W/cm^2.

4. Investigation of fast electrons using dielectric targets

Next, fast electron study was performed in transparent dielectric and layered dielectric target to investigate the core fast electron transport related issues such as electric field inhibition, sheath field dynamics, etc.

4.1 Probing electric field inhibition using dielectric transport layer

First, we performed the fast electron generation from bare mylar (polyethylene terephthalate) foil and its comparison with metallic Cu foil. Figure T.3.6 shows the electron energy spectrum for bare mylar foil and its comparison with Cu. The maximum energy for mylar extends upto ~0.4 MeV with a fitted electron temperature of ~0.07 MeV. In comparison, for Cu foil (7 μm) has maximum energy of ~1 MeV with temperature of ~0.12 MeV. Therefore, the maximum energy and temperature for bare mylar is ~2.5X and ~1.7X smaller, respectively as compared to Cu foil. Similarly, the total charge of electrons with energy >70 keV for bare mylar was ~6.6 X smaller than the Cu foil. The dominant reason for such reduction of electron charge and energy is found to be the electric field inhibition during electron transport through matter due to dielectric nature of the mylar, which is absent in Cu.

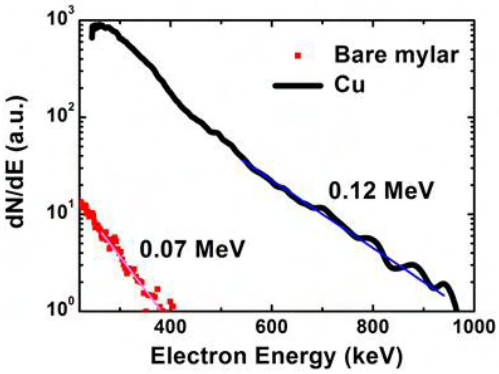

Fig. T.3.6: Energy spectrum of electrons for bare mylar (8 μm) and Cu (7 μm), intensity of ~$1x10^{19}$ W/cm^2, angle of incidence: 30°.

4.2 Improvement in electron energy and probing sheath dynamics using layered dielectric targets

Next, a novel technique was proposed for studying sheath dynamics by creating plasma using metal coating on the front and rear surface of transparent mylar target [16]. The electron flux and energy increased (flux ~1.8 X and energy ~2.5X at I ~1x10^{19} W/cm^2) when a thin (~50 nm) metal (Al) coating was applied in the front of mylar compared to bare mylar as shown in Figure T.3.6. This enhancement is explained from the larger laser absorption in longer pre-plasma in critical density region formed for metal coated mylar. Self-focusing of laser pulse in extended pre-plasma also helps in increase of laser intensity resulting in improvement in electron flux and energy.

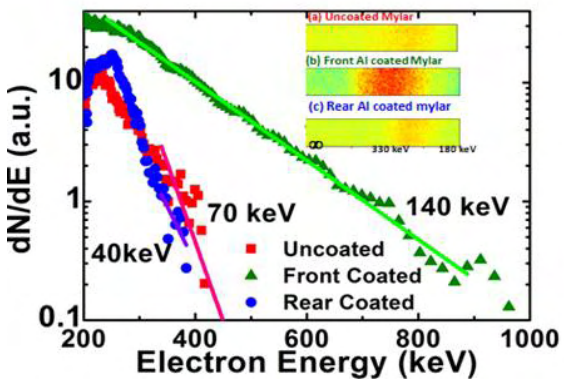

Fig. T.3.7: Fast electron spectrum for uncoated, front Al coated mylar and rear Al coated mylar.

Further, electron flux increased (~1.4 X at I ~1x10^{19} W/cm^2) for rear Al coated mylar but without any change in maximum energy as shown in Figure T.3.7. As the fast electron energy is decided mostly by the front surface pre-plasma condition, the energy was unchanged in case of rear Al coated mylar. However, the enhancement of electron charge is explained by considering the presence of pre-plasma at rear, leading to delay in formation of rear sheath field resulting in larger escaped electron flux. The study brings out important aspects of fast electron generation using a fs laser system by using a layered target design, which could be of interest to control the fast electron generation.

5. Improvement in electron beam properties utilizing grazing incidence interaction

Generally, fast electron generation depends on various laser-solid interaction parameters and broad angular distribution of electrons peaking along laser propagation direction was observed with wide divergence of ~80º - 90º. However, for practical use of such electrons beams, improvement in electron parameters are required particularly the electron beam divergence. It has been found that in the presence of self-induced quasistatic electric and magnetic fields, fast electrons emission direction as well as divergence can be strongly modified. At grazing incidence interaction (incidence angle ~70º), the generation of surface fields and interaction of electrons with the surface field can be enhanced leading to a highly collimated and directional electron beam to be useful for different applications. Further, it is also important to understand the generation and transport of fast electron in the context of hollow re-entrant cone target proposed for the fast ignition experiment as in this case electrons are generated in cone sidewalls at grazing incidence.

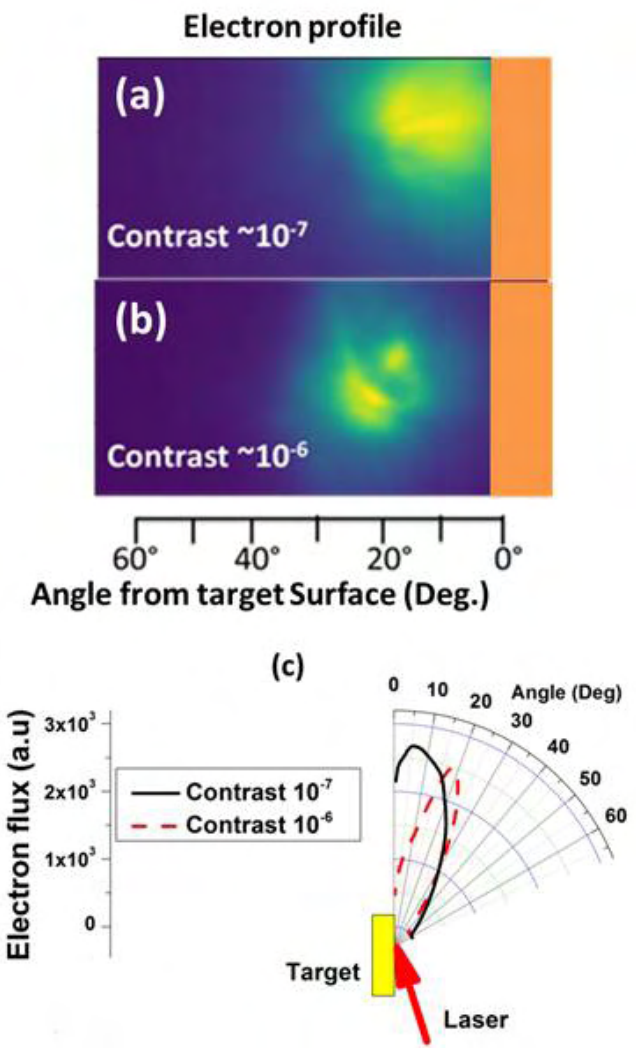

Fig. T.3.8: Typical electron beam profiles as recorded on phosphor screen for (a) contrast of 10^{-7} and (b) contrast of 10^{-6}, and (c) polar plot of electron beam in the incidence plane for the two contrast cases.

First, the grazing incidence interaction study was performed [17] at laser intensity of ~1x10^{18} W/cm^2 as shown in Figure T.3.8. The fast electrons were observed along target surface direction for small pre-plasma scale length at better contrast of ~10^{-7} (Fig. T.3.8(a) and T.3.8(c)). However, with the increased pre-plasma scale length (contrast ~10^{-6}), the collimated (divergence angle ~20^0) fast electron emission was obtained along the specular direction (Fig. T.3.8(b) and T.3.8(c)). The emission direction further moves towards the target normal direction with further increase in pre-plasma scale length. The electron characteristics including emission direction, divergence angle and charge of the fast electron was found to depend strongly on the target material and pulse duration

whereas showed weak dependence on the polarization of laser beam. The electron beam charge was maximum in Si target, which could be attributed to the higher laser absorption depth in the material.

The experimental results were understood considering the role of quasistatic electric and magnetic fields present on the target surface. The 1-D hydrodynamic simulation using HELIOS [18] estimated the scale length of plasma density profiles for different ASE contrast, extent and for different target materials and was useful in understanding the experimental results. The 2D PIC simulation using EPOCH [19] was also run for two different pre-plasma scale lengths of 1 μm and 4 μm, which showed electrons are ejected along the surface direction for smaller pre-plasma scale length.

Next, the grazing incidence study was extended in thin foil target at higher intensity of ~7x10^{19} W/cm^2. Here, we obtained electron beam both along front and rear surface as shown in Figure T.3.9(a) and T.3.9(b). Compared to oblique incidence interaction, the rear electron beam was more inclined towards target surface direction with higher charge (~ 4±0.6 nC) and reduced divergence (~ 65°±5°). On the other hand, the front escaped electrons were highly collimated (~7º) and guided along the target surface direction showing the influence of quasistatic surface fields.

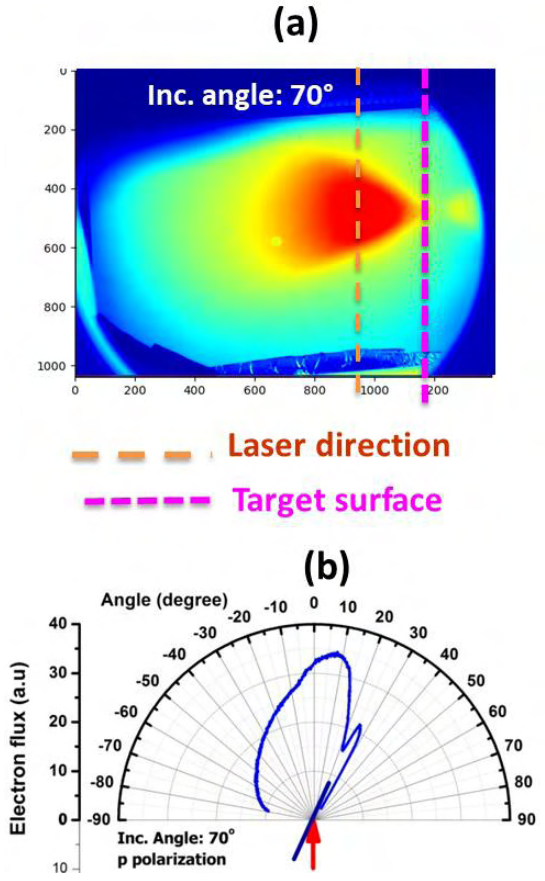

Fig. T.3.9: Electron (a) beam profile and (b) polar plot of fast electrons for 45° and 70° incidence angle.

6. Fast electron transport study through x-rays measurements

By measuring the fast electrons directly, we mostly infer interaction dynamics of escaped electrons. To understand the transport by the confined electrons, x-ray measurements are very important. Some important aspects such as laser to fast electrons conversion efficiency, applicable absorption mechanism, refluxing, reacceleration, etc. can be investigated by measuring flux of x-ray radiation.

High resolution x-ray spectroscopic measurements are generally carried out for investigation of above mentioned aspects. Crystal spectrographs are generally used for the measurement of high resolution x-ray line radiations. Further, the knowledge of x-ray source size is useful for finding the fast electron divergence angle in dense solid. The x-ray source size (akin to the electron source size) measurement can be performed using different techniques such as x-ray shadowgraphy using the knife-edge technique or by monochromatic 2D K_α imaging.

First, 1D imaging [20] of broadband x-ray source size was performed using knife edge shadowgraphy technique. The front as well as rear side source size was measured. Further, the effect of laser intensity, pulse duration and ASE contrast on x-ray source size was studied to investigate the probable role of these laser parameters on electron divergence inside target material. Fast electron divergence was measured using specific layered target consisting a propagation layer and a tracer layer. A half divergence angle of ~37°±10º was estimated by measuring the rear side x-ray source sizes with different thicknesses at a laser intensity of ~1.3×10^{18} W/cm^2.

Next, 2D imaging of monochromatic Cu K_α source from target front and rear surface was performed using a spherically bent quartz crystal spectrograph at a laser intensity of 7x10^{19} W/cm^2. High resolution spherically bent quartz crystal spectrograph was used to image Cu $K_{\alpha 1}$ (8.047 KeV) source size at the target front and rear surface. The schematic of the setup is shown in Figure T.3.10(a). A spherically bent quartz crystal and x-ray CCD camera was used in the spectrograph in an appropriate geometry with a magnification of ~8.1. For front side imaging, incidence angle was kept at ~30°, such that the crystal faces the target front surface and interaction region in the normal direction and therefore will provide near circular x-ray images. For rear side imaging, the target was rotated in clockwise direction keeping the crystal position fixed such that the crystal faces the rear surface. However, the incidence angle was limited to ~70° in this case. Front side source size was calculated to be ~38 ± 2 μm (Fig. T.3.10(b)) whereas the rear side source size was estimated be ~47 ± 2 μm and 58 ± 4 μm for Cu 7 μm and Cu 25 μm foil, respectively. A fast electron half divergence angle of ~17° inside target material was calculated from the fitting of rear side source sizes. Such small divergence indicates the acting role of self-generated mega gauss magnetic fields on collimating fast electrons at high laser intensity.

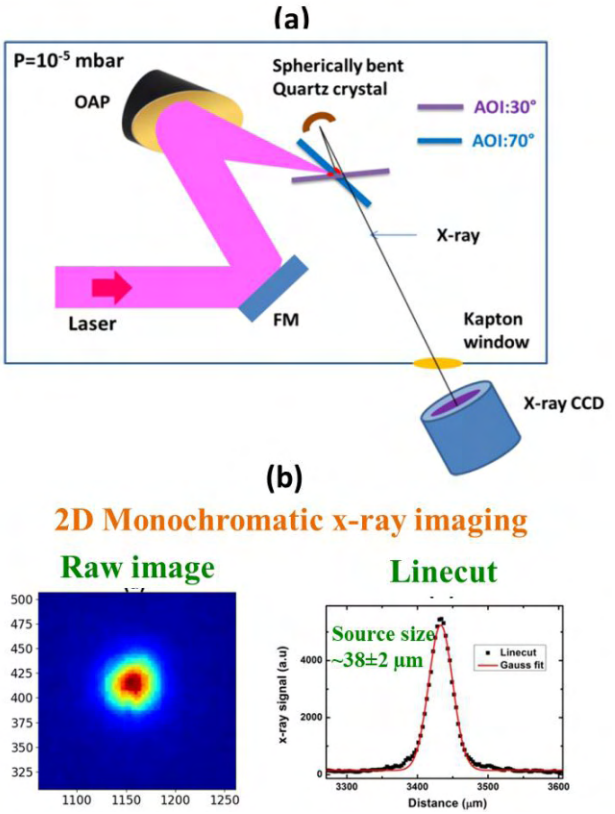

Fig. T.3.10: (a) Experimental setup for monochromatic magnified x-ray imaging for transport studies and (b) raw x-ray images with linecut for source size estimation.

Next, fast electron generation and transport was studied [21] by measuring high resolution Cu K_α lines (Fig. T.3.11) using crystal spectrograph at intensity of ~1x10^{19} W/cm^2 for understanding the generation and refluxing of the electron in subsequent transport through dense matter. Figure T.3.11(a) shows the schematic of the experimental setup for the x-ray measurement. The laser beam of ~30 fs duration was focused by an off-axis parabola (f/ 2.6) on Cu foil at an incidence angle of ~10^0 - 50^0. The intensity on target plane was estimated to be ~1x10^{19} W/cm^2. A cylindrically bent HAPG crystal spectrograph was used to measure high resolution Cu K_α x-ray line emission spectrum in the spectral range of 8.0 – 8.1 keV. Indirect detection x-ray CCD camera was used as detector.

Figure T.3.11(b) shows the spectra of Cu k shell lines containing $K_{\alpha1}$ and $K_{\alpha2}$ for two different polarizations. The conversion of laser energy into K_α radiation increases with the laser intensity as ~$I_L^{0.9}$ and conversion of the order of ~10^{-5} was obtained. The experimentally observed conversion scaling law is in broad agreement with modified model with refluxing considering JxB heating mechanism for fast electron acceleration. The study of x-ray conversion with laser pulse duration demonstrates the role of reacceleration of confined electron after getting reflected from target rear surface. The effect of the transport layer over the target in reducing the sheath field strength was demonstrated. The study with changing the laser polarization shows the signature of the pre-acceleration of electron in the JxB heating by polarization dependent mechanism. The study is useful to identify the parametric regime for increasing the K_α x-ray conversion by maximizing the refluxing efficiency in thin foil target.

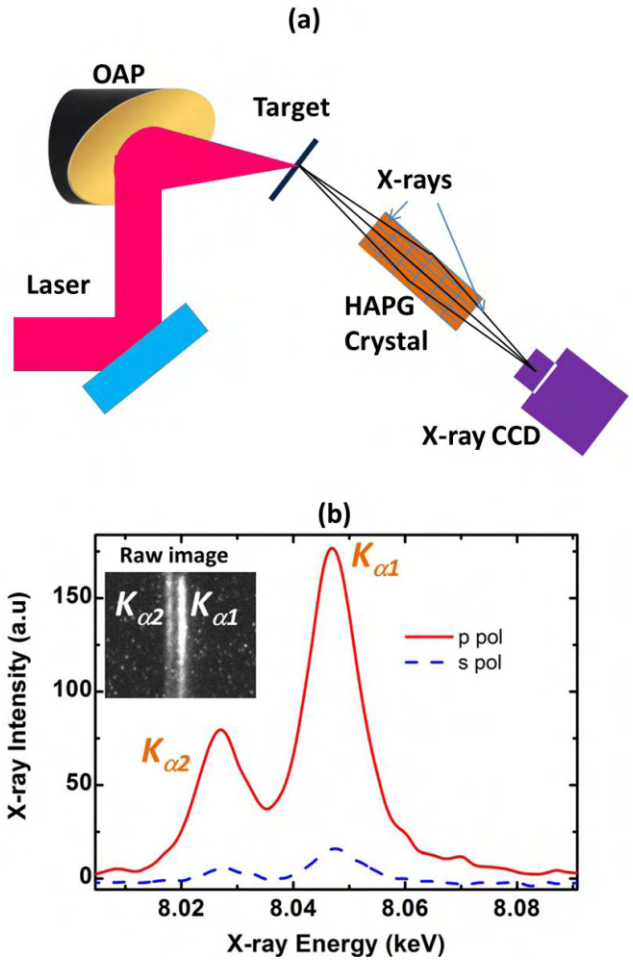

Fig. T.3.11: (a) Experimental setup for high resolution x-ray measurements using HAPG crystal spectrograph and (b) x-ray spectrum from Cu foil for p- and s- polarization at I ~1 x 10^{19} W/cm^2.

7. Conclusion

In conclusion, ultrashort, intense laser plasma interaction was explored through measurement of energetic MeV fast electrons and x-rays. Multiple in-house electron and x-ray diagnostics were developed for the study. The dominance of less explored JxB mechanism was demonstrated in the interaction of ultra-short pulses with foil targets at I~1 - 7x10^{19} W/cm^2. Transverse electron beams along laser polarization direction were found due to ponderomotive scattering. Contrary observation of strong polarization dependence of JxB mechanism was explored and is explained from pre-acceleration in the rising part of laser pulse. The results were supported through detailed PIC simulation, laser absorption and x-ray measurements. Extensive study on electron energy scaling with pre-plasma scale length reveals

that for sharp scale length, electron temperature was lower than the ponderomotive limit whereas for extended scale length, it even produces super-ponderomotive temperature through changes in absorption mechanism in stochastic heating regime. Complex transport phenomena such as refluxing and re-acceleration were clearly demonstrated. Next, electron flux and energy enhancement were obtained using a novel use of simple metallic coated transparent mylar target. Important revelations about the ultrashort rear sheath dynamics was probed by creating a rear plasma using rear metal coating on mylar. Through unique grazing incidence interaction, surface acceleration was demonstrated with high flux and less divergence, which can be a seed for potential practical uses. Finally, the information of refluxed fast electrons confined within the target was obtained through x-ray measurements study, which reveals the important fast electron properties inside target complementing the direct fast electron measurements. The results are very important towards the generation of high charge (nC), high energy (tens of MeV) electron beam, understanding of associated MeV proton beam as well as high flux, hard (keV to MeV) x-ray source for dense plasma and object radiography applications.

Acknowledgement

The present research work has been carried out under the guidance of Dr. A. Moorti, Head, Advanced Plasma Acceleration Section & Laser Electron Acceleration Lab. The author would like to thank Dr. J. A. Chakera, Head, Laser Plasma Division, for valuable suggestions and constant support during the research work. The author sincerely thanks technical advisor Dr. Vipul Arora, for his invaluable advice and suggestions. The author also expresses acknowledgement to Dr. A. Upadhyay for providing PIC simulations support. The author is thankful to Shri R. A. Khan, Shri Ankit, Shri R. A. Joshi and Shri S. Meena for providing laser support and Shri R. P. Kushwaha, Shri S. Sebastin, Shri K. Meena, Shri K. C. Parmar and Shri L. Kisku for providing mechanical support during experiment.

References

[1] P. McKenna, D. Neely, R. Bingham, and D. Jaroszynski, editors, Laser-Plasma Interactions and Applications (Springer International Publishing, 2013).
[2] P. Gibbon, Short Pulse Laser Interactions with Matter (Imperial college press, London, 2005).
[3] D. Strickland and G. Mourou, Opt. Commun. 56, 219 (1985).
[4] M. Tabak et al., Phys. Plasmas 1, 1626 (1994).
[5] A. Macchi, M. Borghesi, and M. Passoni, Rev. Mod. Phys. 85, 751 (2013).
[6] H. Schwoerer et al., Phys. Rev. Lett. 86, 2317 (2001).
[7] S. C. Wilks, W. L. Kruer, M. Tabak, and A. B. Langdon, Phys. Rev. Lett. 69, 1383 (1992).
[8] D. R. Rusby et al., High Power Laser Sci. Eng. 7, (2019).
[9] M. N. Quinn et al., Plasma Phys. Control. Fusion 53, 025007 (2011).
[10] R. J. Gray et al., New J. Phys. 20, 033021 (2018).
[11] H. Chen and S. C. Wilks, Laser Part. Beams 23, 411 (2005).
[12] A. J. Mackinnon et al., Phys. Rev. Lett. 88, 215006 (2002).
[13] A. Yogo et al., Sci. Rep. 7, 1 (2017).
[14] T. Mandal, V. Arora, A. Moorti, A. Upadhyay, and J.A. Chakera, Phys Plasmas 30, 023106 (2023).
[15] T. Mandal et al., Manuscript under preparation (2022). Also presented in 36th PLASMA conference, Dec 13-15, 2021, BIT, Mesra.
[16] T. Mandal, V. Arora, A. Moorti, A. Upadhyay, and J. A. Chakera, Phys. Plasmas 26, 013103 (2019).
[17] T. Mandal, V. Arora, B. S. Rao, A. Moorti, A. Upadhyay, and J. A. Chakera, Phys. Plasmas 26, 043105 (2019).
[18] J. J. MacFarlane et al., J. Quant. Spectrosc. Radiat. Transfer 99, 381–397 (2006).
[19] T. D. Arber et al., Plasma Phys. Controlled Fusion 57, 113001 (2015).
[20] T. Mandal et al., Appl. Phys. B 119, 281 (2015).
[21] T. Mandal, V. Arora, A. Moorti, and J. A. Chakera, Plasma Phys. Control. Fusion, 63, 095009 (2021).

A. Journal Articles

1. Abbot R.*, Bhandare A., Chaturvedi M., Dave I., George J., Khursheed M., Malik A., Pai A., Pant B.C., Raja S., Rajan C., Sharma P., ShyamSundar S., Thondapu R., Verma Y. et al.
Population of merging compact binaries inferred using gravitational waves through GWTC-3
Physical Review X, 13, 011048(1-75) (2023)

2. Abraham S.T.*, Mouni C. T.*, Albert S.K.*, Sagdeo A., Balasubramaniam K.*, Venkatraman B.*
An experimental investigation on the combined effect of plastic deformation and grain size variation on the acoustic nonlinearity parameter
Review of Scientific Instruments, 94, 024903(1-10) (2023)

3. Ahad A.*, Gautam K.*, Majid S.S.*, Dey K.*, Tripathy A.*, Rahman F.*, Choudhary R.J.*, Sankar R.*, Sinha A.K., Kaul S.N.*, Shukla D.K.*
Random magnetic anisotropy driven transitions in the layered perovskite $LaSrCoO_4$
Physical Review B, 107, 214405(1-10) (2023)

4. Ahlawat S., Mukhopadhyay P.K., Singh R., Dixit S.K., Bindra K.S.
Laser textured superhydrophilic silicon for uniform solidification and sensitive detection of water based samples using laser induced breakdown spectroscopy
Journal of Analytical Atomic Spectrometry, 38, 883-892 (2023)

5. Ahlawat S., Singh A., Mukhopadhyay P., Singh R., Dhamgaye V.P., Dixit S.K., Bindra K.S.
Analyte enrichment and sensitive detection over nanosecond laser textured stainless steel superhydrophobic surfaces
Materials Chemistry and Physics, 302, 127755(1-11) (2023)

6. Ajimsha R.S., Mahapatra A., Das A.K., Sahu V.K., Misra P.
High output power density owing to enhanced charge transfer in ZnO-based triboelectric nanogenerator
Energy, 263, 125646 (2023)

7. Alam M.A., Tiwari M.K., Devi D.*, Tripathi S.*, Trivedi A.*, Ojha S.*, Singh S., Gupta M.*
Depth profile analysis of 100 keV Ni ions in Si 〈100〉 substrate
Spectrochimica Acta B, 206, 106707 (2023)

8. Anas M.*, Jain A.*, Gupta M.*, Sagdeo A., Yusuf S.M.*, Maitra T.*, Malik V.K.*
Structural and magnetic properties of $LaVO_3$ absence of anomalous diamagnetism
Ceramics International, 49, 9672-9680 (2023)

9. Arya R.*, Bhisikar A. et al.
Next generation gamma ray shielding blocks developed using alumina industry waste
Construction and Building Materials, 273, 130895(1-11) (2023)

10. Badapanda M.K., Tripathi, A., Upadhyay R., Lad M.
High voltage DC power supply with input parallel and output series connected DC-DC converters
IEEE Transactions on Power Electronics, 38, 6764-6768 (2023)

11. Bairagi S.*, Bartwal K.S., Dhiman S.K.*, Mahajan S.K.*, Ansari G.F.*
Studies on optical and electronic characteristics of ternary zinc-tellurite glasses with varying Zn doping concentration
Materials Today Proceedings, 80, 427-433 (2023)

12. Bera G.*, Surampalli A.*, Prajapat D.*, Mal P.*, Reddy V.R.*, Kumar K.*, Sagdeo A., Das P.*, Turpu G.R.*
An additional simultaneous magnetic ordering and magneto-capacitive behavior with dielectric relaxation besides multiferroicity in $FeTe_xVO_4$
Journal of Physics: Condensed Matter, 35, 125801(1-11) (2023)

13. Bhardwaj K., Sarkar S., Ram S.P., Tiwari V.B., Mishra S.R.
A method for loading magneto-optical trap in an ultrahigh vacuum environment
AIP Advances, 13, 015108(1-5) (2023)

14. Bhattacharjee J., Gupta R.K., Singh S.D.
Assessment of bonding characteristic of β-$(Al_xGa_{1x})_2O_3$ alloys from photoluminescence and x-ray absorption near edge spectroscopy
Applied Physics Letters, 122, 152104(1-7) (2023)

15. Bhattacharjee J., Singh S.D.
Observation of mixed-mode behavior of Raman active phonon modes for β-$(Al_xGa_{1-x})_20_3$ alloys
Applied Physics Letters, 122, 112101(1-7) (2023)

16. Bhattacharya J., Chakrabarti A.
Electronic and transport properties of Heusler alloy based magnetic tunneling junctions: a first principles study
Computational Materials Science, 216, 111852(1-15) (2023)

17. Bhattacharya J., Dutt R., Chakrabarti A.
Ab-initio predictions of mechanical, electronic, magnetic, and transport properties of bulk and heterostructure of a novel Fe-Cr based full Heusler chalcogenide
Journal of Physics and Chemistry of Solids, 178, 111307(1-12) (2023)

18. Chakravarty U., Khare J., Joshi M.P., Mukherjee C.,

Singh R.
Broad band optical absorption and thermoplasmonic response from bio-inspired hierarchical
copper nanostructures fabricated by pulsed laser deposition
Optics & Laser Technology, 167, 109772(1-14) (2023)

19. Chakravarty U., Kumar A., Kuruvilla A., Asok A.*, Jain R.K., Singh R., Ekka B., Upadhyaya B.N., Bindra K.S.
Thulium-doped all-fiber laser oscillator with more than 100 W of output power at 1940 nm and study of self-pulsing behaviour
Optics & Laser Technology, 164, 109452 (2023)

20. Chandra J., Rao P.N., Rai S., Manekar M.
Effect of chemo-mechanical polishing on the surface and superconducting properties of niobium coupons: a comparative Study
Journal of Superconductivity and Novel Magnetism, 36, 777–791 (2023)

21. Changdar S.*, Ghosh S.*, Vijay K., Kar I.*, Routh S.*, Maheshwari P. K.*, Ghorai S.*, Banik S., Thirupathaiah S.*
Nonmagnetic Sn doping effect on the electronic and magnetic properties of antiferromagnetic topological insulator $MnBi_2Te_4$
Physica B, 657, 414799(1-8) (2023)

22. Chaturvedi A., Mondal P., Srihari V.*, Joshi M.P.
Visible light sensitive Au–TiO_2 nanocomposites formed by effective attachment of Au with TiO_2 nanoparticles using liquid-phase pulsed-laser ablation
Optical Materials, 138, 113732(1-7) (2023)

23. Chetia S.K., Das A.K., Ajimsha R.S., Singh R., Padhi P.S., Misra P.
Al_2O_3 barrier layer for enhancing UV to visible rejection ratio in p-Si/n-MgZnO heterojunction visible blind UV photodetectors
Physica B, 663, 415021 (2023)

24. Daiya D., Patidar R.K., Moorti A., Benerji N.S., Bindra K.S.
Online monitoring and active control of alignment errors in a tiled grating assembly using single wedge plate
Optics and Lasers in Engineering, 161, 107355 (2023)

25. Dasgupta R., Majumder S.K.
A simulation of undiagnosed population and excess mortality during the COVID-19 pandemic
Results in Control and Optimization, 12, 100262(1-15) (2023)

26. Dastider S.G.*, Abhishek R.*, Banerjee A., Haldar K.K.*, Fortunelli A.*, Mondal K.*
Does water play a crucial Role in the growth of ZnO nanoclusters in ZnO/Cu Catalyst?
Journal of Physical Chemistry C, 127, 8993-9001 (2023)

27. Deshmukh P.S.*, Yadav S., Sathiaraj G.D.*, Paul C.P.
Nano to macro-mechanical properties of laser directed energy deposited CoCrNi medium entropy alloy
Materials Today Communications, 35, 106351 (2023)

28. Dhamgaye V., Laundy D.*, Khosroabadi H.*, Moxham T.*, Baldock S.*, Fox O.*, Sawhney K.*
Alvarez varifocal x-ray lens
Nature Communications, 14, 4582 (2023)

29. Dhole V.J.*, Souframanien J.*, Reddy K.S.*, Petwal V.C.
Comparison of effectiveness and efficiency of electron beam over gamma rays to induce novel mutations in mungbean (Vigna radiata L. Wilczek)
Applied Radiation and Isotopes, 194, 110719(1-9) (2023)

30. Dutt R., Chakrabarti A.
Effect of substitution of 3d, 4d and 5d elements on structural, electronic, magnetic properties and XMCD spectra of Co-based full Heusler alloys: a DFT study
AIP Advances, 13, 1-5 (2023)

31. Dutt R., Chakrabarti A.
First-principles study to probe the effect of substitution at X and Z sites on the electronic, magnetic and transport properties of Co_2X(V, Nb, Ta)Z(Al, Ga, In, Si, Ge, Sn) Heusler alloys
Solid State Communications, 359, 115022 (2023)

32. Dutt S., Rambadey O.V.*, Sagdeo P.R.*, Sagdeo A.
Absence of presumed ferroelectricity in methylammonium lead chloride single crystals representing organic-inorganic hybrid perovskites
Materials Chemistry and Physics, 295, 127169 (2023)

33. Dwari G.*, Banik S. et al.
Large unsaturated magnetoresistance and electronic structure studies of single-crystal GdBi
Physical Review B, 107, 235117(1-11) (2023)

34. Dwivedi P.K.*, Rai A.K., Ganesh P., Ranganathan K., Bindra K.S., Dutta K.*
Effect of laser shock peening on microstructure and micro-texture evolution in high-strength low-alloy steel upon electrochemical interaction
Journal of Materials Engineering and Performance, 32, 1-17 (2023)

35. Fakhri A.A., Kant P.
Double bend achromat structure for insertion devices
Nuclear Instruments & Methods in Physics Research A, 1049, 168049(1-7) (2023)

36. Gaur A.*, Pundir V.*, Kaur R.*, Jha S.N., Bagchi V.*
Curtailing the excess eg-orbital filling of a Ni atom by enhanced interatomic charge transfer within a bimetallic bimetallic 2D metal–organic framework for the oxygen evolution reaction

ACS Applied Energy Materials, 6, 5360-5367 (2023)

37. Gayathri V.*, Amaladass E.P.*, Sathyanarayana A.T.*, Kumary T.G.*, Pandian R.*, Gupta P., Rai S.K., Mani A.*
Interfacial interaction driven enhancement in the colossal magnetoresistance property of ultra-thin heterostructure of $Pr_{0.6}Sr_{0.4}Mn0_3$ in proximity with With $Pr_{0.5}Ca_{0.5}Mn0_3$
Scientific Reports, 13, 2315(1-13) (2023)

38. Ghosal A.M.*, Gupta R.K., Chandra K.*, Bhardwaj V., Upadhyaya B.N., Ganesh P.
Laser surface melting of 304L SS: increase in resistance to transpassive dissolution and pitting corrosion
Corrosion Engineering, Science and Technology, 58, 1-14 (2023)

39. Ghosh S.*, Ghosh Haranath
As k-edge absorption at high pressures in AFeAs (A=Na/Li): first principles results
Journal of Electron Spectroscopy and Related Phenomena, 263, 147286(1-11) (2023)

40. Gopal K.*, Singh A.P.*, Kundu M.*, Upadhyay A., Varshney P.*
Mid-infrared radiation from semiconductor plasmas using extraordinary mode of lasers
Brazilian Journal of Physics, 53, 118 (2023)

41. Gopi D.*, Karthika A.*, Rajeswari D.*, Kavitha L.*, Pramod R., Dwivedi J.
Retraction: Investigation on corrosion protection and mechanical performance of minerals substituted hydroxyapatite coating on HELCDEB-treated titanium using pulsed electrodeposition
RSC Advances, 13, 10015-10015 (2023)

42. Goud B.K.*, Shinde D.D*, Kamath M.P., Kumar R.S.*, Raju S.D.V.S.J.*, Kumar K.*, Sanyal D.N.*, Rao K.D.*, Sinha S.K.*, Udupa D.V.*
Pressure tube replica imaging system for PHWR reactors based on optical coherence tomography
Annals of Nuclear Energy, 189, 109837 (2023)

43. Gupta P.K., Singh C.P., Mukhopadhyay P.K., Dixit S.K., Bindra K.S.
Vector dark–bright pulses from a ytterbium doped fiber laser mode-locked by nonlinear multimode interference
Laser Physics, 33, 045105(1-5) (2023)

44. Gupta S., Sinha M.*, Dhawan R., Jangir R., Bose A., Gupta P., Swami M.K., Modi M.H.
Study of oxidation behaviour of Ruthenium thin film after thermal annealing in oxygen environment
Thin Solid Films, 764, 139606 (2023)

45. Hegde G.S.*, Prabhu A.N.*, Chattopadhyay M.K.
Influence of indium and selenium co-doping on structural and thermoelectric properties of Bi_2Te_3 alloys
Journal of Materials Science: Materials in Electronics, 34, 1234(1-18) (2023)

46. Hinge V.K.*, Bairagi M.*, Yadav N.*, Shrivastavab B.D.*, Jha S.N., Bhattacharya D., Gaur A.*
XAFS study of mixed ligand benzimidazole copper complexes having distorted coordination geometry
Journal of Molecular Structure, 1289, 135909 (2023)

47. Hong W.*, Zhou H.*, Li Z.*, Li Y.*, Stuhr U.*, Pokhriyal A., Ghosh Haranath et al.
Interlayer coupling in the superconducting state of iron-based superconductors
Physical Review B, 107, 224514(1-11) (2023)

48. Jamal M.S.*, Gupta P., Sergeev I.*, Leupold O.*, Kumar D.*
Interface-resolved study of magnetism in MgO/FeCoB/MgO trilayers using x-ray standing wave techniques
Physical Review B, 107, 075416(1-11) (2023)

49. Jamal M. S.*, Singh S.*, Dev A.S.*, Gupta N., Gupta P. et al.
Atypical magnetism in Pt/MgO/FeCoB/Pt waveguide structure by exchanging the order of MgO and FeCoB layers
Acta Materialia, 257, 119150 (2023)

50. Jegadeesan P.*, Sen S.*, Padmaprabu C.*, Srivastava S.K., Das A.*, Amirthapandian S.*
Morphological and optical investigations on Gd_2O_3 nanostructures
Inorganic Chemistry Communications, 150, 110493 (2023)

51. Jena S.*, Choi W.Y.*, Gardner J.*, Jung M.H.*, Srivastava S.K., Verma V.K.*, Amemiya K.*, Singh V.R.*
Evolution of bulk magnetic structure in MnSi thin film: a soft x-ray magnetic circular dichroism study
Physica Scripta, 98, 075927 (2023)

52. Kamlesh P.*, Mehra P.*, Tavar D.*, Prakash S.*, Sharma R.K., Srivastava A.K.*, Paul A.*, Singh A.*
One-step high-temperature electrodeposition of Fe-based films as efficient water oxidation catalysts
Langmuir, 39, 6088–6101 (2023)

53. Kaur N.*, Khanna A.*, Kaur P.*, Singh M.N., Sinha A.K.
Comparative study of the short-range structure of α-V_20_5 α-TeO_2 and xV_20_5–$(100 - x)TeO_2$ glasses using x-ray diffraction, rietveld analysis and reverse Monte Carlo simulations
Acta Crystallographica B, 79, 55-63 (2023)

54. Khan A.K.*, Wani S.S.*, Shaikh A., Yamin Y.*, Shah N.A.*, Aitenov Y.O.*, Faizal M.*, Lone S.*
Deformation of nanowires and nanotubes
Europhysics Letters, 141, 52001(1-7) (2023)

55. Khan S.*, Vasudevan S.*, Maurya M.*, Ansari M.S.
Development of a compact, cost-effective photoacoustic spectral response measurement system for biomedical applications
IEEE Transactions on Instrumentation and Measurement, 72, 4007611(1-11) (2023)

56. Kumar A.*, Swain S.*, Upadhyay J., Upalekar Y.*, Arya R., Prabhudesai V.S.*
Predissociation dynamics of negative-ion resonances of H2 near 12 and 14.5 eV using the velocity slice imaging technique
Physical Review A, 107, 062803(1-9) (2023)

57. Kumar M., Singhal H., Chakera J. A.
Design and performance of a double-solenoid magnetic bottle photoelectron spectrometer for attosecond metrology
Review of Scientific Instruments, 94, 023303(1-11) (2023)

58. Lakhani P.*, Chodvadiya D.*, Jha P.K.*, Gupta V.K.*, Trzybiński D.*, Wozniak K.*, Kurzydłowski K., Goutam U.K.*, Srivastava H., Modi C.K.*
DFT stimulation and experimental insights of chiral Cu(ii)–salen scaffold within the pocket of MWW-zeolite and its catalytic study
Physical Chemistry Chemical Physics, 25, 14374-14386 (2023)

59. Mahapatra A., Ajimsha R.S., Ittoop M.O., Sharma A.*, Karmakar S., Shaikh A., Sankar P.R., Misra P.
Flexible ZnO:PVDF based free standing piezoelectric nanogenerator for vibrational energy harvesting and wearable shoe insole pedometer sensor
Journal of Alloys and Compounds, 960, 170898 (2023)

60. Mandal T., Arora V., Moorti A., Uphadhyay A., Chakera J.A.
Addressing key aspects of J × B driven MeV fast electron generation in ultra-short ultra-intense laser foil interaction
Physics of Plasmas, 30, 023106 (2023)

61. Mangavati S.*, Gurukrishna K.*, Rao A.*, Petwal V.C., Verma V.P., Dwivedi J.
Enhancement of thermoelectric power factor in Cu_2Se superionic conductor via high energy electron beam irradiation
Journal of Materials Science: Materials in Electronics, 34, 87 (2023)

62. Manivannan S.*, Mandal D.*, Dabhade P.A.*, Chamfekar M.*, Paul C.P.
Decomposition kinetics of sodium amalgam in fixed bed of WC-coated tubular SS-304 packing: modelling and validation
Asia-Pacific Journal of Chemical Engineering, 18, e2893 (2023)

63. Maru B.A.*, Bhatt G.J.*, Lad U.*, Deota P.T.*, Kane S., Goutam U.K.*, Modi C.K.*
$Fe@g\text{-}C_3N_4$: an effective photocatalyst for Baeyer–Villiger oxidation under visible light condition
New Journal of Chemistry, 47, 9797-9805 (2023)

64. Mishra N.K.*, Shwetabh K.*, Gautam U.K., Kumar K.*
Probing multimodal light emission from Tb^{3+}/Yb^{3+}-doped garnet nanophosphors for lighting applications
Physical Chemistry Chemical Physics, 25, 11756-11770 (2023)

65. Mishra S.*, Rudrapal K.K.*, Jana B.*, Islam K.P.*, Sagdeo A., Chaudhuri A.R.*, Adyam V.*, Choudhury D.*
Structural origin of room-temperature ferroelectricity in spark-plasma sintered $DyCrO_3$ and $LaCrO_3$
Physical Review B, 107, 214104 (2023)

66. Mistry K.A.*, Shenoy N.S.*, Bhanja K.*, Kohli D.K., Shenoy K.T.*
Modeling and experimental investigation for development of combined electrolysis and catalytic exchange process for hydrogen isotope separation
Chemical Engineering Research & Design, 192, 487-499 (2023)

67. Modi M.H., Gupta R.K., Yadav P.K., Gupta S., Mukherjee C., Idir M.*
Effect of electronic transitions on near edge opticalproperties of off-stoichiometric boron carbide thin films
Journal of Applied Physics, 133, 165302(1-8) (2023)

68. Mrinaleni R.S.*, Amaladass E.P.*, Sathyanarayana A.T.*, Amirthapandian S.*, Jegadeesan P.*, Gupta P., Kumary T.G.*, Rai S.K., Mani A.*
Anisotropic magnetic and magnetotransport properties in morphologically distinct $Nd_{0.6}Sr_{0.4}MnO_3$ thin films
Physica Scripta, 98, 075919(1-12) (2023)

69. Mrinaleni R.S.*, Rao P.N., Gupta P., Rai S.K. et al.
Enhanced temperature coefficient of resistance in nanostructured $Nd_{0.6}Sr_{0.4}MnO_3$ thin films
Thin Solid Films, 779, 139933 (2023)

70. Muthukumaran G.*, Rai A.K., Gautam J.*, Babu P.D.*, Ranganathan K., Bindra K.S.
A study on effect of multiple laser shock peening on microstructure, residual stress, and mechanical strength of 2.5 Ni-Cr-Mo (EN25) low-alloy steel
Journal of Materials Engineering and Performance, 32,4361-4375(2023)

71. Nayak P.*, Nanda S.S.*, Pattnaik S.*, Rai V.K.*, Sharma R.K., Dash S.*
Yb-Mn dimer tailored upconversion luminescence in $CaWO_4:Er^{3+}/Yb^{3+}/Mn^2$ green phosphors for thermometry and optical heating
Optics & Laser Technology, 159, 108990(1-10) (2023)

72. Ojha A.*, Megha*, Bulusu S.S.*, Banerjee A.
Structure and dynamics of 38-atom Ag-Pt nanoalloys using ANN based-interatomic potential
Computational and Theoretical Chemistry, 1220, 113985 (2023)

73. Padhi P.S., Ajimsha R.S., Rai S.K., Bose A., Misra P.
Effect of Al_2O_3 layer thickness on leakage current and dielectric properties of atomic layer deposited $Al_2O_3/TiO_2/Al_2O_3$ nano-stack
Journal of Materials Science: Materials in Electronics, 34, 1160 (2023)

74. Padhi P.S., Ajimsha R.S., Rai S.K., Goutam U.K.*, Bose A., Bhartiya S.*, Misra P.
Process temperature-dependent interface quality and Maxwell–Wagner interfacial polarization in atomic layer deposited Al_2O_3/TiO_2 nanolaminates for energy storage applications
Nanoscale, 15, 8337-8355 (2023)

75. Pal D.*, Banik S. et al.
Multiple magnetic phases and anomalous hall effect in $Sb_{1.9}Fe_{0.1}Te_{2.85}S_{0.15}$ topological insulators
Journal of Physical Chemistry C, 127, 2508–2517 (2023)

76. Pal S., Kamparath R., Subrahmanyam V.V.V., Sharma N., Jana S.*, Karwal S.*, Rajput P.*, Shaikh A.*, Mukherjee C., Jha S.N.*, Benerji N.S.
Sol-gel prepared amorphous Ta_2O_5 thin film for application in high LIDT antireflection coating and UV photodetection
Optical Materials, 142, 114097(1-12) (2023)

77. Pandey A., Gupta S.M., Sahlot P.*, Awasthi A.M.*, Rao T.V.C.*, Nigam A.K.*
Magneto-dielectric signature of Gd^{3+}-substituted $PbMg_{1/3}Nb_{2/3}O_3$ ceramics
Journal of Materials Science: Materials in Electronics, 34, 1349(1-11) (2023)

78. Pandya S.*, Chandra L.S.S., Ganesan V.*
Low-temperature thermoelectric power behavior of $Nd_{1-x}Gd_xCo_2$: insights from impurity and spin wave scattering
Journal of Low Temperature Physics, 212, 69-78 (2023)

79. Pant P.*, Agarwal H.*, Bharadwaj S.*, Srivastava S., Sagdeo A., Shaz M.A.*
Structural correlation to enhanced magnetodielectric properties of Pr-doped polycrystalline $Gd_{0.55}Pr_{0.45}.MnO_3$ at low temperatures
Journal of Magnetism and Magnetic Materials, 572, 170621(1-14) (2023)

80. Parida S.K.*, Ganguly D.*, Barik T.*, Sharma R.K., Amirthapandian S.*, Jena H.*, Sundara R.*
Design and performance enhancement of cobalt-encapsulated nitrogen-doped carbon nano fiber electrocatalyst through ionic liquid modification for efficient oxygen reduction
ACS Applied Nano Materials, 6, 1975–1984 (2023)

81. Patra P.*, Rani P.A.*, Sharma N., Mukherjee C., Jha H.C.*
Unraveling the connection of epstein–barr virus and its glycoprotein $M_{146-157}$ peptide with neurological ailments
ACS Chemical Neuroscience, 14, 2450–2460 (2023)

82. Pokhriyal A., Ghosh A.*, Sen S.*, Ghosh Haranath
Interplay of magnetic interaction and electronic structure in new structure RE-12442 type hybrid Fe-based superconductors
Magnetochemistry, 9, 164(1-24) (2023)

83. Pokhriyal A., Ghosh A.*, Ghosh Haranath
Electronic structure, magnetic order and Lifshitz transition in electron doped new structure 12442 type Fe-based superconductors
Journal of Physics and Chemistry of Solids, 172, 111085 (2023)

84. Pradhan S., Deshmukh P., Kambale R.C.*, Darvade T.C.*, Satapathy S., Majumder S.K.
Effect of nano-size on magnetostriction of $BiFeO_3$ and exceptional magnetoelectric coupling properties of $BiFeO_3$_P(VDF-TrFE) polymer composite films for magnetic field sensor application
Smart Materials and Structures, 32, 045017(1-12) (2023)

85. Ramadas H.*, Sarkar S.*, Kaul R., Majumdar J.D.*, Nath A.K.*
Enhancing the static and dynamic mechanical properties of laser powder bed fusion process built 15–5 precipitation hardening stainless steel specimens by laser shock peening
Materials Science and Engineering A, 866, 144657 (2023)

86. Ramawat S.*, Kukreti S.*, Kale A.*, Dutt R., Chakrabarti A., Dixit A.*
Cs_2KMnCl_6: a possible half-metallic double perovskite for spintronics
Journal of Applied Physics, 133, 165102(1-11) (2023)

87. Ramjan S.K., Chandra L.S.S., Singh R., Chattopadhyay M.K.
Effect of Gd addition on the superconducting properties of Ti-based V, Nb, Ta alloys
Superconductivity, 6, 100048 (2023)

88. Rao S.P.*, Saw A.K.*, Chotia C.*, Verma V.P., Petwal V.C., Dwivedi J., Okram G.*, Dayal V.*
Structural, transport, and thermoelectric properties of electron beam-irradiated $Bi_{1.2}Pb_{0.33}Sr_{1.54}Ca_{2.06}Co_3O_y$ cobalties
Journal of Materials Science: Materials in Electronics, 34, 548 (2023)

89. Rathore R., Pathak A.*, Gupta M.K.*, Mittal R.*, Kulkarni R.*, Thamizhavel A.*, Singhal H., Said A.H.*, Bansal D.*
Evolution of static charge density wave order, amplitude mode dynamics, and suppression of Kohn anomalies at the hysteretic transition in $EuTe_4$
Physical Review B, 107, 024101(1-9) (2023)

90. Rathore R., Singhal H., Kamal C., Chakera J.A.
Long-lasting deformation potential effect in Ge induced by UV photoexcitation
Journal of Applied Physics, 134, 035101 (2023)

91. Raut S.*, Chakravarty S.*, Mohanty H.S.*, Mahapatra S.*, Bhardwaj S.*, Awasthi A.M.*, Sharma R.K. et al.
Effect of magnetic phase coexistence on spin-phonon coupling and magnetoelectric effect in polycrystalline $Sm_{0.5}Y_{0.5}Fe_{0.58}Mn_{0.42}O_3$
Physica B, 651, 414593 (2023)

92. Rohidas P.R., Borage M., Singh A., Dwivedi V.K., Srivastava A.
Estimation of output voltage ripple in phase-staggered series-connected two-quadrant power converters for electromagnets in particle accelerators
Power Electronics and Drives, 8, 174-195 (2023)

93. Saha U.*, Dutta A.*, Konkati C.*, Chakraborty S.*, Dey S.*, Chauhan A.*, Srivastava S., Gayathri N.*, Mukherjee P.*
Microstructure and defect evolution in oxygen ion-irradiated pure nickel – insights from experimental probes and molecular dynamics simulations
Materials Chemistry and Physics, 305, 127916(1-14) (2023)

94. Sahu M.C.*, Jena A.K.*, Mallik S.K.*, Roy S.*, Sahoo S.*, Ajimsha R.S., Misra P., Sahoo S.*
Reconfigurable low-power TiO_2 memristor for integration of artificial synapse and nociceptor
ACS Applied Materials Interfaces, 15, 25713-25725 (2023)

95. Sahu V.K., Das A.K., Ajimsha R.S., Misra P.
On origin of resistive and capacitive contributions to impedance of memory states in $Cu/TiO_2/Pt$ RRAM devices by impedance spectroscopy
Ceramics International, 49, 2215-2223 (2023)

96. Samantaray K.S.*, Amin R.*, Maneesha P.*, Bhaumik I., Sen S.*
Effect of electrical poling on the structural, vibrational, and electrical properties of $0.94(Na_{0.5}Bi_{0.5}TiO_3)$-$(0.06\text{-}x)\,CaTiO_{3-x}$ $(BaTiO_3)$ lead-free ceramics
Ceramics International, 49, 14310-14326 (2023)

97. Sarkar P.*, Biswas A.*, Ravi K.*, Rai S., Jha S.N.*, Bhattacharyya D.*
Role of C and B_4C barrier layers in controlling diffusion propagation across the interface of Cr/Sc multilayers
Physical Chemistry Chemical Physics, 25, 3072-3082 (2023)

98. Sarkar S.*, Bhattacharya J., Dutt R., Chakrabarti A. et al.
Charge density wave induced nodal lines in $LaTe_3$
Nature Communications, 14, 3628(1-11) (2023)

99. Selvamani R.*, Kumar S.*, Singh G., Sen D.*, Sastry P.U.*
Effect of particle and pore morphology on optical transmission of yttria based laser host ceramics: a small-angle scattering investigation
Nuclear Instruments & Methods in Physics Research B, 537, 104-110 (2023)

100. Sen S.*, Ghosh Haranath
Magnetic-moment-induced metal–insulator transition inThMnXN (X = As, P): a first principles study
Magnetochemistry, 9, 1-9 (2023)

101. Sen S.*, Kabbour H.*, Ghosh Haranath
Pressure-induced antiferromagnetic-tetragonal to nonmagnetic-collapse-tetragonal insulator-metal transition in ThMnAsN
Journal of Materials Science, 58, 8398–8414 (2023)

102. Shaikh A., Singh B.K.*, Purnendu K.*, Kumari P.*, Sankar P.R., Mundra G., Bohm S.*
Utilization of the nickel hydroxide derived from a spent electroless nickel plating bath for energy storage applications
RSC Sustainability, 1, 294-302 (2023)

103. Sharma A., Yadav P., Bhaumik I., Singh M.N., Sathe V.*, Singh G.
Structural evaluation in vicinity of composition induced non-ergodic to ergodic crossover in niobium doped $(Na_{0.41}K_{0.09}Bi_{0.5})TiO_3$
Journal of Applied Physics, 134, 044105(1-12) (2023)

104. Sharma A.K.
A simple intra-beam alignment setup for tiled grating assembly based laser pulse compressor of high energy ultrashort pulse laser systems
Sadhana, 48, 121 (2023)

105. Sharma B., Deshmukh P., Satapathy S., Majumder S.K.
Infrared-to-visible conversion in strontium sulphate through a defect-based infrared stimulated visible emission phenomenon
Luminescence, 38, 1-11 (2023)

106. Sharma V.*, Singh I.*, Arora S.K.*, Sanchez F.*, Singh F.*, Tripathi S., Jha S.N.
Influence of ion irradiation on the surface electronic structure of epitaxial lanthanum nickelate films
Surfaces and Interfaces, 38, 102776 (2023)

107. Sharma V.K., Manekar M.

Estimation of barocaloric effect across the magnetostructural transition in Mn–Co–Ge alloy from magnetization measurements under pressure
Journal of Magnetism & Magnetic Materials, 565, 170236 (2023)

108. Shreevalli M.*, Kumar R.V.*, Ramachandran D.*, Padmaprabu C.*, Karthik V.*, Sagdeo A.
X-ray diffraction line profile analysis of defects in neutron-irradiated austenitic stainless steels at low displacement damage levels
Journal of Nuclear Materials, 577, 154338 (2023)

109. Sidden C.*, Paulraj R.*, Bhatt R., Bhaumik I., Soharab M., Perumalsamy R.*
Direction dependent crystalline perfection, Z-scan studies and fabrication of type-I and type-II SHG elements using imidazolium L-tartrate crystals for optical modulator applications
Journal of Physics and Chemistry of Solids, 172, 111065 (2023)

110. Singh A., Srivastava H., Chari R., Jayabalan J.
Effect of the orientation of non-spherical metal nanoparticle with respect to light polarization on its transient optical response
Nanotechnology and Precision Engineering, 6, 023005(1-8) (2023)

111. Singh H.*, Gupta M.*, Gupta P., Penacchio F.S.*, Morelhao S.L.*, Kumar H.*
Role of nitrogen partial pressure, deposition rate and annealing on stability of β-W phase
Applied Physics A, 129, 312 (2023)

112. Singh M.K., Banerjee A.
Role of different solvents and tailor-made additives in asymmetry in growth rates along the opposite ends of the polar axis: the riddle of α-resorcinol
Crystal Growth & Design, 23, 180−196 (2023)

113. Singh R., Singh R., Srihari V.*, Makde R.D.
In vitro investigation unveiling new insights into the antimalarial mechanism of chloroquine: role in perturbing nucleation events during heme to β-hematin transformation
ACS Infectious Diseases, 9, 1647–1657 (2023)

114. Singh S.*, Khichi P.*, Dahiya S.*, Punia R.*, Saini P.K., Satapathy S., Tripathi R.*, Ohlan A.*
Enhanced magnetoelectric coupling in novel rare earth metal substituted Sr based Z-hexaferrites/P(VDF-HFP) composites
Ceramics International, 49, 26135-26140 (2023)

115. Singh S.*, Palani I.A.*, Dehgahi S.*, Paul C.P., Prashanth K.G.*, Qureshi A.J.*
Influence of the interlayer temperature on structure and properties of CMT wire arc additive manufactured NiTi structures
Journal of Alloys and Compounds, 966, 171447 (2023)

116. Singh S.*, Palani I.A.*, Dehgahi S.*, Qureshi A.J.*, Jinoop A.N., Paul C.P., Prashanth K.G.*
Development of Cu-based shape memory alloy through selective laser melting from elemental powder mixture: processing and characterization
Journal of Alloys and Compounds, 961, 171029 (2023)

117. Singh V., Tiwari V.B., Shukla R., Mukherjee C., Mishra S.R.
Development and characterization of atom chip for magnetic trapping of atoms
Journal of Applied Physics, 133, 084402(1-9) (2023)

118. Singh Y.*, Chowdhury A., Dasgupta R., Majumder S.K.
The effects of lithium on human red blood cells studied using optical spectroscopy and laser trap
European Biophysics Journal, 52, 91-100 (2023)

119. Soharab M., Bhatt R., Khan S., Singh A., Sharma A., Bhaumik I.
Investigation of the effect of Cr co-doping on the refractive index, spectroscopic parameters and lasing of Nd:$GdVO_4$ crystals
Journal of Luminescence, 263, 119973 (2023)

120. Sumit, Kane S.R., Ganguli T., Shukla R.
Measurements for static shape control optimization of silicon mirror using nonlinear piezoceramic actuators
Smart Materials and Structures, 32, 035035(1-11) (2023)

121. Sumit, Kane S.R., Sinha A.K., Ganguli T., Shukla R.
Iterative piezo response function-based optimization for static shape control of cantilever beam using nonlinear piezoactuators
Smart Materials and Structures, 32, 015005(1-12) (2023)

122. Supakar S.*, Singh V., Tiwari V.B., Mishra S.R.
Ultrahigh vacuum pressure measurement using magneto-optical trap on atom chip
Journal of Applied Physics, 134, 024403(1-5) (2023)

123. Supekar S.*, Ghuge R.*, Shinde M.*, Manda S.*, Sivalingam Y.*, Ganesh P., Kumar S.S., Pareek P., Rane S.*
Effect of annealing conditions on structural and magnetic properties of 36Ni-64Fe laminates
Journal of Physical Chemistry C, 567, 170357(1-12) (2023)

124. Swain A.*, Verma P.*, Singh M.N., Rajput P.*, Sharma R., Giri S.*
K^+-doped P crystals of NIR-upconverting $NaYF4:Yb^{3+}/Ho^{3+}$ conform to the 'strain–intensity'

relationship
CrystEngComm, 25, 3528-3538 (2023)

125. Swain D.*, Ghosh S.*, Bera K.*, Friedemann S.*, Ghosh Haranath, Roy A.*, Das S.*
Possible Raman signature of broken symmetry states near the quantum critical point in P doped $BaFe_2As_2$: experiment and theory
Physica C, 606, 1354211(1-9) (2023)

126. Syamlal S.K.*, Gupta N., Perumal H.P.*, Kumar D.*, Gupta M.*, Gupta P., Sinha J.*
Interfacial electronic structure modulated magnetic properties in Ta/CoFeB/Ta multilayers
Surfaces and Interfaces, 40, 103043 (2023)

127. Tanwar M.*, Rani C.*, Kandpal S.*, Ghosh T.*, Mondal P., Kumar R.*
Etching-induced longitudinal phase inhomogeneity in fractal silicon: identification through depth-profiled Raman mapping
Journal of Physical Chemistry C, 127, 12606-12612 (2023)

128. Tiwari M.K., Singh A.*, Khooha A., Goutam U.K.*
Structural investigation of Ayurveda Lauha (Iron) Bhasma
Journal of Ayurveda and Integrative Medicine, 14, 100690(1-8) (2023)

129. Tripathi S.*, Kumar Y.*, Nand M.*, Jangir R., Bahadur J.*, Shrivastava H., Sharma R.K.*, Mohan S.R., Srihari V.*, Jha S.N.*
Effect of annealing environment on the luminescence and structural properties of pure $CePO_4$ and Tb: $CePO_4$ nanowires
Journal of Luminescence, 257, 119666 (2023)

130. Vachhani D.M., Arya R., Bhatt U.R.*
Design, implementation and performance evaluation of different digital control techniques for current controlled DC-DC Buck converter
International Journal of Power Electronics, 17, 97-128 (2023)

131. Verma S., Bitra V.S.*, Singh R., Rao T.
Optical response of Au films for reproducible Si nano-structuring and its application for efficient micro-drop SERS with portable Raman system
Materials Chemistry and Physics, 306, 128058 (2023)

132. Vijay K., Chandra L.S.S., Ali K.*, Sagdeo A., Tiwari P., Chattopadhyay M.K., Arya A.*, Banik S.
Tunable magnetoresistance driven by electronic structure in Kagome semimetal $Co_{1-x}Fe_xSn$
Applied Physics Letters, 122, 233103(1-6) (2023)

133. Vijay K., Vavilapalli D.S.*, Arya A.*, Srivastava S.K., Singh R., Sagdeo A., Jha S.N.*, Kumar K.*, Banik S.
Magneto-strain effects in 2D ferromagnetic van der Waal material $CrGeTe_3$
Scientific Reports, 13, 8579(1-12) (2023)

134. Vishwakarma P.*, Sharma G.*, Modi M.H., Gupta M.*, Stahn J.*, Gupta A.*
Boron migration during amorphous to crystalline transformation in CoFeB/MgO multilayers: a reflectivity study
Materials Research Bulletin, 161, 112150 (2023)

135. Yadav P.K.*, Gupta R.K.*, Gupta S.*, Mukherjee C., Goutam U.K.*, Modi M.H.
Boron carbide thin film surface characterization after graphitic carbon removal using low-pressure oxygen gas RF plasma
Applied Optics, 62, 1399-1405 (2023)

136. Yadav S., Paul C.P., Rai A.K., Singh R., Dixit S.K.
Elucidating laser directed energy deposition based additive manufacturing of copper-stainless steel functionally graded material: Processing and material behavior
Journal of Manufacturing Processes, 92, 107-123 (2023)

B. Invited Talks

1. Abdurrahim
Simulation of transverse single bunch instabilities in HBSRS booster synchrotron
11th Indian Particle Accelerator Conference (InPAC-2023), BARC, Mumbai, Mar. 13-16, 2023

2. Agrawal R.K.
Control software and networking infrastructure for Indian Synchrotron Radiation Sources: present and future
Asian Forum for Accelerators and Detectors (AFAD-2023), The University of Melbourne, Melbourne, Australia, Apr. 12-14, 2023

3. Banik S.
Photoemission studies on spintronic materials using Indus synchrotron
Theme meeting on Spectroscopy using Indus Synchrotron Radiation (SISR-2023), RRCAT, Indore, Mar. 24-25, 2023

4. Baraik K., Garg S.R., Garg C.K., Lal S., Nath S.K., Jangir R., Kane S.R., Raghuwanshi V.K., Singh S.D., Ganguly T.
Development and initial results of x-ray magnetic circular dichroism beamline at Indus-2 synchrotron source
Theme meeting on Spectroscopy using Indus Synchrotron Radiation (SISR-2023), RRCAT, Indore, Mar. 24-25, 2023

5. Borage M.B.
Future accelerators at RRCAT: High Brilliance Synchrotron Radiation Source (HBSRS)
11th Indian Particle Accelerator Conference (InPAC-2023), BARC, Mumbai, Mar. 13-16, 2023

6. Borage M.B., Srivastava A., Singh A.
Fast-ramped power converters with energy storage and grid power control
National Symposium on High Voltage- Energy Storage Capacitors and Applications (HV-ESCA-2023), BARC, Mumbai, June 22-24, 2023

7. Fatnani P.
Control system of Indus-2 and future SRS
RRCAT-ISPA Theme meeting on Control Systems and Instrumentation for Future Accelerator Projects, RRCAT, Indore, May 26, 2023

8. Dwivedi J.
ARPF (RRCAT)
11th Indian Particle Accelerator Conference (InPAC-2023), BARC, Mumbai, Mar. 13-16, 2023

9. Dwivedi J.
Electron beam services and industrial Linac technology from RRCAT
8'th International Conference on Radiation Technologies: Challenges and Opportunities for Sustainable Development (NICSTAR 2023), Lulu Bolgatty International Convention Centre (LBICC), Kochi Kerala, Jan. 9-12, 2023

10. Ganguli T.
Materials science research at Indus beamlines
Asian Forum for Accelerators and Detectors (AFAD-2023), The University of Melbourne, Melbourne, Australia, Apr. 12-14, 2023

11. Kumar V.
Beams in cavities
11th Indian Particle Accelerator Conference (InPAC-2023), BARC, Mumbai, Mar. 13-16, 2023

12. Lad M.
High power RF systems for future accelerators
11th Indian Particle Accelerator Conference (InPAC-2023), BARC, Mumbai, Mar. 13-16, 2023

13. Modi M.H.
Soft x-ray reflection spectroscopy using synchrotron source
Theme meeting on Spectroscopy using Indus Synchrotron Radiation (SISR-2023), RRCAT, Indore, Mar. 24-25, 2023

14. Moorti A.
Laser wakefield accelerators
11th Indian Particle Accelerator Conference (InPAC-2023), BARC, Mumbai, Mar. 13-16, 2023

15. Nakhe S.V.
Future accelerators at RRCAT
11th Indian Particle Accelerator Conference (InPAC-2023), BARC, Mumbai, Mar. 13-16, 2023

16. Pant K.K.
IR-FEL (RRCAT)
11th Indian Particle Accelerator Conference (InPAC-2023), BARC, Mumbai, Mar. 13-16, 2023

17. Pathak K.
RF characterization of 32 KW and 40 KW, 650 MHz solid state RF power amplifiers
11th Indian Particle Accelerator Conference (InPAC-2023), BARC, Mumbai, Mar. 13-16, 2023

18. Puntambekar T.
INDUS-2 (RRCAT)
11th Indian Particle Accelerator Conference (InPAC-2023), BARC, Mumbai, Mar. 13-16, 2023

19. Raghavendra S.
Challenges in cavity processing
11th Indian Particle Accelerator Conference (InPAC-2023), BARC, Mumbai, Mar. 13-16, 2023

20. Rana R.
Orbit feedback systems in synchrotron radiation sources
RRCAT-ISPA Theme meeting on Control Systems and Instrumentation for Future Accelerator Projects, RRCAT, Indore, May 26, 2023

21. Rao B.S., Mishra S., Moorti A., Chakera J.A.
Generation and application of high energy electron beams and hard-x-rays from laser wakefield accelerator
Asian Forum for Accelerators and Detectors (AFAD-2023), The University of Melbourne, Melbourne, Australia, Apr. 12-14, 2023

22. Shrivastava P.
Indian institutions & Fermilab collaboration
11th Indian Particle Accelerator Conference (InPAC-2023), BARC, Mumbai, Mar. 13-16, 2023

23. Shrivastava P.
Proton accelerator and related technology development at RRCAT
Asian Forum for Accelerators and Detectors (AFAD-2023), The University of Melbourne, Melbourne, Australia, Apr. 12-14, 2023

24. Singh S.N.
Design, development and deployment of accelerator magnets in RRCAT and future challenges

Asian Forum for Accelerators and Detectors (AFAD-2023), The University of Melbourne, Melbourne, Australia, Apr. 12-14, 2023

25. Tiwari M.K.
X-ray fluorescence spectroscopy using Indus-2 facility
Theme meeting on Spectroscopy using Indus Synchrotron Radiation (SISR-2023), RRCAT, Indore, Mar. 24-25, 2023

26. Tiwari N.
Operational experience of digital LLRF system for particle accelerators at RRCAT
11th Indian Particle Accelerator Conference (InPAC-2023), BARC, Mumbai, Mar. 13-16, 2023

27. Yadav S.
Beam diagnostics system for Indus-2 and future challenges for HBSRS
RRCAT-ISPA Theme meeting on Control Systems and Instrumentation for Future Accelerator Projects, RRCAT, Indore, May 26, 2023

C. Seminar/Conference Presentations

C.1. 11th Indian Particle Accelerator Conference (InPAC-2023), BARC, Mumbai, Mar. 13-16, 2023

1. Abdurrahim, Kumar P.
Simulation of transverse single bunch instabilities in HBSRS booster synchrotron

2. Agrawal G., Patel H.K., Gilankar S.G., Ghosh R., Lakshminarayanan A., Jain A., Tiwari A., Arzare D., Khare P., Shrivastava P., Vincent R.*, Chandrasekaran S.*
Design of vacuum vessel for HB 650 MHz cryomodule at RRCAT

3. Aditya L., Ahlawat M., Meena M., Pareek P., Singh S.N.
Design and development of NiAlCo ferrites for high power circulator at S-band

4. Arora P., Jana P.K., Kulkarni N.S., Kumar V.
Numerical studies for evolving measurement methodology for characterization of single cell in constant gradient traveling wave Linac

5. Babbar L.K., Vaishnav D., Soni A.K., Sisodia B., Tiwari S.K.
Design and development of ultrahigh vacuum compatible upgraded fluorescent screen monitor for Indus-1 upgrade

6. Babbar L.K., Vaishnav D., Soni A.K., Sharma S.K., Sisodia B., Sankar P.R., Kamath M.P., Mukherjee C., Tiwari S.K.
Design and development of ultrahigh vacuum compatible upgraded synchrotron light monitor for Indus-1 upgrade

7. Bagduwal P.S., Sharma D., Mishra E., Mishra N., Gothwal P., Tiwari N., Lad M.
Design and development of up-graded digital RF gap voltage and phase regulation control system

8. Bagre M., Jain V., Moulali S., Vijayakumar V., Singh A., Maratha S., Maurya T., Yedle A., Yadav A., Verma V., Srivastava V.K., Mohania P., Mahawar A., Kamble P.B., Chouksey S., Shrivastava P.
Experience of dumbbells fabrication for five-cell HB 650 (β=0.92) SCRF cavities in Indian industries

9. Biswas B., Chandran S., Saini R.S., Dave T., Lal S., Kumar A., Pandit R.K., Nerpagar P., Kale U., Gupta S.K., Pant K.K.
Performance optimization of the IR-FEL at RRCAT

10. Chalisgaonkar A., Ghodke D.V., Jain R., Singh K.K., Amban A.K.
Design and development of FPGA based data acquisition card for hydrogen ion source beam current measurements

11. Dave T., Lal S., Kumar A., Pant K.K.
Design studies for a pill box type accelerating structures with beam ports and coupling loop using analytical and perturbation techniques

12. Deepchand, Gandhi M.L.
Design and fabrication of cold plates for dipole power converter of Indus-2 at RRCAT

13. Dey S.K., Sinha G., Aich S.*
Effect of Dy substitution at Nd sites in melt-spun Nd-Fe-B permanent magnet ribbons

14. Dhingra R., Kulkarni N.S., Kumar V.
Development of a computer program for longitudinal beam dynamics studies in a traveling wave constant impedance electron Linac

15. Dhingra R., Kumar V., Kulkarni N.S.
Three-dimensional electromagnetic simulations of a constant gradient traveling wave accelerating structure integrated with RF couplers

16. Dwivedi V.K., Madhu B., Koli M., Singh A., Borage M.
Design and development of 125 A, 25 V power converters for combined function corrector magnets in Indus-1 storage ring

17. Garg A.D., Ojha A., Puntambekar T.A.
Measurement of electron beam size by using synchrotron radiation interferometer in Indus-2

18. Gaur R., Kulkarni N.S., Kumar V., Kane G. V., Sharma N.K., Chaturvedi A., Prasad V., Singh K.A.P., Rajput V.,

Baxy D., Lad M., Shrivastava P.
Cold test and RF tuning of the first section of 3 MeV, 35 MHz RFQ at RRCAT

19. Gauttam V. K., Kasliwal A.
Design and development of 3kW, active PFC pre-regulator for super conducting wavelength shifter magnet power supply.

20. Gothwal P., Mishra N., Bagduwal P.S., Mishra E., Sharma D., Tiwari N., Lad M.
Prototype development of digital controllers for multi-module current sharing power supply for RF amplifiers

21. Gupta A.K., Jain A., Lad M.
Power combining topology for CW 32 kW-650 MHz solid state RF amplifier (SSPA) installed at horizontal test stand (HTS) facility, RRCAT

22. Gupta P.K., Sharma R. K., Nema V., Kumar M., Raghavendra S., Shrivastava P.
Design, development and installation of cryogenic safety system of horizontal test stand

23. Jain M.K., Deo R.K., Kanyal G., Lad M.
Design study on solid-state RF power system for 10MeV re-circulating high power accelerator (RHPA)

24. Jain R., Holikatti A.C., Yadav S., Babbar L.K., Sonawane B.B., Fatnani P., Puntambekar T. A.
Development of beam position based interlock system for Indus-2

25. Jain V., Bagre M., Moulali S., Srivastava V., Singh K.K., Kane G.V., Bose A., Suhane S., Raghavendra S., Mohania1 P., Park H.*, Eremeev G.*, Furuta F.*, Chandrasekaran S.*, Grimm C.*, Chouksey S., Shrivastava P.
Development Journey of elliptically shaped high beta 650 MHz superconducting RF cavity: an overview

26. Jena S.K., Fakhri A.A.
Study of on-axis longitudinal beam injection in storage ring of high brilliance synchrotron radiation source

27. Kanyal G., Jain M.K., Deo R.K., Lad M.
Design and development of 100 kW, 325 MHz tetrode tube based high power RF pulse amplifier

28. Karnewar K., Maurya N.K., Holikatti A.C., Jain R., Kumar M., Arora P., Yadav H., Kumar A., Sisodia B.N., Sandha R.S., Fatnani P., Dwivedi J., Puntambekar T. A.
Development of energy measuring device and the measurement of energy and energy spread for the industrial Linac

29. Kelkar Y., Srinivas L., Barothiya R., Karandikar U., Singh Y.P.
Vertical pinger magnet power supply for Indus – 2

30. Koli M., Madhu B., Kumar V., Prajapati S. K., Somkuwar V., Mani S., Rohidas P.R., Srivastava A., Dwivedi V. K., Singh A., Borage M.B. Development of high-stability true-bipolar power converters for upgraded closed orbit distortion correction scheme in Indus-1 storage ring

31. Kumar A., Ruwali K., Kumar S., Das S., Singh S.N.
Development of helmholtz coil based measurement system for characterization of permanent magnet blocks

32. Kumar A., Yadav R.P., Borage M.B., Fatnani P.
Disciplined software clock for new VME CPU

33. Kumar N., Vyas D., Jain A., Kumar R., Lad M.
Development and commissioning of a thermal profile data logging and protection subsystem for Indus-2 RF cavity

34. Kumar V.
Understanding the RF coupling, beam loading and wake field in accelerator physics

35. Kumar V., Sharma A.
A review of calculation of emittance growth for some common cases in accelerator physics

36. Mahawar A., Mohania P., Namdeo R. K., Baxy D., Lad M.
Design and development of pulse 2 kW solid state amplifiers for energizing s-band pre-buncher cavity of 10 MeV, 10 kW Linac developed at RRCAT

37. Malik R., Sinha G., Sreeramulu K., Sisodia B., Chatarji U., Prasad R. K., Srinivasan B., Singh K., Mishra A., Ruwali K., Singh B., Kumar P., Rajesh L., Shah P., Awale N., Veerbhadraiah T., Singh S. N.
Design and development of an improved 270 degree dipole magnet for energy filtering system for the Linac at RRCAT

38. Maurya V., Chaudhari S., Tomar S., Rajan A.
Our experiences in establishing and managing reliable and secure network connectivity over public communication channels for mission critical accelerator applications

39. Meena V.K., Prakash S., Husain R.
Proposed closed orbit correction scheme for Indus-1 storage ring

40. Mishra D.K., Purohit D., Dutta S., Kumar P., Dwivedi J.
Electromagnetic simulation of 107.5 MHz co-axial RF cavity and its higher order mode identification

41. Mishra E., Sharma D., Mishra N., Bagduwal P. S., Gothwal P., Tiwari N., Lad M.
Auto-configurable clock divider for digital low-level radio frequency system of infrared free electron laser

42. Mishra N., Bagduwal P.S., Tiwari N., Sharma D., Gothwal P., Mishra E., Prasad M., Lad M.
Design and development of PLC based RF cavity tuner system for 31.6MHz RF cavities in Indus complex

43. Mishra R., Singh K.K., Kumar R., Pathak M., Ghodke D.V., Prasad V.
Remote control applications for operation of hydrogen negative ion source

44. Mohania P., Mahawar A., Namdeo R.K., Baxy D., Lad M.
Design and development of s-band low level RF system for 10 MeV, 10 kW electron linear accelerator KIRTI-1010

45. Mohania P., Namdeo R., Mahawar A., Baxy D., Lad M., Jain S.K., Shrivastava P.
Design and development of a 1 kW pulse RF amplifier with integrated power meter and pulse generator for ECR proton source

46. Moulali S., Kumar V., Maurya T., Singh A., Yedle A., Bagre M., Jain V., Chouksey S., Shrivastava P.
Study and development of various dissimilar metal joints of superconducting radio frequency cavities

47. Musuku J., Seema M., Jatin. J., Pawnarkar P., Satheesan T.V., Fatnani P.
Development of multi-channel programmable trigger generator for Linac of electron beam radiation processing facility

48. Nayak V.K.*, Kale U., Chaudhari B.B.*, Rath M. C.*
Design and development of pulse transformer for pico-second electron accelerator klystron modulator at RPCD, BARC

49. Nigam N., Mandle S., Sharma N.K., Kane G.V., Prasad V., Shrivastava P.
Mechanical design of spoke resonator cavity for high energy pulsed proton accelerator

50. Nigam N., Mandle S., Sharma N.K., Kane G.V., Prasad V., Shrivastava P.
Design methodology for forming tooling of SCRF cavities

51. Pal M.K., Jana A.R., Kumar V.
Development of a computer program for design of diode type electron gun

52. Pal M.K., Gaur R.
Study of cumulative beam breakup instability in spoke resonator section of a 1 GeV pulsed H- Linac

53. Pandey A., Gupta A., Mulchandani J., Wanmode Y., Lad M., Shrivastava P.
Design and development of floating pulse power supply for triode electron gun

54. Pareek P., Gaud V., Singh K., Kumar S.S., Veerbhadraiah T., Sisodia B., Sreeramulu K., Singh S.N.
Development of pinger magnets for Indus- electron storage ring

55. Patel H.K., Agrawal G., Gilankar S.G., Ghosh R., Lakshminarayanan A., Jain A., Tiwari A., Shukla A., Arzare D., Khare P., Shrivastava P., Vincent R.*, Chandrasekaran S.*
Design analysis of strongback and cavity support for high beta 650 MHz cryomodule at RRCAT

56. Pathak K., Sharma D.K., Gupta A.K., Jain A., Lad M.
RF characterization of 3 kW and 40 kW, 650 MHz solid state RF power amplifiers

57. Pathak M., Mohania P., Jain S.K., Naika R., Ghodke D.V., Prasad V., Baxy D., Lad M., Shrivastava P.
Optimization of operating parameters of ECR proton source in pulsed mode

58. Patidar A., Vohra A., Shelke A., Bilaiya S.K., Nayak M.K., Parchani G., Haridas G., Mundra G.
Holistic approach for design and construction of THz-FEL building at RRCAT

59. Prakash R., Jana A.R., Kumar V.
Dark current calculation in SRF elliptic cavities

60. Prakash R., Sharma A., Kumar V.
Development of a 3D particle in a cell (PIC) solver for multipacting study

61. Prakash S., Meena V.K. Husain R.
Preliminary simulation studies on closed orbit correction in HBSRS storage ring

62. Prasad M., Bagduwal P.S., Mishra N., Mishra E., Sharma D., Gothwal P., Tiwari N., Lad M.
Design, development and RF characterization of tunable RF cavity for LLRF control systems

63. Prasad M., Mishra N., Bagduwal P.S., Tiwari N., Sisodia B., Veerbhadraiah T., Prasad P. K., Chaterji U., Sharma S., Chouksey S., Mundra G., Lad M.
Design, fabrication and characterization of HOM damped RF cavity

64. Rana M., Pramod R., Sriharsha V., Sindal B.K., Joshi S., Yadav D.P.
Effect of wehnelt potential on the beam parameters of a 20 keV strip type DC electron gun and its initial beam trials

65. Rathi S., Tyagi R.K., Tripathi A., Upadhyay R., Badapanda M.K., Lad M.
Installation and commissioning of high voltage DC power supply with electron gun for power testing of photon absorbers

66. Raturi S., Dhingra R., Kumar V., Kulkarni N.S.
Numerical studies and simulation of field stabilization and tuning of a 35 MHz drift tube Linac

67. Rohidas P.R., Srivastava A., Singh A., Borage M.B.
Simulation studies on series connected fast-ramped power converter modules for booster synchrotron

68. Saurabh., Kutbuddin S., Ansari M.S., Satheesan T.V., Sanga S., Fatnani P.
FPGA based VME bus compatible location monitor board

69. Sharma D., Bagduwal P.S., Mishra E., Mishra N., Gothwal P., Tiwari N., Lad M.,
Digitally controlled precision RF signal synthesis for LLRF applications

70. Sharma N.K., Chaturvedi A., Kane G.V., Prasad C., Shrivastava P.
Thermal characteristics and frequency tuning methodology for 325 MHz RFQ structure

71. Sharma R.K., Gupta P. K., Raghavendra S., Shrivastava P.
Design and fabrication of cryogenic distribution box for horizontal test stand at RRCAT

72. Sharma S.K., Sindal B.K., Bais V. S., Das S., Yadav D. P., Shrivastava P.
Design and simulation analysis of vacuum system of SWLS insertion device for Indus-2 synchrotron radiation Source

73. Shrivastava B. B., Yadav S., Holikatti A., Ojha A., Jain R., Babbar L.K., Kumari A., Khan R., Nayak A., Merh B. N, Puntambekar T.A.
Development and preliminary evaluation results of prototype 100 nm spatial resolution digital beam position monitor envisaged for high brilliance synchrotron radiation source

74. Sindal B.K., Sharma S.K., Bais V. S. Kumar K.V.A.N.P.S., Shankar A., Sisodia B., Bhange N. J., Bhatnagar P., Joshi S., Yadav D. P., Shrivastava P.
Design, simulation, development and UHV testing of upgraded prototype dipole vacuum chamber for Indus-1 SRS at RRCAT

75. Singh, A., Borage M.
Design and simulation of upgraded 800 A, 140 V power converter for Indus-1 dipole magnet

76. Singh G., Kasliwal A.
Design and dvelopment of ethernet based remote card for generation of programmable reference for bipolar current controlled power supply

77. Singh K.A.P., Rajput V., Mohania P., Mahawar A., Pandey U. P., Namdeo R., Baxy D., Lad M., Shrivastava P.
Simulation and development of 650 MHz high power dummy coupler of superconducting RF cavity for qext measurement

78. Singh K.K., Jain V. K., Ghodke D.V., Prasad V., Chouksey S., Shrivastava P.
Development of transfer function measurement system for elliptical high beta superconducting RF dressed cavity

79. Singh M.K., Pandey R.M., Kumar R., Kumar Y., Parkash R., James J., Puntambekar T.A.
Improvement in Indus-2 coolant temperature stability suring beam energy ramp up with flooded evaporator type chiller system

80. Singh M.S., Pareek P., Bais V.S., Sindal B.K., Kumar K.V.A.N.P.S., Singh S.N., Yadav D. P., Srivastava P.
Design and impedance simulation of RF-shielded bellow and pumping manifold for Indus-1 upgradation

81. Sinha G., Malik R., Sreeramulu K., Srinivasan B., Singh K., Mishra A., Singh B., Kumar P., Rajesh L., Shah P., Awale N., Ruwali K.
Design and characterisation of anodised aluminium strip solenoids

82. Sriharsha V., Sindal B.K., Bais V.S., Pramod R., Monika R., Chaterji U., Sisodia B.N., Pandey V., Joshi S., Yadav D.P., Shrivastava P.
Development of a 20 KeV, 2 kW DC strip type electron gun system for testing photon absorber of Indus-2 SRS

83. Srinivas L., Kelkar Y., Singh Y.P.
Design and development of digitally controlled power converter for thyratron auxiliary power supplies

84. Srivastava A., Borage M., Singh A.
Development of a prototype fast-ramp power converter with grid power control

85. Srivastava V.K., Maurya T., Chouksey S., Shrivastava P.
Development of titanium gr-2 bellows for HB 650 MHz 5-cell SCRF cavities

86. Suhane S., Bose A., Chauhan S.K., Das K.K., Kokil S.V., Singh A., Rajput D S., Hussain A., Prasad K., Raghavendra S., Shrivastava P.
Processing and cleanroom preparation of SCRF cavities for performance testing in VTS cryostat

87. Tripathi A., Badapanda M. K., Upadhyay R., Tyagi R. K., Rathi S., Lad M.
Power factor correction techniques employed with DC power supplies of various RF amplifiers in Indus-2

88. Tiwari A., Gilankar S.G., Ghosh R., Patel H.K., Lakshminarayanan A., Jain A., Agrawal G., Sinnarkar D., Khare P., Shrivastava P., Vincent R*., Chandrasekaran S*.
Selection of HB 650 cryomodule control valves & development of excel VBA program

89. Tiwari M., Reghu T., Arya R., Lad M.
Design and development of isolated two winding bouncer scheme for droop correction in hard switched modulator

90. Tiwari N., Pritam S., Bagduwal ., Sharma D., Mishra E., Mishra N., Gothwal P., Prasad M., Lad M.
Operational experience of digital LLRF system for particle accelerators at RRCAT

91. Upadhyay R., Badapanda M.K., Tripathi A., Tyagi R. K., Rathi S., Lad M.
Control protection interlock system of 50 V, 700 A DC power supply for solid state RF amplifier in Indus-2

92. Valecha A., Satheesan T.V., Sanga S., Saifee K., Fatnani P.
Development of prototype serial bus communication analyzer system

93. Vijayakumar V., Singh A., Moulali S., Maurya T., Yedle A., Srivastava V. K., Bagre M., Jain V. K., Chouksey S., Shrivastava P.
EB welding of helium vessel assembly for 650 MHz SCRF dressed cavities

C.2. Theme Meeting on Spectroscopy using Indus Synchrotron Radiation (SISR-2023), RRCAT, Indore, Mar. 24-25, 2023

1. Bharti A.S.*, Jaiswal A.*,Tiwari M.K., Uttam K.N.*
Elemental investigation of the garlic by synchrotron radiation induced x-ray fluorescence

2. Chattaraj A.*, Sinha A.K., Jha S.N., Claverie A.*, Kumar V.*, Kanjilal A.*
Oxygen driven phase transition from α to β in tungsten

3. Tiwari A.*, Bharti A.S.*,Tiwari M.K., Uttam K.N. *
Elemental composition of the mentha leaf by synchrotron radiation induced energy dispersive x-ray fluorescence spectroscopy

4. Tripathi A.*, Bharti A.S.*, Tiwari M.K., Uttam K.N.*
Elemental investigation of the leaf and seed of coriander plant by synchrotron radiation x-ray fluorescence spectroscopy

5. Samanta A.*, Chattaraj A.*, Sagdeo A., Kanjilal A.*
Study of nickel oxide thin film as a hole transport layer for solar cell devices

6. Nag J.*, Vijay K., Bandyopadhyay B.*, Banik S., Alam A.*, Suresh K.G.*
Direct observation of the electronic structures of the quaternary heusler alloys probed by photoemission

7. Bharti A.S., Baran C.*, Tiwari M.K., Uttam K.N.*
Elemental investigation of the onion by synchrotron radiation induced x-ray fluorescence spectroscopy

8. Vijay K.*, Vavilapalli D.S., Arya A., Kumar K., Banik S.
Electronic structure of 2D van der waal ferromagnetic semiconductor $CrGeTe_3$

9. Rajput P.*, Kumar M.*, Nayak M., Jha S.K.*
On the splitting of surface plasmon resonance band of gold nanopillars developed on rippled si surface

10. Padhi P.S. *, Ajimsha R.S., Rai S.K., Banik S., Misra P.
Synchrotron radiation spectroscopy studies on atomic layer deposited Al_2O_3/TiO_2 nanolaminates to tune interfacial polarization for high-density storage capacitors

11. Dawn R.*, Urkude R., Tripathi S., Roy J. *, Jha S.N., Bhuniya S., Singh V.R.*
Advanced spectroscopic studies to investigate electronic properties of cobalt doped TiO_2 nanoparticles: an effect of annealing temperatures

12. Tripathi S., Kumar Y., Nand M., Baral M., Jha S.N.
Resonance photoemission in Tb:$CePO_4$ nanowires

13. Sharma S.*, Tiwari M.K., Uttam K.N.*
Nutrient profiling of the underutilized seeds using synchrotron radiation induced x-ray fluorescence spectroscopy

14. Dubey S.*, Dubey K.*, Gautam U.K., Sharma R.K., Pagare G. *, Gaur N.K. *
Structural, electronic and optical spectroscopy of $LiTaO_3$ ceramic: an experimental and DFT study

15. Sharma S.*, Singh A.K., Tiwari M.K., Uttam K.N.*
Prompt screening of the alterations in mineral profile of wheat plants stressed with chromium using x-ray fluorescence excited by synchrotron radiation

16. Kumar Y., Tripathi S., Nand M., Jha S.N., Sengupta P.*, Arya A.*
Local structure analysis of Indian zircon

C.3. 8th International Conference on Radiation Technologies: Challenges Opportunities for Sustainable Development (NICSTAR-2023), Lulu Bolgatty International Convention Centre (LBICC), Kochi Kerala, Jan. 9-12, 2003

1. Kumar P., Kumar S., Purohit D., Goswami S. G., Sandha G.S., Soni R.K., Pal V., Verma, A.K., Choudhary R.S., Yadav R., Petwal V.C., Dwivedi J., John R., Rawlani B.K., Parchani G., Mulchandani J., Acharya M., Wanmode Y., T Reghu, Mohania P., Mahawar A., Lad M., Arora P., Jana A.R., Kulkarni N.S., Kumar V., Jotangia J.D., Seema M.,

Agrawal R.K., Karnewar A., Shrivastava B.B., Fatnani P., Gauttam V.K., Singh V., Kasliwal A., Sharma H., Sindal B.K.,Yadav D.P., Sreeramulu K., Sinha G., Singh S.N., Dhara P., Haridas G, Puntambekar T.A., Mundra G.
Roadmap for industrialisation and deployment of RRCAT developed Linac

2. Sandha R.S., Goswami S.G., Dwivedi J., Choudhary J.R., kumar P., Soni R., Kumar A., Yadav H., Petwal V.C., Verma V.P., Khandelwal D., Dutta S., Wanmode Y., Reghu P., Mahawar A., Lad M., Seema M., Janardhan M., Jatongia J., Gupta A., Fatnani P., Arora P., Jana P.K., Sharma A., Kulkarni N., Kumar V., Pramod R., GauttamV., Kasliwal A., Singh G., SinhaG., Sreeramulu K.,Karnewar A.K., Holikatti A.C., Jain R., Shrivastava B.B., Sindal B.K., Sharma H., Bhatnagar P., Yadav D.P., Bhatnagar V.K., Kumar A., Dhara A., Pandey R.M., Suryavanshi S.D., Kumar R., Puntambekar T.A., Mundra G., Shrivastava P.
Development, testing and qualification of 9.5 MeV, 10 kW food irradiation Linac at RRCAT

3. Petwal V.C., Verma V.J., Mishra A.S.,Chaudhary R.S., Kumar A., Soni R., Makwana K., Purohit D., Khandelwal D., Goswami S.G., Yadav H., Waghmare D., Kumar P., Sandha R.S., Dutta S., Pramod R., Jotangia J.,Seema M.,Gupta A., Janardhan M.,Srivastava B.S.K., Bansal A., Agrawal R.K., Holikatti A.C., JainR., KarnewarA., GauttamV., Kasliwal A.,Chand D., Singh S., Mulchandani J.K., WanmodeY., Reghu T., Acharya M., Mohania P., Mahawar A, Jain L., Sindal B.K., Sharma H., Kumar M., Nanda D., Haridas G., Kulkarni N., Kumar V., Bhatnagar V.K., Lambhate Y., Rawlani B.K., John R., Yadav D.P., Fatnani P., Parchani G., Lad M., Dwivedi J., Puntambekar T.A., Mundra G., Shrivastava P.
E-beam facility for sterilization of medical devices using RRCAT Linacs

C.4. Other Seminar/Conference Presentations

1. Chaudhari S., Thankur A., Rajan A.
An efficient malicious URL detection approach using machine learning
2nd International Conference on Women Researchers in Electronics and Computing, Dr B. R. Ambedkar National Institute of Technology, Jalandhar, Punjab, Apr. 21–23, 2023

2. Radke N.K., Tomar S.S., Rajan A.
Study on machine learning models for IPv6 address lookup in large block lists
IEEE 29th National Conference on Communications (NCC-2023), IIT Guwahati, Feb., 23- 26, 2023

Note: '*' indicates author affiliation other than RRCAT, Indore.

N.1: Workshop on "Intellectual Property Rights" at RRCAT, Indore

A one-day workshop on "Intellectual Property Rights" was organized at Convention Centre, RRCAT, Indore by DAE-Intellectual Property Right (IPR) Cell and Incubation Centre-RRCAT on February 3, 2023. The workshop was sponsored by Administrative Training Institute (ATI), DAE. The objective of the workshop was to create awareness about IPR and its impact on commercialization of the developed technologies; to introduce the patent filing provisions and elaborate patent filling procedure of DAE; and also to discuss and resolve the difficulties faced while processing patent applications. The workshop was attended by 82 nominated officers and 18 HBNI Ph. D. scholars.

During the inauguration address, Dr Shankar V. Nakhe, Director, RRCAT briefed about the importance of IPR in present context and emphasized on adopting professional approach with an awareness about the potential commercialization of the developed know-how to develop marketable products/processes. The first session of the workshop was conducted by Smt. Anuradha Maheshwari, where she gave a brief overview on IPR, PCT filling and International Patents, journey from patent to technology, conversion of the novel research works into patents and benefits of patent search for searching novelty in technology.

Smt. Anuradha Maheshwari briefing about IPR to workshop participants.

Subsequently, Shri. Dani Rajiah, Head, IPR Cell, DAE introduced DAE patent filing methodology and procedure to the participants. He also shared his experience in managing patent filling cases. Thereafter Shri Daniel Babu explained DAE technology transfer framework to the workshop participants. Later, Dr. C. P. Paul, Head, Technology Transfer Cell (TTC) gave a brief overview of DAE incubation framework and various initiatives taken at RRCAT for commercialization of developed know-how. He also explained the support being offered by TTC and Incubation Centre-RRCAT to technology developer to translate the RRCAT developed technology into a successful product or process. The workshop concluded with the vote of thanks by Shri Praveen Agarwal, Co-convener, Incubation Centre-RRCAT.

Reported by:
C. P. Paul (incubation@rrcat.gov.in)

N.2: Four incubation and one technology transfer agreement signed during 40th Foundation Day celebration of RRCAT

RRCAT is closely working with many industries/ start-ups to translate the RRCAT developed technologies to industries, MSMEs and start-ups contributing towards the self-reliance mission of Government of India through incubation and technology transfer activities. Dr. Shankar V. Nakhe, Director, RRCAT signed four incubation agreements with various industries/start-ups and exchanged the documents for one technology transfer on 40th Foundation Day celebration of RRCAT on Feb. 20, 2023. Shri K. N. Vyas, Chairman, Atomic Energy Commission and Secretary, Department of Atomic Energy (DAE), Government of India was the Chief Guest for the function with Prof. U. Kamachi Mudali, Vice-chancellor, VIT Bhopal and former Chief Executive, Heavy Water Board, DAE as Guest of Honour.

'TVASHTR' is selected as commercial name for LAM-DED technology going in public domain. First agreement was signed with a new start-up Unnati 5G Manufacturing System Pvt. Ltd., Navi Mumbai, which will be catering the product in academia and R&D labs by providing a cost-effective TVASHTR in the price range of ₹50 - 100 lakhs. Mr. Hrishikesh V. Iyer, CEO, Unnati 5G exchanged the incubation agreement.

Dr. S. V. Nakhe, Director, RRCAT (second from left) exchanging incubation agreement with Hrishikesh V. Iyer, CEO, Unnati 5G Manufacturing System Pvt. Ltd., Navi Mumbai. Shri K. N. Vyas (at center) and Prof. U. Kamachi Mudali (first from right) gracing the occasion.

Next agreement was signed with M/s VFuse Metal 4 Manufacturing Pvt. Ltd., Bhopal, a new start-up for the incubation of TVASHTR with the target market segment for VFuse is Indian industries and National Labs and projected price of TVASHTR is in the price range of ₹ 200 - 350 lakhs. Mr. Manoj Jain, CEO, M/s VFuse Metal 4 Manufacturing Pvt. Ltd., Bhopal exchanged the incubation agreement.

Dr. S. V. Nakhe, Director, RRCAT exchanging incubation agreement with Mr. Manoj Jain, CEO, VFuse Metal 4 Manufacturing Pvt. Ltd., Bhopal. Shri K. N. Vyas (at center) and Prof. U. Kamachi Mudali (first from right) gracing the occasion.

The third agreement was signed with M/s Lokesh Machines Limited, Hyderabad - a well-known name in CNC machines. The company has annual turnover of ₹ 200+ Crores with 15% export of the CNC machines in 22 countries across the globe. Lokesh will jointly develop the TVASTHR by developing an additive-subtractive machine and push the product to Indian and global market. The projected cost of the machine is in the range of ₹ 150 - 250 lakhs. Mr. M. Srinvasan, Director, Lokesh Machine Limited exchanged the incubation agreement.

Dr. S. V. Nakhe, Director, RRCAT (second from left) exchanging incubation agreement with Mr. M. Srinvasan, Director, Lokesh Machines Ltd., Hyderabad. Shri K. N. Vyas (at center) and Prof. U. Kamachi Mudali (first from right) gracing the occasion.

A collaborative incubation agreement for 'Circumferential TIG Welding – Special Purpose Machine (CTW-SPM)' was signed with M/s Metal and Membrane Pvt Ltd., Rau, Indore, wherein the technological expertise developed at RRCAT would be utilized to solve industrial problems as part of collaborative incubation. Mr. Rahul Dalal, the founder of M/s Metal and Membrane Pvt. Ltd., Rau, Indore exchanged the incubation agreement.

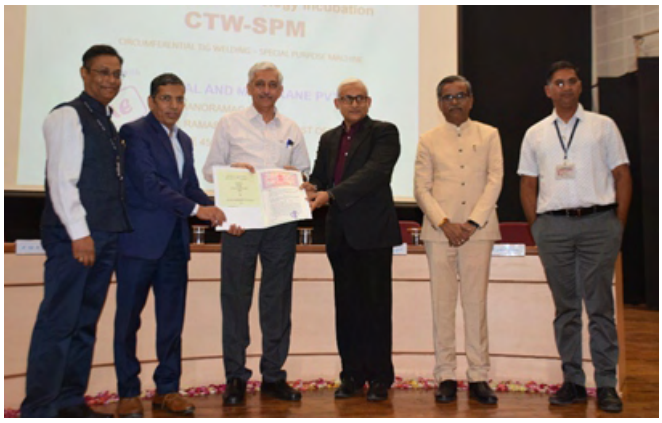

Dr. S V. Nakhe, Director, RRCAT (second from left) exchanging collaborative incubation agreement with Mr. Rahul Dalal, Founder, Metal and Membrane Pvt. Ltd. Rau, Indore. Shri K. N. Vyas (third from left) and Prof. U. Kamachi Mudali (second from right) gracing the occasion.

In addition, technology transfer (TT) of 'Agni-Rakshak' - a Raman optical fibre based distributed fibre sensor system has been licensed on non-exclusive basis to M/s Technica Fibre Tech Pvt. Ltd., New Delhi. Mr. Dhurv Goyal, CEO, Technica Fibre Tech Pvt. Ltd., New Delhi collected the TT agreement. Dr. Om Prakash, Head, Fibre Sensors & Optical Spectroscopy Section (FSOSS), RRCAT and Dr. Manoj Saxena, SO/G, FSOSS witnessed as technology developer.

Dr. S V. Nakhe, Director, RRCAT (third from left) exchanging technology transfer agreement with Mr. Dhurv Goyal, CEO, Technica Fibre Tech, New Delhi. Shri K. N. Vyas (third from right) and Prof. U. Kamachi Mudali (first from right) gracing the occasion.

Reported by:
C. P. Paul (incubation@rrcat.gov.in)

N.3: Technology transfer of Agni-Rakshak and RF amplifier modules

In a significant advancement for technological innovation, two cutting-edge technologies developed by RRCAT have been successfully transferred to Indian industries on 8th June 2023. These technology transfers (TTs) involve the 'Agni-Rakshak' and 'RF amplifier modules'. TT agreement was signed between Dr. S. V. Nakhe, Director, RRCAT on behalf of Department of Atomic Energy, Government of India and representatives of industries. All these efforts are contributing to "Atma Nirbhar Bharat" mission of Government of India. The ceremony was witnessed by Shri Purushottam Shrivastava, Shri M. Lad, Dr. S. K. Dixit, Dr. Om Prakash, Dr. Akhilesh Jain, Dr. C. P. Paul, Dr. Manoj Saxena along with members of Coordination Committee for Patent, Technology Transfer, and Incubation (CCPTTI), Coordination Committee of Incubation Centre (CCIC), and Technology Transfer Cell, RRCAT.

'Agni-Rakshak' is a Raman optical fiber distributed temperature sensor, which has applications in fire monitoring in hospitals, buildings, road & rail tunnels, stations, cable trays of power cables, high-capacity transformers, coal conveyors, warehouse and storage, cement industry, oil & gas industry, nuclear industry and sensitive installations, etc. The system is very useful in detecting the onset of fire by sensing the heat. It has the capability to provide information about the location, width and temperature of the fire zone to which the sensing fiber is subjected to. The system can generate audio-visual alarms for various fire zones in the fiber. This revolutionary system, utilizing Raman optical fiber technology, enables the creation of a distributed fire sensor network, providing real-time and accurate fire detection in a wide range of environments. The technology is poised to transform fire safety protocols by offering an early warning system that can significantly reduce the risk of fire-related incidents. Two firms, M/s Indiyo, Indore and M/s B C Technomation Pvt. Ltd., Bhopal, have been granted licenses for the groundbreaking Agni-Rakshak technology.

TT Agreement handed over to M/s Indiyo, Indore by Dr. S. V. Nakhe, Director, RRCAT.

TT Agreement handed over to B C Technomation Pvt. Ltd., Bhopal by Dr. S. V. Nakhe, Director, RRCAT.

TT Agreement handed over to M/s Technopower International, Mumbai by Dr. S. V. Nakhe, Director, RRCAT.

Solid-state RF amplifier modules are an indispensable part of any high-power system/ transmitter. They have been widely used in radio frequency systems such as radar, mobile communication, jamming and identification, and occupy a very important position. This technology has distinct advantages in terms of small size, low cost, durability, high efficiency, and in-built safety. The potential deployment of this technology is in the domestic microwave, industrial furnaces and communications in defense and space, etc. This sophisticated technology is designed to amplify radio frequency signals with high efficiency and precision. The RF amplifier module holds immense potential in the realm of communication and wireless technology, with applications spanning telecommunications, broadcasting, radar systems, and more. By TT of solid state RF amplifiers to industries, India joined the elite group, where this technology is available to the industry within the country. M/s Technopower International, based in Mumbai, has acquired the license for the RF amplifier module technology.

Reported by:
C. P. Paul (incubation@rrcat.gov.in)

N.4: RRCAT celebrated its 40th Foundation Day on 20th February 2023

Raja Ramanna Centre for Advanced Technology, Indore, a unit of the Department of Atomic Energy, Government of India celebrated its 40th Foundation Day Function on February 20, 2023. The Chief Guest on the occasion was Shri K. N. Vyas, Chairman, Atomic Energy Commission, and Secretary, Department of Atomic Energy, Government of India, a highly accomplished nuclear energy technocrat and scientific administrator. The Guest of Honour of the function was Prof. U. Kamachi Mudali, former Chief Executive and Chairman, Heavy Water Board, Department of Atomic Energy, and the present Vice-Chancellor, VIT Bhopal University. Dr. Shovan K. Majumder, Chairman, Seminar Committee, introduced the Chief Guest as well as the Guest of Honour.

Dr. S. V. Nakhe, Director, RRCAT welcoming the Chief Guest, Shri K. N. Vyas, Chairman, AEC and Secretary, DAE.

Shri Purushottam Shrivastava, Director, Proton Accelerator Group, welcoming the Guest of Honour Prof. U. Kamachi Mudali, Vice-Chancellor, VIT Bhopal University.

Dr. S. V. Nakhe, Director RRCAT, presented an overview of the important scientific accomplishments of the Centre achieved during the past one year. He presented the current status of the synchrotron radiation sources Indus-1 and Indus-2, highlighting in particular, the new beamlines made operational and the upgradations carried out in the facility for improving the performance. He briefed that the Free Electron Laser, which is a unique facility in India, has been made available to users and the first set of experiments have also been carried out. Another important milestone mentioned was the successful commercial utilization of Electron-Beam Radiation Processing Facility, which is the first such facility in the country, for sterilizing medical products. He mentioned about the development of indigenous computer codes, machine components and setting of various facilities towards capacity building for the proton accelerator. Dr. Nakhe also mentioned that 40 kW/650 MHz Solid State RF Amplifier delivered to Fermi Lab under IIFC Collaboration has been tested and qualified. Other important accomplishments elaborated were development of lasers systems for material processing, cutting and welding in nuclear applications, deployment of fiber Bragg grating based multi-point temperature monitoring system in nuclear power plant, development of laser additive manufacturing systems, machine-vision based metrology systems for inspection of nuclear fuel components, and development of technology for laser diode bonding and packaging. He also mentioned about deployment of OncoDiagnoScope, a photonics technology based cancer screening device, in several medical camps in remote areas and in the Life-Line Express in Maharashtra. At the end of his talk, he emphasised that R&D institutes, academia, and industries working together with innovative ideas can write success stories for Atma Nirbhar Bharat.

Dr. S. V. Nakhe, Director, RRCAT delivering his lecture during the Foundation Day function.

Another highlight of the Foundation Day Function was an event in which a few technologies developed at RRCAT were transferred to industry, and incubation agreements were signed with a few other industrial partners. The technology of Agni-Rakshak, a Raman optical fiber based distributed temperature sensor system, was transferred to M/s Technica Fiber Tech Pvt.Ltd., New Delhi. Three agreements were signed for incubation of in-house developed technology for laser additive manufacturing systems with M/s Ideas AM Systems, Navi Mumbai, M/s VFUSE Metal 4 Manufacturing Pvt. Ltd., Navi Mumbai, and M/s Lokesh Machines Ltd., Hyderabad. A collaborative technology incubation was signed with M/s Metal and Membrane Pvt. Ltd., Indore for development of special purpose machine for circumferential TIG welding.

Dr. S. V. Nakhe presenting the technology transfer and incubation agreement documents to the industrial partners in the presence of Shri K. N. Vyas.

The Guest of Honour of the function Prof. U. Kamachi Mudali delivered an engrossing talk to the staff members of the Centre. He mentioned that RRCAT is the leading institute in the Country in the areas of lasers, accelerators, and non-nuclear advanced technologies. He highlighted the importance of sustainable developmental goals set up by the United Nations, wherein he specifically elaborated on the role of Artificial Intelligence in achieving goals of Industry 4.0 and Education 4.0.

Prof. U. Kamachi Mudali, former Chief Executive and Chairman, Heavy Water Board, Department of Atomic Energy, and the present Vice-Chancellor, VIT Bhopal University delivering his talk during the Foundation Day function.

The Chief Guest of the function Shri K. N. Vyas delivered a motivating talk to the staff members of the Centre. He congratulated RRCAT fraternity for its excellent scientific and technological accomplishments during the past one year under the leadership of Dr. Nakhe. He elaborated on the role of nuclear power to meet the goal of "Net Zero" by 2070. He presented the advantages of nuclear energy vis-a-vis other sources of energy such as thermal power and solar power plants. In this regard, he described the role of small modular reactors, which could be industry built. He advised to utilize the unique strengths of different DAE units by establishing collaborations among each other as well as with academics and industries. He expressed his happiness that many industrial partners came forward to absorb the high-end technologies developed at RRCAT.

Shri K. N. Vyas, Chairman, AEC and Secretary, DAE delivering the Foundation Day address.

The vote of thanks was proposed by Shri Purushottam Shrivastava, Director, Proton Accelerator Group, RRCAT. The function was attended by several dignitaries from DAE including the former Directors of RRCAT, Dr. P. D. Gupta, Dr. P. K. Gupta and Shri S. C. Joshi, and the Directors of DAE-UGC CSR, Prof. Amlan J. Pal and Prof. Vasant Sathe. Many eminent personalities from outside DAE also graced the occasion including Dr. Dhruv Ghai, Pro Vice-Chancellor of Oriental University, Indore, Dr. Prithvi Yadav, Vice-Chancellor, Symbiosis University of Applied Science, Indore, Dr. Dilip K. Pattnaik, Vice-Chancellor, Medicaps University, Indore, Dr. Rajeev Vishwakarma, Pro Vice-Chancellor, APJ Abdul Kalam University, Indore, Dr. R. K. Khare, Dean (Administration), SGSITS, Indore, Dr. V. Ganesan, Dean, Medicaps University, Indore, Shri Dev Kumar Vasudevan, an eminent Social Worker, and several senior officials of District Administration and Police Department of Indore. The proceedings of the function were telecast live at different centres of DAE and also at several locations within RRCAT.

Reported by:
Shovan. K. Majumder (shkm@rrcat.gov.in)

N.5: Theme meeting on "Control Systems and Instrumentation for Future Accelerator Projects"

A one-day theme meeting on "Control System and Instrumentation for Future Accelerator Projects" was organized by RRCAT in collaboration with Indian Society for Particle Accelerators on May 26, 2023 at Convention Centre, RRCAT, Indore. The theme meeting had inaugural session and two invited talk sessions. Shri Uday Vaidya, Head, RCnD, BARC was the Chief Guest and Dr. S. V. Nakhe, Director, RRCAT chaired the inaugural session. Shri T. A. Puntambekar, Group Director, Electron Accelerator Group, RRCAT, gave the inaugural address giving the relevance of the meeting and covered major challenges associated with the control system of particle accelerators. Addressing the meeting Dr. Nakhe highlighted the importance of this meeting in light of upcoming high brilliance synchrotron radiation source (HBSRS) project. Shri Uday Vaidya gave a talk on "Challenges & Approach in Design of Control and Instrumentation for Future Accelerator Projects". He emphasized on a systematic, documented & well controlled, life cycle-based design process for system development.

Dr. S. V. Nakhe, Director, RRCAT along with other dignitaries lighting the lamp during inauguration of Theme meeting.

The invited talk sessions had ten talks by eminent experts in the field of control and instrumentation from major Indian institutes involved in the development of particle accelerators. The various topics covered were related to control and instrumentation including SCADA system, embedded system design and development, beam diagnostics & related instrumentation, application of AI/ML in control systems, precision timing and synchronization system and, development of detectors and sensors and ASICs for particle accelerators. The meeting was concluded with a panel discussion in which panellist highlighted importance of documentation and suggested for initiation of V&V process. The meeting was attended by more than 130 registered participants from various DAE units and academic institutes along with invited guests and senior officials of RRCAT. This theme meeting has generated a lot of enthusiasm among the participants and generated collaboration possibilities among institutes on various aspects of control and instrumentation for particle accelerators and in particular for development of detectors and sensors using ASICs. This meeting will serve to foster better networking among participants for realization of robust control and instrumentation systems for particle accelerator projects.

Reported by:
R. K. Agrawal (ragrawal@rrcat.gov.in)

N.6: National Science Day Celebration at RRCAT

National Science Day (NSD) is celebrated in India on 28th February of each year to commemorate the discovery of the Raman Effect by Prof. C. V. Raman who was awarded Nobel Prize in Physics in the year 1930 and Bharat Ratna in 1954. RRCAT celebrated the National Science Day on last Saturday and Sunday of February 2023 i.e., on 25th and 26th February by holding an open house for the school and college students, teachers, family members and guests of RRCAT staff and invitees from public. The theme of this year's National Science Day was "Global Science for Global Wellbeing".

Dr. S. V. Nakhe, Director, RRCAT addressing the students during celebrations of NSD-2023.

On Saturday, February 25, 2023, students of Class XI and teachers from schools in and around Indore, were invited for a full day visit. About 850 students and teachers invited from 57 schools of Indore and nearby places visited RRCAT. The program started with an address by Dr. S. V. Nakhe, Director, RRCAT on the basics of Raman Effect and working principles of accelerators and lasers, which are the main areas of research and development at RRCAT. His lucid explanation in simple Hindi language was very much appreciated by the students and the teachers. A few small movies depicting importance of hygiene and cleanliness were also shown to students and teachers under "Swachcha Bharat Abhiyaan".

Special arrangements were made for the Hearing and Speech impaired students invited from special schools to participate in the celebrations accompanied by interpreter-teachers. Director, RRCAT, along with senior members of organizing committee, interacted with about 50 special students in a separated interactive session and tried to address their queries with the help of interpreter-teachers. The students participated actively in this interaction session.

After the address, all the students were taken to exhibit places at laboratories and RRCAT Convention Centre, in organized groups, under the guidance of RRCAT volunteers.

Enthusiastic participation of specially-abled students in an interaction session with the expert panel.

There were working exhibits on lasers like use of light and lasers for biomedical applications, demonstrations on applications of lasers like: laser cutting and marking, laser additive manufacturing and Nd:YAG and fibers lasers, etc. To explain some basic science concepts, special experiments had been set up like Raman effect, Michelson interferometer, glow discharge, laws of motion, gas laws, conservation of momentum, change in physical properties of materials at low temperature, etc. To explain some technological applications, live demonstration with models of superconducting magnetic levitated trains, Agni-Rakshak, CNC machining, induction heating, glass blowing, etc. were shown. Videos on Indus Synchrotrons and their uses, development of superconducting radio frequency cavities, indigenous 10 MeV linear accelerator, optical diagnosis of cancer, laser additive manufacturing, laser cutting, detection of RF and microwave signals, etc. were shown.

Students visiting exhibits at RRCAT laboratories.

About 40 exhibits related to technologies of accelerators, lasers, cryogenics, superconductivity, RF and microwave, magnets, along with demonstration of Fire & Safety aspects were set up at RRCAT Convention Centre and in different laboratories to explain the scientific and technical activities of RRCAT as well as to demonstrate a few concepts in basic sciences and engineering.

Important scientific achievements and in-house technological developments were showcased, with emphasis on "Make in India", with the help of illustrated posters, working models, and actual components. These included instruments like TuBerculoScope, Raman Probe, OncoDiagnoScope, Agni-Rakshak, laser micro welding machine for brachytherapy sources and development of laser technologies related with maintenance of Indian PHWRs, diode pumped laser marker, technology for LN2 based REEFER, SCRF cavity, superconducting corrector magnets, solid state RF amplifier, high stability power converters, glass-tube based sealed-off CO_2 laser, crystal growth, fiber Bragg grating (FBG) sensor, UV-NIR laser beam visualizer and machine for fiber polishing, etc., which greatly enthused the young visitors.

Visitors experiencing an interesting demonstration on laser cutting.

The overall response of the students and teachers was very enthusiastic showing keen interest in the exhibits and had lively discussions with the RRCAT officials. Exhibits like demonstration of laser cutting, magnetic levitated train, shaping glass using glass blowing technique, artificial cloud creation by liquid nitrogen and live demonstration of fire-fighting created a vivid impact on young minds and earned applause from students, teachers, family members of staff and guests.

An "Ask-a-Question" event was organized for the students with an aim to create an opportunity for free discussion between these young minds and the working scientists. Several RRCAT scientists interacted with the students encouraging them to ask questions. The discussions ranged from questions arising out of the exhibits at RRCAT for Science Day to basic scientific concepts. The event also encouraged the accompanying teachers to discuss their problems in teaching particular concepts of science. Participation prizes were also given to curious students. The specially-abled students also visited various laboratories and took part enjoyably in "Ask-a-Question" event with great enthusiasm.

Students visiting exhibits at RRCAT Convnetion Centre.

All the students and accompanying teachers were offered refreshments and lunch in the morning and noon, respectively. Souvenir caps were also distributed to all the students and teachers. Buses were arranged for movement of the students to various exhibits and labs. The overall response of the students was extremely enthusiastic as demonstrated by the number of queries they put in during the visits to the exhibits and at the "Ask-a-Question" event. They went back full of admiration for the scientific activities being pursued by DAE in general, and RRCAT in particular. They were also impressed by the cleanliness, greenery and lakes in the RRCAT picturesque campus.

On Sunday, February 26, 2023, family members and guests of RRCAT staff, college students, and invitees were given opportunity to visit RRCAT laboratories. More than 3000 persons including about 750 college students and teachers visited the laboratories and expressed their happiness on getting an opportunity to learn about the important R&D activities being carried out at the Centre.

The whole event was managed, under keen supervision of Dr. S. V. Nakhe, Director, RRCAT, by an Organizing Committee with Shri Rajesh Arya as the Convener and Dr. S. K. Majumder as the Co-convener for the event. The committee had made quite elaborate arrangements for the event with the help and enthusiastic cooperation of a large team of volunteers, exhibitors, administrative staff, and security personnel. The event was covered by different major national and state level newspapers.

Reported by:
Rajesh Arya (rajarya@rrcat.gov.in)

N.7: Industrial and radiation safety activities in RRCAT

Fire and Safety Section, RRCAT is taking care of the safety compliance for the improvement of safety culture among the staff members. Different safety activities are being carried out to meet the said objectives.

Periodic inspection and maintenance of breathing apparatus sets: Every month, the inspection of breathing apparatus sets, which are kept in different labs of the RRCAT technical area is carried out to check their healthiness. The main features include checking of face mask, warning whistle, air pressure, harness assembly, low and high pressure hose, pressure gauge, pressure reducer, back plate and cylinder valves in each assembly. Wherever a fall in pressure in the cylinder is observed to be less than the permissible limit, it is topped. A total of 30 numbers of breathing apparatuses are installed in different buildings of the RRCAT technical area and two sets are also kept in the Agricultural Radiation processing Facility (ARPF).

Inspection of breathing apparatus set.

Noise & illumination measurement: Fire & Safety Section is regularly conducting sound level measurement tests in various buildings of RRCAT. The sound level have been measured quarterly. Measurement of sound produced by various machines and their sub-systems at different places of RRCAT like Workshop-A & B, LCW & Power Conditioning Unit, etc. for occupational safety of employees working at noisy area was done. Wherever sound level is more than permissible limit, concerned employees have been suggested to use proper PPE. Wherever sound level is very high, employees are suggested to use various engineering control methods like damping, isolation & machine guards, etc.

Similarly illumination measurements are done as per the guidelines set in Atomic Energy Factory Rules - 1996 and corrective measures are taken to improve the observed deficiencies, if any. Illumination measurements have been carried out at various labs of RRCAT with the help of digital lux meter -Lutron Lx-101A.

Noise and illumination survey in DMTD.

Issuing of height passes: RRCAT ensures the safety of the employees and workers working at height. For this purpose, height pass test were conducted. Height pass certificates were issued to 06 workers of CSD. Height pass document is prepared and record of issued height pass is also maintained.

Height pass test for workers.

Routine inspection of fire hydrants, isolation valves, and water/foam monitors: Monthly routine inspection, preventive maintenance, cleaning, oiling, checking for smooth valve operation of 79 fire hydrants, 30 isolation valves, and 20 water/foam monitors, spread all over the technical area of RRCAT are being carried out. A monthly report of these works was prepared and corrective measures were taken.

Preparation of various safety reports: Regular coordination and data collection from Administration, Medical Centre, Security, CISF, and other Sections/Divisions on various aspects of industrial safety and reporting to the regulator was done in the form of "Quarterly Status Report of RRCAT on Safety, Health and Environment, Industrial Hygiene Surveillance Report, Industrial Safety Award Report, Plant Accidents details report, etc". These reports include data on injury statistics of different categories of employees including contractor workers, number of reportable injuries (both fatal & non-fatal), man days lost, frequency rate (FR), severity rate (SR) and injury index (II), fire incidents, significant events and dangerous occurrences as per Factory Act, 1948.

Radiation safety: Radiation surveillance was provided to all radiation facilities to ensure radiation safety of staff and workers. During the period of Jan. – June, 2023 radiological surveillance was provided during the operation of the synchrotron radiation facilities and their beam lines. Induced radioactivity measurement on accelerator components and performance check of area radiation monitors & survey meters were carried out during Indus shutdown. Detailed radiation measurements were carried out at H^- ion source (RF based) within the shielded vault at H^- ion building and the recommendations were made to plug the glass viewing windows (with SS flange or lead glass) through which low energy x-rays were streaming out. Personal dosimetry for 499 workers (including temporary) of RRCAT was carried out during the period. The biometric data of 24 new radiation workers was uploaded on National Occupational Dose Registry System. From the dose data (of first quarter), the maximum individual dose recorded is 0.15 mSv, which is well within acceptable limit. Quarterly testing of various equipment /instruments of Radiation Emergency Response Centre was carried out and kept in a preparedness state for responding to any radiological emergency. Elementary training on radiations protection were imparted to 182 users of synchrotron radiation source of Indus-1 and Indus-2. The environmental radiation monitoring data from 11 locations of RRCAT campus and ARPF site indicated no increase in radiation level due to operation of the radiation facilities.

Reported by:
Vivek Kumar Bhatnagar (vivek@rrcat.gov.in)

N.8: Fire safety activities at RRCAT

Fire activities group of Fire and Safety Section (FSS), RRCAT is involved in fire fighting during fire emergencies. Along with this, they are also conducting first-aid fire fighting training program and fire safety awareness program. Different fire safety activities were carried out to meet the said objectives.

Live demonstration during National Science Day 2023: The Fire and Safety Section organized a science exhibit during the National Science Day Celebration in RRCAT, Indore on 25th & 26th February 2023. During this event, different types of fire safety equipment like Fire Entry Suit-3000 Series, Fire Proximity Suit-750 Series, Water Turbine based Smoke Extractor, Fire-fighting Hose with water branch, Aqueous Film Forming Foam (AFFF) Compound, DCP type Fire Extinguishers, CO_2 type Fire Extinguishers, Portable Fire Pumps, Breathing Apparatus Sets, Breathing Apparatus Compressor, etc. were displayed.

Fire fighting demonstration on National Science Day-2023.

Students from different schools were briefed about their operations and applications for mitigating the emergencies. A live operation of the High Expansion Foam Generator was also demonstrated, the foam discharge of this generator is 02 lakh liters per minute. Various types of fire-fighting water branches with different patterns of the water jet, donning & doffing of breathing apparatus set, and Multi-purpose Fire Tender with high-pressure hose reels, water monitors & remote controlled Light Mast were also demonstrated. The event was conducted at RRCAT Fire Station. Visitors from various schools, and colleges along with RRCAT colony residents and their relatives participated in this program.

Periodic training for fire fighting equipment and breathing apparatus set: Fire and Safety Section is regularly conducting training on fire-fighting and the breathing apparatus set. This monthly training program is imparted to RRCAT employees, using the latest training aids along with power point presentations, safety video clips and short movies, Hands-on experience with fire extinguishers & B.A. sets. During this period, total of 99 RRCAT employees were trained. Fire mock drills were also conducted in RRCAT technical area, which includes the Free Electron Laser (FEL) building and Indus Complex. A fire hazard analysis including fire load density & smoke filling calculation for the Indus Complex including MPS & RF hall was also conducted. A drive to control fire in the grass area of the unoccupied technical area was also

initiated and results remained successful, as during the summer season a few incidences of small fire in this area could be contained and controlled safely.

Training on fire fighting for employees.

In the month of January-2023, the recruitment for driver cum pump operator cum fireman was initiated through different levels of examination, which include medical test, written test, physical endurance test (PET) and vehicle driving test. For this recruitment, physical endurance test (PET) and vehicle driving test was organized by FSS.

Observance of National Fire Service Week-2023: Fire and Safety Section observed National Fire Service Week-2023 from 14th April to 20th April 2023. During this week, Martyr's Day on 14th April was observed in the presence of Dr. Shankar V. Nakhe Director, RRCAT, and other dignitaries at the Fire Station. A week-long program for RRCAT employees like a fire quiz competition, slogan competition, poster competition, and essay competition (Hindi and English) on the fire safety topic "Awareness in Fire Safety for Growth of National Infrastructure (AGNI)", basic fire-fighting training to AECS school children, Lecture on fire safety in Hindi, Screening of movie "The Tower" (in Hindi) based on fire disaster in the 108 stories tower sky building, etc. were successfully organized in RRCAT. On 20th April 2023, a prize distribution ceremony followed by a live fire safety demonstration by fire staff including high-rise building emergency and rescue operations, operation amidst the fire flames wearing fire entry suit was organized at RRCAT Fire Station.

Shri Purushottam Shrivastava, Chairman, Apex Safety Committee was the Chief Guest of this function. This event was presided by Dr. K. S. Bindra, Director, Laser Group & Outstanding Scientist. About 300 officials of RRCAT observed the fire safety demonstration.

Fire safety demonstration during National Fire Safety Week-2023.

Prize distribution ceremony during National Fire Service Week-2023.

Reported by:
Vivek Kumar Bhatnagar (vivek@rrcat.gov.in)

N.9: Activities of RRCAT Staff Club

RRCAT Staff Club is working under the aegis of RRCAT to promote sports and cultural activities to its members and their families. In addition to regular on-going activities, several events have been organized during the period January to June 2023.

RRCAT Staff Club successfully conducted 37th DAE Sports and Cultural Meet of Basket-ball during 13th to 17th February, 2023. A total of 88 participants from eight group teams of DAE units participated in the meet. The meet was commenced with beautiful inaugural function on 13th February, 2023. Mrs. Savita Kharadkar (Former International Basket-ball player) was Chief Guest for the inaugural function. The inaugural function was chaired by Dr. Shankar V. Nakhe, Director, RRCAT.

Inauguration of newly constructed Basket-ball court by Mrs. Savita Kharadkar near In-door Sports Complex.

Address by Director, RRCAT to the participants of 37th DAE Sports & Cultural Meet 2022-23 (Basket-ball).

A new Basket-ball court was constructed in mission mode to conduct the event and the same was inaugurated by Chief Guest, Mrs. Savita Kharadkar.

A total of 15 matches were played during league and knock-out stages. A certified team of tournament officials were assigned to conduct the matches. The meet was concluded with delightful valedictory function on 17th February, 2023. The prizes were distributed by Shri Sunil Hardia, Vikram Awardee and Vice-President MP Basket-ball association, who was the Chief Guest in the valedictory function.

Glimpses of match during 37th DAE Sports & Cultural Meet 2022-23 (Basket-ball).

RRCAT Staff Club has successfully organized a summer camp for children of RRCAT staff members from 6th May to 9th June, 2023. A total of 339 children participated in 18 different activities. More importantly, telescope making workshop and classes for computer coding and drama were also organized during the summer camp. In the last week of summer camp, competitive matches were organized in individual activity and prizes were distributed to the winners during valedictory function on 10th June, 2023.

Children of RRCAT Staff Club members in different events during Summer Camp-2023.

A motivational talk by B. K. Shaktiraj of Bhramakumaris (Mt. Abu) on 11th May 2023 and lecture series by Chinmaya Mission (10-17 June, 2023) were also organized. On 21st June, 2023 RRCAT Staff Club organized Yoga event on the 9th International Day of Yoga (IDY) in line with directives received from the department as per the guideline of Ministry of AUYUSH, Government of India. About 200 staff including family members participated in the event.

Participants attending Yoga event on the eve of International Day of Yoga.

Reported by:
Gurvinderjit Singh (gjit@rrcat.gov.in)

N.10: Accomplishments of AECS, Indore

Competitive exams cleared by AECS students: Sachin Ghongde Cleared JEE Advanced and joined IISc, Bangalore. Sanjit Satheesan cleared JEE Advanced, NEET and IISER and joined AIIMS, Mangalagiri. Vishesh Srivastava cleared JEE Advanced and joined IIT Pallakad. Gargi Tiwari cleared JEE Advanced and joined IIT Patna. Prathamesh Sangale cleared JEE Mains and joined SGSITS, Indore. Vivek Agrawal cleared JEE Mains and joined NIT, Bhopal. Sakshi Sharma and Mohit Nimje cleared VITEEE and joined VIT Bhopal. Tanmay Janbandhu cleared IPM 2023 and joined IIM Indore. Divyansh Dev cleared IPL 2023 and joined IIM Rothak. Maitri Jha joined Nirma University, Ahmedabad. Manvir Singh cleared JEE Mains and joined National Forensic Sciences University – Dharwad campus.

Board results of classes X and XII: The result of class X and XII is 100% pass. Class X scored Q.I. of 8.18 and E.I. 93.59. Class XII scored Q.I. of 7.3 and E.I. of 85. Prisha Mahawar of Class X topped the board results of our school with 97.6% Ramsha Riyasat Fatima stood second with 96.8%, Mitali Kulkarni and Samyak Baj were third with 96%. Gargi Tiwari of Class XII topped the board results of our school with 97.4%. Vishesh Srivastava stood second with 97% and Sanjit Satheesan was third with 96.8%.

JSO/JMO: Junior Science and Mathematics Olympiad 2023 was held during 5th to 14th June 2023 at AECS-05, Anushakti Nagar, Mumbai. Diva Shrivastava, K. Yaazhvendan, Akshat Pratap Singh and Aditya Patil of Class X participated in this enrichment programme. Diva Shrivastava won the First prize in Physics and Biology for which she also received cash prize along with Shri Sunil Mehta Memorial award for being topper in Physics and Biology. She also got the third prize in the Team Quiz Competition.

Vidyarthi Vigyan Manthan (VVM) 2022-23: Vidyarthi Vigyan Manthan (VVM) 2022-23 was organized by Vijnana Bharati (VIBHA) in association with Vigyan Prasar, Department of Science and Technology, Govt. of India and National Council of Educational Research and Training (NCERT), Ministry of Education, Govt. of india. Prarabdhi Nagar (Class 8), Ushraayush Mukherjee (Class 8) and Gyanvi Jain (Class 10) were selected for participation in State Level camp (Madhya Pradesh Region). Ushraayush Mukherjee (Class 8) bagged the first position in the State Level Camp (5th Feb. 2023 at Bhopal) and was selected for the National Camp (May 2023, IISER, Trivandrum).

Bhatiya Sanskriti Gyan Pariksha 2022-23: Prarabdhi Nagar (Class 8) received the Third Prize in Indore district of Madhya Pradesh.

IAPT: National Standard Examination (27.11.2022):
Sanjit Satheesan of Class XII, has secured his position in Top 10% in Biology.

TERI, The Green Olympiad 2022-23: Prarabdhi Nagar (Class 8) received a Certificate of Merit and Sachidanand Tiwari (Class 8), Shubham Chahar (Class 9) and Gyanvi Jain (Class 10) have received Certificate of Distinction. Gyanvi Jain also secured Global Winner- Second Rank in TERI Olympiad 2022-23.

Reported by:
Chinmoy Basu (aecsprincipal@rrcat.gov.in)

N.11: Clean and green campus activities at RRCAT

At RRCAT, concerted and coordinated efforts have been made involving innovative integrated approaches for sustainable, clean and green environment in the campus. The innovative approaches for developing an eco-friendly institutional culture covers all aspects of swachhata, like waste segregation and management, energy conservation, rain water harvesting, paperless office procedures, plantation drives, cleanliness campaigns, and public awareness programmes. Three R's – Reduce, Reuse and Recycle are being followed as a policy in the Centre. In view of the recent pandemic, the cleanliness activities in the campus have become even more important. As per the directive from the Secretary, DAE, all units were to observe "Swachhata Pakhwada" from February 16 to 28, 2023, and undertake innovative cleanliness related initiatives during the fortnight. The objective of the celebration of the 'Swachhata Pakhwada', as part of the 'Swachh Bharat Abhiyaan', is to take up sanitation initiatives, mobilize people, and reinforce the mass movement for cleanliness to contribute to Mahatma Gandhi's dream of a clean India. In this direction various activities were carried out at RRCAT which were coordinated by the Advisory Committee for Clean and Green Campus (ACCGC) of RRCAT. The activities included: (i) Two workshops for increasing awareness about hygiene and cleanliness among housekeeping staff and Work-Assistants working in various Divisions of RRCAT on Feb. 17 and Feb. 22, 2023, respectively. During the workshops, special lectures were delivered in Hindi language by the doctors of RRCAT Medical Centre, on the topic of "Hygiene and cleanliness issues in the current scenario"; (ii) Quiz for employees of RRCAT was organized on Feb. 21, 2023, on the topic of "Swachhata guidelines as well as general Swachhata initiatives taken by the Government of India"; (iii) A few award winning films on the topic of "swachhata" were screened during celebration of the National Science Day in RRCAT on Feb 25, 2023; (iv) Special Swachhata drive was organized in the RRCAT colony; (v) Special Swachhata drive was conducted in the technical area of RRCAT; (vi) Special drive for collection of waste papers and scrap from all the buildings; (vii) Competition for cleanest office, cleanest mechanical workshop, optical workshop and civil construction site of RRCAT; (viii) Competition on swachhata related topics for students of AECS, Indore and also specially abled children of Mook-Badhir Sangathan, Indore; (ix) Cleaning of water bodies (lakes) at RRCAT colony; (x) Installation of Nirmalya Kalash at three locations in RRCAT colony for collecting discarded waste or remains of puja; (xi) Special campaign for collection of saleable scrap from all the Divisions; (xii) Enhancing the capacity of composting from garden waste generated in the campus from 80 MT to 100 MT using bioreactors (bacteria, fungus and earthworms); (xiii) Air quality measurement at different locations in the technical area of RRCAT, (iv) Renovation of Baggi Khana building for use as a part of Indoor Sports Complex; (xv) Arrangement of bird nests from available wooden scrap in Nakshtra Udyan and City Forest in the Campus; and (xvi) In order to maintain the cleanliness and

hygiene, four open Bhatties (Chullhas) have been constructed near RRCAT Welfare Center and the surrounding area has been paved using old paver blocks. In case of cleanliness related competitions, a few best performers were awarded. In view of the recent pandemic, all the precautions and necessary guidelines issued by the Government of India from time to time were strictly followed during organization of Swachhata Pakhwada and other cleanliness initiatives. A few photographs of the events organized are given below:

Swachhata pledge taking ceremony before the cleanliness drive in RRCAT colony.

Dr. S. V. Nakhe, Director, RRCAT (2nd from right) leading the Swachhata campaign in the colony.

Organizers and participants in the workhop for house-keeping staff on the topic of cleanliness.

Swachhata related short films being screened during the National Science Day -2023 celebrations.

Drawing and painting competition being organized by RRCAT officials for specially-abled students.

Team of judges inspecting the civil construction site for debris management and general cleanliness.

Air quality measurements being performed in the Technical Area of RRCAT.

Baggi-khana before (top) and after (below) renovation.

Open Bhatties (Chullhas) constructed near RRCAT Welfare Center to reduce air-pollution.

All the Divisions in RRCAT technical area actively participated in cleanliness campaigns, which included cleaning inside-and-around each building, rearrangement of equipment in the Labs for efficient utilization, identifying the non-functional materials and shifting to a selected place to declare them as scrap, etc. The waste collected in each of the Division was placed at selected location near the individual building, which was then collected by the Stores Unit of RRCAT for further segregation and proper disposal as per the norms set by the Indore Municipal Corporation. A tractor trolley ferried from building to building for collection of the waste and its disposal. In addition, a special cleanliness drive was also conducted in the residential premises of RRCAT for collection of wastes from the residences of the employees. This exercise was in-addition to the regular collection of domestic waste, which is done in a door-to-door manner on daily basis from every residence of the RRCAT colony.

One of the Labs of RRCAT, before (top) and after (bottom) cleanliness drive in the technical area.

RRCAT has been consistently receiving awards from Indore Municipal Corporation for the clean and green campus activities. This year also, RRCAT received award from IMC for the "Cleanest Colony of the Cleanest City of India". In addition, the waste management model of RRCAT was appreciated by a team of IMC officials led by Smt. Harshika Singh, Commissioner, IMC, which received wide publicity in the local newspapers.

"Cleanest Colony of the Cleanest City of India" award (certificate and shield) received by RRCAT from Indore Municipal Corporation.


ये होगा नया बदलाव: शहर के जलस्रोतों के पास रखे जाएंगे निर्माल्य कलश

स्वच्छ शहर को भाया आरआर कैट का वेस्ट मैनेजमेंट मॉडल

पत्रिका न्यूज नेटवर्क
patrika.com

इंदौर. देश के सबसे स्वच्छ शहर को राजा रम्मन्ना प्रगत प्रौद्योगिकी केंद्र (आरआर कैट) से सफाई का नया मंत्र मिला है। नगर निगम आयुक्त ने जब कैट परिसर का दौरा किया तो वेस्ट मैनेजमेंट का नया मॉडल सामने आया। अब शहर में इसे अमलीजामा पहनाने के लिए नगर निगम की टीम कैट का दौरा करेगी। इसके बाद कुछ नए बदलाव लागू किए जाएंगे, जिसमें निर्माल्य कलश रखना सबसे अहम है।

निगमायुक्त हर्षिका सिंह राजा रम्मन्ना प्रगत प्रौद्योगिकी केंद्र पहुंची तो उन्होंने यहां की सफाई की जमकर तारीफ की। यहां के वेस्ट मैनेजमेंट की सराहना करते हुए निगम अफसरों को यहां का विजिट करने के लिए कहा है। निगमायुक्त अपने रूटीन दौरे पर थीं, यहां जल संरक्षण के लिए तालाब के आसपास किए गए कार्यों को उन्होंने देखा। कैट क्षेत्र में पर्याप्त सफाई व्यवस्था तथा वेंकटाइन सफाई भी देखी। वेंकलेन बहुत सुंदर थी।

यहां सीनरेट से कंपोस्ट खाद और बायो सीएनजी गैस का निर्माण किया जा रहा है। यहां का कचरा बाहर नहीं आता है। कैट के तालाब के पास निर्माल्य रखने के लिए कलश भी रखा गया है। यहां के लोग तालाब में निर्माल्य न डालते हुए कलश में रखते हैं। निगमायुक्त ने ऐसे कलश शहर में सभी जगह रखने के निर्देश दिए।

कृष्णपुरा छत्री पर देखी सफाई व्यवस्था

निगमायुक्त गुरुवार को सुबह कृष्णपुरा छत्री भी पहुंची। नदी किनारे स्थित घाट पर सफाई व्यवस्था के साथ ही पेंटिंग और रंगन करने के निर्देश दिए गए। उन्होंने गणगौर घाट, पंचकुइयां, राम मंदिर घाट, पीतिया खाल घाट का भी निरीक्षण किया।

News about the waste management model of RRCAT being appreciated by the IMC officials.

The activities carried out at RRCAT during Swachatta Pakhwada-2023 from Feb. 16 to 28, 2023, were evaluated by a committee constituted at DAE level, and RRCAT was adjudged "Second" among all the DAE units in this regard. A "Certificate of Excellence" was awarded to RRCAT by Secretary, DAE along with "Swachhata Pakhwada Award – 2023" by the Department of Drinking Water and Sanitation, Government of India.

"Certificate of Excellence" awarded to RRCAT by Secretary, DAE and "Swachhata Pakhwada Award – 2023" by the Dept. of Drinking Water and Sanitation.

RRCAT won the Championship trophy at the 35th Annual Rose Show held on 14th and 15th January 2023 at Indore, which was jointly organized by the Department of Horticulture & Food Processing, Govt. of M.P. and Malwa Rose Society, Indore. RRCAT bagged several other prizes as well in the competitions under the Institutional category. The prizes include First prize in Best Largest Rose Garden, First prize in Best Landscape / Ornamental Garden, 6 second prizes and 7 Consolation prizes in various categories for Cut Flower participation under HT, Floribunda and Polyantha Rose Categories.

The championship trophy and the certificate won by RRCAT during 35th Annual Rose Show by the Malwa Rose Society.

The clean and green campus activities in RRCAT are coordinated by the Advisory Committee for Clean and Green Campus (ACCGC), RRCAT under the keen supervision and guidance of Dr. Shankar V. Nakhe, Director, RRCAT, and with the strong support of Construction and Services Division, RRCAT. These activities receive active participation from RRCAT employees, Administration, Accounts, Security, CISF personnel, AECS students and teachers, HBNI scholars, project trainees, stipendiary trainees, and residents.

Reported by:
Sunil Verma (greencampus@rrcat.gov.in)

N.12: Activities of Women's Welfare Committee (WWC)

Essential Financial Awareness for Women: On 6th January 2023, a lecture was organised on "Essential Financial Awareness for Women" at Convention Centre, RRCAT for the benefit of all women employees and female family members of RRCAT employees. The lecture was delivered by renowned Indore High Court advocate Ms. Mini Ravindran. Advocate Shri Avinash M. Sirpurkar was the special guest of the program. It was a very informative and educating lecture about the financial rights and liabilities of an Indian woman. The lecture received overwhelming response with over 150 women participants.

Indore High Court advocate Ms. Mini Ravindran (center) and Advocate Shri Avinash M. Sirpurkar (left) during the lecture program.

UDYAM-2023: On 21st January 2023 WWC organized one day entrepreneurship fair by women "UDYAM-2023". The fair was organized on the theme "Women empowerment through financial independence" at Welfare Centre, RRCAT. Around 60 female participants had put up 30 stalls showcasing herbal products, handicrafts, self-written books, clothes/saris from various states, homemade food products, etc. The exhibition was inaugurated by Smt. Revati Nakhe who motivated participants to take their entrepreneurship journey to a long distance ahead. WWC members distributed memento to all participants.

Inauguration of UDYAM-2023 by Smt. Revati Nakhe (center).

International Women's Day-2023:

International Women's Day-2023: A week long program from 1st to 8th March 2023 was organized by Women's Welfare Committee to celebrate International Women's Day-2023. This year's International Women's Day was celebrated on the theme #EmbraceEquity. The events conducted during the week included poetry and slogan writing competitions. Around 60 staff participated with full zeal and enthusiasm in these competitions. On 6th March 2023, online pledge on the theme #Embrace Equity was taken by all RRCAT staff. On 7th March 2023, "Cultural Programme" was organized. Staff members, Smt. Arti Shelke, Smt. Madhuri Sinnarkar, Smt. Abha Uppal and Smt. Sujata Joshi due to retire in the coming year were felicitated. The chief guest of the cultural program Smt. Sujata Joshi was welcomed by Smt. Beena Jain. Smt. Joshi shared her experiences of professional life in RRCAT and gave a useful insight to all present. WWC members enthusiastically conducted various activities during the week.

Celebration of International Women's Day-2023.

On 16th January 2023 an orientation session on "Awareness about Workplace Conduct" was jointly organized by WWC and ICC for educating TSOs, Ph. D. scholars, M. Tech./M. Sc. students, and TASAR apprentice about workplace conduct.

On 17th February 2023, ACCGC and WWC jointly organized a workshop on "Health-Hygiene Awareness" for housekeeping staff during Swachhata Pakhwada.

Reports of all programs are available at WWC page on RRCAT Infonet.

Reported by:
Beena Jain & Shradha Tiwari (beenaj@rrcat.gov.in)

N.13: Orientation session on "Awareness about Workplace Conduct"

An orientation session on "Awareness about Workplace Conduct" was organized on January 16, 2023 for TSOs, Ph. D. scholars, M. Tech/ M. Sc./other students, Indus beamline users (specially students) and apprentices undergoing training of one year under TASAR programme of RRCAT. Dr. Shankar V. Nakhe, Director, RRCAT addressed the audience and explained about workplace conduct, importance of mutual respect and shouldering responsibilities for self-growth as well as growth of organization. He also expressed that there is need for a well defined code of conduct for all students, trainees, apprentices working in RRCAT.

Dr. Alpana Rajan and Dr. Beena Jain delivered a very informative talk on "General Workplace Conduct". The session helped the audience to gain insight on importance of utilizing the time for their professional benefit and growth, importance of discipline and conduct to be followed at workplace. Dr. S. Bhavani gave a very educative talk on "Hygiene: Understanding & Compliance" for making everyone aware of the importance of cleanliness and hygiene in daily life and its effect on persons behaviour. Dr. C. P. Paul and Dr. Suparna Pal explained in very interesting manner about how to make the hostel at RRCAT a better place to live. This talk made students, trainees aware of the rules and regulations to be followed in RRCAT Guest House.

Smt. Gitika Khare briefed the audience about mandate of Internal Complaints Committee and Smt. Shradha Tiwari gave an overview about the mandate of Women's Welfare Committee. The Chairpersons including members of Coordination Committee for HBNI Ph. D. Programme, Students Grievance Redressal Committee, Projects Placement Committee, Coordination Committee for Apprenticeship Program, Internal Complaints Committee and Women's Welfare Committee attended the Orientation Session along with the students.

The programme was conducted by Dr. Ajit Upadhyay and vote of thanks was proposed by Dr. Sunil Verma. The programme was attended by over 150 students, which included TSOs, Ph. D. scholars, M. Tech./ M. Sc./other students, Indus beamline users (students only) and TASAR apprentices undergoing one year training in RRCAT.

Dr. S. V. Nakhe, Director, RRCAT addressing the participants about workplace conduct.

Dr. Alpana Rajan (left) and Dr. Beena Jain (right) delivering a talk on "General Workplace Conduct".

Dignitaries and participants attending orientation session on "Awareness about Workplace Conduct".

Reported by:
Shradha Tiwari & Gitika Khare (shradha@rrcat.gov.in)

N.14: Awards and Honours

N.14.1: Award of Doctor of Philosophy (Ph. D.) Degree

The Homi Bhabha National Institute (HBNI), a Deemed University has awarded Ph. D. Degree to following employee / students of RRCAT:

1. Dr. Soumyadeep Ghosh was awarded Doctor of Philosophy in Physical Sciences on the dissertation, titled "Theoretical studies on core electron spectroscopy of some novel iron based and chalcogenide materials", which was supervised by Dr. Haranath Ghosh.

2. Dr. Chiranjit Debnath was awarded Doctor of Philosophy in Physical Sciences on the dissertation, titled "Synthesis and characterization of Lithium Niobate nanoparticles and nanocomposites for optical applications", which was supervised by Dr. Sunil Verma.

N.14.2: ISPA Young Engineer Award 2023

Shri Nitesh Mishra, SO/D, RF Systems Division, Proton Accelerator Group, RRCAT received ISPA Young Engineer Award 2023 sponsored by the Indian Society for Particle Accelerators (ISPA), during Indian Particle Accelerator Conference (INPAC-2023) held at BARC, Mumbai during March 13-16, 2023. This award was conferred on him in recognition of his outstanding contributions in the field of particle accelerators. The award carries a certificate and a cash prize of ₹10000.

N.14.3: Best Thesis Award

Dr. Surendra Yadav, SO/G, Accelerator Controls & Beam Diagnostics Division, Electron Accelerator Group, RRCAT received Best Thesis Award sponsored by the Indian Society for Particle Accelerators (ISPA), during Indian Particle Accelerator Conference (INPAC-2023) held at BARC, Mumbai during March 13-16, 2023. The title of the thesis was "Intelligent approach to study transverse coupled bunch instabilities and their effects on performance of electron synchrotron". The award carries a certificate and a cash prize of ₹10000.

N.14.4: Best Poster / Paper Awards

1. Four posters of RRCAT received the Best Poster Awards sponsored by Indian society for Particle Accelerators (ISPA), during Indian Particle Accelerator Conference (INPAC-2023) held at BARC, Mumbai during March 13-16, 2023. The award carries a certificate and a cash prize of ₹3000. The details of the posters are given below:

1.1 *Title:* Development and preliminary evaluation results of prototype 100 nm spatial resolution digital beam position monitor envisaged for high brilliance synchrotron radiation source
Authors: B. B. Shrivastava, Surendra Yadav, Anil Holikatti, Avanish Ojha, Rahul Jain, L. K. Babbar, Ankita Kumari, Raja Khan, Abhisek Nayak, Bhavna N. Merh, and T. A. Puntambekar

Shri B. B. Shrivastava, SO/G, Accelerator Controls & Beam Diagnostics Division, Electron Accelerator Group, RRCAT, presented the poster and received the award.

1.2 *Title:* Cold test and RF tuning of the first section of 3 MeV, 325 MHz RFQ at RRCAT
Authors: R. Gaur, N. S. Kulkarni, V. Kumar, G. V. Kane, N. K. Sharma, A. Chaturvedi, V. Prasad, K. A. P. Singh, V. Rajput, D. Baxy, M. Lad and P. Shrivastava

Shri Rahul Gaur, SO/F, Accelerator & Beam Physics Section, Proton Accelerator Group, RRCAT, presented the poster and received the award.

1.3 *Title:* Design methodology for forming tool of SCRF cavities
Authors: Nitin Nigam, S. Mandle, N. K. Sharma, G. V. Kane, Vijendra Prasad, Purushottam Shrivastava

Shri Nitin Nigam, SO/E, Proton Linac Development Division, Proton Accelerator Group, RRCAT, presented the poster and received the award.

1.4 *Title:* Design and impedance simulation of RF-shielded bellow and pumping manifold for Indus-1 upgradation
Authors: M. K. Singh, P. Pareek, V. S. Bais, B. Sindal, K. V. Kumar, S. N. Singh, D. P. Yadav, P. Shrivastava

Shri Manish Kumar Singh, SO/C, Ultra High Vacuum Technology Section, Proton Accelerator Group, RRCAT, presented the poster and received the award.

N.15: New Recruits

RRCAT welcomes the following personnel who have joined during January 2023 to June 2023:

- Shri Manjeet Kumawat, SAC, DMTD

N.16: Superannuations

The following RRCAT colleagues retired during January 2023 to June 2023. RRCAT family wishes them a happy and healthy post-retirement life.

- Shri Pravin Fatnani, OS, ACBDD
  DoJ: 01.08.1986, DoR: 31.05.2023.
- Shri Rakesh Kumar Gupta, SOH, EDMS
  DoJ: 21.12.1984, DoR: 30.06.2023.
- Shri Ram Mohan Pandey, SOH, CSPCS
  DoJ: 16.03.1988, DoR: 30.06.2023.
- Dr. Mukesh Kumar P. Joshi, SOH, PNL
  DoJ: 01.08.1988, DoR: 30.06.2023.
- Smt. Arti Shelke, SOH, CSDC
  DoJ: 24.02.1997, DoR: 31.05.2023.
- Shri Niketan Kumar Sethi, SO/G, GHMDWC
  DoJ: 03.09.1984, DoR: 30.04.2023.
- Dr. Abha Uppal, SOG, APML
  DoJ: 27.12.1990, DoR: 30.06.2023.
- Shri Om Prakash Joshi, TOE, HPLEL
  DoJ: 26.04.1990, DoR: 31.03.2023.
- Shri S. William Amalraj, SAG, HEOS
  DoJ: 23.11.1987, DoR: 31.05.2023.
- Shri R.K. Jain, SAG, ILAS
  DoJ: 02.05.1988, DoR: 30.06.2023.
- Shri Sudarshan Ramgopal Patwa, SAG, HEOS
  DoJ: 18.11.1987, DoR: 30.06.2023.
- Shri C.B. Panwar, SAG, LTD
  DoJ: 15.01.1990, DoR: 31.03.2023.
- Shri Akhilesh Kumar Pathak, SAG, EWC
  DoJ: 06.09.1984, DoR: 30.04.2023.
- Shri Surendra Singh Kushwah, SAF, CVLEL
  DoJ: 20.11.1987, DoR: 31.01.2023.
- Shri Lakshman Chowdhry, SAF, PLDD
  DoJ: 28.11.1989, DoR: 30.04.2023.
- Shri Praduman Krishen Bhan, SAF, ESLM
  DoJ: 18.07.1994, DoR: 30.04.2023.
- Shri S.M. Sharma, Foreman/C, LMIL
  DoJ: 01.01.1990, DoR: 31.01.2023.
- Shri C.B. Kulkarni, Tech. Sup./B(Drg.), UHVEL
  DoJ: 26.11.1987, DoR: 31.05.2023.
- Shri Bhimsen Verma, Tech. Sup./A, MTL
  DoJ: 13.09.1988, DoR: 30.06.2023.
- Shri Jose S. Pulickal, Tech. Sup./A, MTL
  DoJ: 12.08.1988, DoR: 31.03.2023.
- Shri Umashankar Babulal Yadav, Sr. Techn./H, CCMS
  DoJ: 02.04.1985, DoR: 30.06.2023.
- Shri Kanhaiya Sukhlal, Techn./G, CTL
  DoJ: 03.09.1984, DoR: 31.05.2023.
- Shri Nirbhay Singh Balram, Techn./F, Dir. Off.
  DoJ: 05.09.1984, DoR: 31.05.2023.
- Shri Prakash Jumman, Sr. Wrk. Ast./B, CTL
  DoJ: 04.04.1991, DoR: 31.05.2023.
- Shri Khyali Ram, Sr. Wrk. Ast./B, MTL
  DoJ: 19.02.2003, DoR: 31.03.2023.
- Shri S.C. Satapathy, SubOff(C), FSS
  DoJ: 04.03.2013, DoR: 31.05.2023.
- Shri Om Prakash, HSG, Security
  DoJ: 23.04.1986, DoR: 30.04.2023.

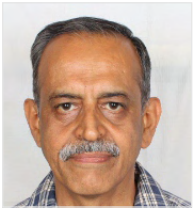

Shri Pravin Fatnani, Outstanding Scientist and Head, Accelerator Control Systems Division and Head, Beam Diagnostics & Coolant Systems Division superannuated on May 31, 2023 after a meritorious service of ~37 years in the Department of Atomic Energy. Shri Fatnani graduated in Electrical Engineering from NIT Raipur in 1985. After completing orientation course from the 29th batch of BARC Training School, he joined Accelerator Controls team at RRCAT in 1986. Right from his early days, he was actively involved in planning and setting up the laboratories and infrastructure of the data acquisition and control system lab. He has made immense contribution in the indigenous development of VME control system hardware. He was involved in the development and commissioning of control systems for Microtron, Booster Synchrotron, Transport Lines-1 & 2, and Indus-1 Synchrotron Radiation Source (SRS). Subsequently, he spearheaded and led the controls team in realizing Indus-2 SRS control system. He was actively involved in planning, building and integrating several critical interfaces and control system aspects for various Indus-2 sub-systems including beam orbit controls, SCADA, database, web technologies, machine information system, etc. He has also guided the development of control and data acquisition system of industrial electron Linacs, Vertical Test Stand (VTS) and Horizontal Test Stand (HTS) for superconducting radio frequency (SCRF) cavity testing, H^- ion source for proton Linac, etc. He has been conferred with DAE Science & Technology Excellence award and several Group Achievement awards. RRCAT family wishes him and his family a very happy, healthy and fulfilling post-retired life.

Shri Rakesh Kumar Gupta, Scientific Officer/H and Head, Laser Components Design and Fabrication Section superannuated on June 30, 2023, after a meritorious service of 38 years in the Department of Atomic Energy. Shri Gupta's educational background includes Diploma in Mechanical Engineering (1983) and B. E. in Mechanical Engineering (1991) from SGSITS, Indore. He joined BARC in 1984 and transferred to RRCAT in 1986. Throughout his tenure at RRCAT, Shri Gupta played a key role in procuring, installing and commissioning of various critical equipment including precision measuring instruments, CNC machines, fabrication facilities, and glass-blowing furnaces. His significant contributions include metrology and quality control of crucial components for various projects such as microwave cavities for 12 MeV and 20 MeV Microtron, Dipole magnets and RF cavity for Indus-1, Dipole UHV chambers and straight UHV chambers for Indus-2 at M/s HAL, Nasik, 505.8 MHz RF cavity for Indus-2, Components and cups for LINAC of ARPF, Forming tooling, half-cell, components for 1.3 GHz and

650 MHz Niobium SCRF cavity. He further distinguished himself by contributing to the design and development of flow control needle valves, Laser alignment system, Horizontal beam scraper, and Beam position monitor. These advancements were instrumental for beamlines of Indus-1 and Indus-2. Shri Gupta also played a vital role in manufacturing various precision UHV-compatible components for ongoing projects within the Laser and Accelerator programs. In recognition of his outstanding contributions, Shri Gupta received ten DAE Group Achievement Awards. Since 2010, he has also led the successful implementation of a two-year Stipendiary Training Programme (STP) at RRCAT, overseeing the training and induction of over 150 trainees across various disciplines. RRCAT family wishes him and his family a very happy, healthy and fulfilling post-retired life.

Dr. Mukesh Kumar P. Joshi, Scientific Officer/H and Head, Photonic Nanomaterials Lab, Laser Materials Processing Division, superannuated on June 30, 2023, after a meritorious service of 36 years in the Department of Atomic Energy. He obtained M. Sc. in Physics from IIT Bombay, Mumbai in 1987. He joined RRCAT in 1988 as SO/C after graduation from 31st batch of BARC training school, Mumbai. He started his research career in the field of nonlinear optics and obtained Ph. D. degree from IIT Bombay while working on the optoelectronic properties of Fullerene C60 and its nanocomposites for optical limiting device application. He also spent two years (1996-1998) at University of Buffalo NY, USA, and carried out research on polymer-based nanocomposites for optical limiting, 3D data storage, and microfabrication. He was also a Professor at Homi Bhabha National Institute (HBNI), Mumbai, and guided three Ph. D. and several M. Tech. and M. Sc. project students. At RRCAT, he made substantial contribution in the field of growth and characterization of photonic nanomaterials for energy conversion and storage applications such as solar cells, solar fuels, photodiodes, NLO devices, etc. He developed methods of fabricating thin films and nanostructures using nano and femtosecond lasers. He also developed material characterization tools such as transient photoconduction and photoluminescence, soft x-ray excited visible luminescence, etc. for investigating optoelectronic properties of nanostructured materials. RRCAT family wishes him and his family a happy, healthy, and fulfilling post-retirement life.

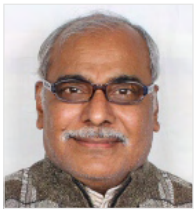

Shri Ram Mohan Pandey, Scientific Officer/H and Head, Coolant Systems and Process Control Section, superannuated on June 30, 2023 after a meritorious service of 35 years in the Department of Atomic Energy. Shri Pandey graduated in Mechanical Engineering from Maulana Azad College of Technology (now MANIT, Regional Engineering College), Bhopal in 1985. He joined RRCAT in March 1988 as Scientific Officer/SC in Cryogenics Division and was involved in developing cryomodule. Later in the year 1989, he was given the responsibility of development of low conductivity water (LCW) coolant system for Indus accelerators. He has vast experience in the field of design, development, installation, and operation & maintenance of coolant systems in round-the-clock mode. He has played a pivotal role in the commissioning of LCW plants for the operation of Indus-1 and Indus-2 synchrotron radiation sources and contributed in various upgrade activities for enhancement of their performance. He has also played a key role in the development and deployment of precision cooling systems for Indus-2 RF cavities. RRCAT family wishes him and his family a very happy, healthy and fulfilling post-retired life.

Smt. Arti Shelke, Scientific Officer/H & Head, Civil Structural Design Cell, Construction & Services Division, RRCAT superannuated on May 31, 2023. She did her Bachelor of Engineering (Civil) in the year 1983 and Master of Engineering (Structural Engineering) in 1986. She joined DAE in November 1985 and Construction & Services Division of RRCAT in February 1997. At RRCAT, she was associated with planning, analysis and detailed structural design of civil structures meeting multidisciplinary stringent requirements. Her contribution includes analysis and structural design of various structures like Petawatt laser lab building, SCRF cavity test stand lab, IRFEL lab building, etc. She was also entrusted with additional responsibility of quality assurance and quality control of RCC structures. She was also a member of the various committees including SSC to grade SO/C, Infrastructure Committee, etc. RRCAT family wishes her and her family a very happy, healthy and fulfilling post-retired life.

Dr. Abha Uppal, Scientific Officer/G, Laser Biomedical Applications Division, superannuated on June 30, 2023 after a meritorious service of 33 years in the Department of Atomic Energy. She did Ph. D. in Biochemistry from Devi Ahilya Viswavidyalaya, Indore. She joined RRCAT in December 1990 and since then she has been associated with Laser Biomedical Applications activity. Her principal areas of interest and expertise include use of light based approaches for diagnosis of diseases, cell micromanipulation and selective therapy. In particular, she contributed significantly to the activities related to design and development of silica nanostructures for photosensitizer delivery to mammalian cancer cells. She has 38 research papers published in international journals and 43 conference proceedings to her credit. She is a recipient of two DAE Group Achievement Awards in the year 2012 and 2013 related to the "Development of Optical Trapping Set ups" and "Design, Development and utilization of Optical Techniques for high resolution biomedical imaging", respectively. She also guided five M. Sc. students during her tenure. RRCAT family wishes her and her family a happy, healthy and fulfilling post-retirement life.

N.17: राराप्रप्रौके में राजभाषा गतिविधियाँ: जनवरी 2023 – जून 2023

01 जनवरी 2023 से 30 जून 2023 तक राजभाषा निरीक्षण से संबंधित विभिन्न गतिविधियां इस प्रकार रहीं:

दिनांक 28.04.2023 को केंद्र में राजभाषा वार्ता का आयोजन किया गया जिसमें 'आधुनिक जीवन शैली में स्वस्थ रहने के लिए योग का महत्व' विषय पर बी. के. बांद्रे द्वारा व्याख्यान दिया गया। राजभाषा कार्यान्वयन समिति की दो बैठकें दिनांक 27.03.2023 तथा 28.06.2023 को निदेशक, राराप्रप्रौके की अध्यक्षता में आयोजित की गईं। दिनांक 20.03.2023 तथा 25.05.2023 को नियमित हिंदी कार्यशालाओं का आयोजन किया गया जिनमें क्रमशः 27 तथा 21 पदाधिकारियों ने भाग लिया। जन संपर्क प्रकोष्ठ, सुरक्षा अनुभाग, अग्निशमन एवं संरक्षा, संगणक प्रभाग, रेडियो आवृत्ति प्रणाली प्रभाग एवं लेसर नियंत्रण एवं उपकरणीकरण प्रभाग का आंतरिक राजभाषा निरीक्षण किया गया। जनवरी-मार्च, 2023 एवं अप्रैल-जून 2023 की तिमाहियों में परमाणु ऊर्जा राजभाषा कार्यान्वयन योजना (अटॉलिस) के अंतर्गत कुल 133 पदाधिकारियों ने भाग लिया तथा 72 पदाधिकारियों को प्रोत्साहन पुरस्कार प्रदान किए गए। दिनांक 09.02.2023 को नराकास, इंदौर की 77 वीं बैठक में केंद्र से श्री पुरुषोतम श्रीवास्तव,निदेशक,प्रोटोन त्वरक वर्ग ने भाग लिया।

प्रस्तुति:
विमल कुमार शुक्ल (vimalks@rrcat.gov.in)

Career and Research Opportunities

Join as Scientific Officer

BARC Training School

The selection of the Scientific Officers is done in a centralized manner by BARC, Mumbai, for all BARC Training Schools situated in various units of the Department of Atomic Energy.
http://oces.hbni.ac.in/ | http://www.barc.gov.in/careers/index.html#sandt

Join as Scientific Assistant

Graduates in science and diploma holders in various engineering branches are recruited through a two-year Stipendiary Training Scheme (Category-I) and they are absorbed as Scientific Assistant-C
https://www.rrcat.gov.in/hrd/Openings/Current_Openings.html

Join as Technician

Candidates having qualification of HSC (Science) or SSC followed by ITI certificate, are recruited under a two-year Stipendiary Training Scheme (Category-II), and they are absorbed as Technician-B or Technician-C
https://www.rrcat.gov.in/hrd/Openings/Current_Openings.html

Ph. D. Programme

RRCAT invites students with appropriate qualifications to pursue Ph.D. program of the Homi Bhabha National Institute (HBNI), a Deemed University with NAAC "A" grade under Department of Atomic Energy.
https://www.rrcat.gov.in/hrd/advt/phdad.html

Projects for Students

RRCAT offers opportunities to the students pursuing M.Tech. / M.E. / M.Phil. / M.Sc. degree in India for carrying out project work towards partial fulfilment of their post graduate degree.
https://www.rrcat.gov.in/hrd/advt/project.html

Trade Apprenticeship Scheme at RRCAT (TASAR)

TASAR is a skill development scheme for young ITI trained personnel, by providing them access to modern engineering infrastructure and opportunity to work under the guidance of experienced engineers and technicians at RRCAT.
https://www.rrcat.gov.in/hrd/Openings/tasar.html#

Dr. S. V. Nakhe, Director, RRCAT exchanging incubation agreement on Foundation Day (20th Feb. 2023) with Mr. Manoj Jain, CEO, VFuse Metal 4 Manufacturing Pvt. Ltd., Bhopal. Chief Guest Shri K. N. Vyas, Chairman, AEC and Secretary, DAE, and Guest of Honour Prof. U. Kamachi Mudali, Vice-Chancellor, VIT Bhopal University gracing the occasion (left). Students visiting exhibits at RRCAT Convention Centre during National Science Day (NSD-2023) celebration at RRCAT (right).

"Cleanest Colony of the Cleanest City of India" award (certificate and shield) received by RRCAT from Indore Municipal Corporation (left). "Certificate of Excellence" awarded to RRCAT by Secretary, DAE for activities carried out at RRCAT during Swachatta Pakhwada-2023 from February 16-28, 2023 (center) and "Swachhata Pakhwada Award – 2023" by the Dept. of Drinking Water and Sanitation (right).

Inauguration of newly constructed Basket-ball court by Mrs. Savita Kharadkar (Former International Basket-ball player) on Feb. 13, 2023 near In-door Sports Complex (left). Glimpses of match during 37th DAE Sports & Cultural Meet 2022-23 (Basket-ball) during February 13-17, 2023 (right).

RRCAT Newsletter is a publication of Raja Ramanna Centre for Advanced Technology, Indore 452013
Website : www.rrcat.gov.in/newsletter/NL
Email : newsletter@rrcat.gov.in
(For private circulation only)